NEW ULTRA- LOW CARBON HIGH STRENGTH STEELS WITH IMPROVED BAKE HARDENABILITY FOR ENHANCED STRETCH FORMABILITY AND DENT RESISTANCE

by

Ritesh Kumar Seal

B.Tech, Indian Institute of Technology (I.I.T.)- Bombay, 2000

Submitted to the Graduate Faculty of

School of Engineering in partial fulfillment

of the requirements for the degree of

Master of Science in Materials Science and Engineering

University of Pittsburgh

2006

UNIVERSITY OF PITTSBURGH

SCHOOL OF ENGINEERING

This thesis was presented

by

Ritesh Kumar Seal

It was defended on

July 30, 2003

and approved by

Dr. I. Nettleship, Associate Professor, Materials Science and Engineering Department

Dr. C. I. Garcia, Materials Science and Engineering Department

Thesis Advisor: Dr. A. J. DeArdo, William Keplar Whiteford Professor, Materials Science and Engineering Department

NEW ULTRA- LOW CARBON HIGH STRENGTH STEELS WITH IMPROVED BAKE HARDENABILITY FOR ENHANCED STRETCH FORMABILITY AND DENT RESISTANCE

Ritesh Kumar Seal, M.S.

University of Pittsburgh, 2006

The threat to future legislation regarding fuel consumption and emission has forced the automotive industry to develop lighter, more fuel-efficient vehicles.

The two main objectives of this industry are the reduction in car weight and improvement in safety. To achieve this, most of the panels that make up the car bodies prefer high strength materials coupled with better formability. The performances of conventional high strength steels are not sufficient. It has been found out that bake hardenable steel sheets are an excellent solution to the above problem. These steels offer good formability (low yield strength for good shape fixability) during press operations and also higher final yield strength during paint baking operations for good dent resistance.

Paint bake hardening is essentially the strain aging increment found after forming and aging for 20 minutes at 180°C. It is commonly assumed in the steel industry that the carbon and nitrogen in solution in the ferrite at the time of paint bake hardening is responsible for the bake hardening strengthening increment observed. However, numerous studies have shown that there is little correlation between the interstitial solute level and the measured paint bake hardening response

It was tried to develop ultra low carbon steel that can provide a consistent BH increment of 100MPa, while retaining good formability. It is to maximize the paint bake hardening increment in ultra low carbon, high strength steel sheets in a consistent and reproducible manner and hence to obtain cost savings in steel plants from improved product yield

The focus was to develop criteria for bake hardening based on the fundamental understanding of the interaction between the strain sources- temper rolling and pre- strain, interstitial character and content, and the bake hardening time-temperature response.

Characterization of the grain boundary distribution, and hence establishing a correlation between the grain boundary hardening, segregation of interstitial solutes and the grain boundary mis-orientation have been established. This will tend to improve our understanding of the nature of the ferrite or final microstructure on the BH response.

The processing condition dependence of the segregation of carbon in low carbon bake hardenable steel, taking account of the variation of the segregation on the individual grain boundaries and to elucidate the relation between the grain boundary segregation and the crystallographic orientation of grain boundaries is also accomplished.

The successful completion of this program will result in large energy savings for steel plants and in the transportation sector.

TABLE OF CONTENTS

LIST OF TABLES

LIST OF FIGURES

PREFACE

There are lots of people who immensely needs to be acknowledged from the core of my heart for helping me in my endeavor. They are as follows:

To GOD, first and foremost, for my life and my existence, without which, I would not have been here to acknowledge others.

To my wonderful parents whose constant support and motivation each and every day helped me where I am today.

To my wonderful wife Antara, who came in later and provided me immense emotional support all the way.

To Dr. DeArdo and Dr. Garcia, for providing me with this wonderful opportunity to work with them and for their intellectual support.

To Dr. Goldman for always making us feel at home, reviewing the thesis and motivating us in any way he can.

To Dr. Mingjian Hua and Peter Wray for providing useful suggestions throughout the research work.

My special thanks goes to all the BAMPRI Graduate students, esp. Mukul Renavikar and Arturo Ruiz Aparicio, for providing help throughout my stay and also for being such great friends.

To Oak Ridge National Lab (ORNL), USS Steel and Dr. Lydia Storajeva from Russia, for providing me access to their experimental equipments like TEM, APFIM, IF (Internal Friction) and Nanoindentor-II, without which it would have been difficult to get some of the results.

To Carolyn Chuha for really helping me with all the long distance workload when I was working in Boston.

Finally, I would like to thank Dr Nettleship for taking time and effort to be in my evaluation committee.

1.0 INTRODUCTION

The threat of future legislation regarding fuel consumption and emission has forced the automotive industry to develop lighter, more fuel-efficient vehicles. At the same time, competition in the market place demands that each car offer more than its competitor. Accessories such as air bags, impact protection, electric windows and air conditioning add considerable weight to the car and this must be balanced by a reduction in weight of the "body in white" if fuel efficiency is to be maintained. The weight reduction is being achieved through close collaboration between the automotive sector and the major steel manufacturers, with the development of, among other measures, higher strength steels. The superior strength of these steels allows them to be used in thinner gauges than existing steel products, reducing the weight of the vehicle while retaining the rigidity of the finished component [1].

The development of new and existing steels is a continual process, as better solutions are sought to the problem of weight saving. Typically, thinner, stronger products are desired, but there is often a trade-off between strength and formability, a problem that can be solved to some extent by the use of bake hardening steels.

1.1 BACKGROUND OF BAKE HARDENABLE STEELS

The primary consumer of sheet steels produced in this country is the automobile industry. Hence, sheet steels must have both excellent formability and high strength.

The two main objectives of the automobile industry are the reduction in car weight and improvement in safety. To achieve this, most of the panels that make up the car bodies prefer higher strength materials coupled with better formability [1-3]. Deterioration of panel stiffness and dent susceptibility is an obstacle to the down gauging. The use of high strength steel makes it possible for

dent resistance of the panel to be kept unchanged even when its gauge is reduced. Researchers have found that bake hardenable steel sheets are an excellent solution to the above problem.

Bake hardenable steel sheets make up a relatively new class of products that have both the above properties. These steels offer good formability (low yield strength for good shape fixability) during press stamping operations and also provide higher final yield strength during paint baking operations for good dent resistance.

This concept was unsuccessfully tried to be put into practice during the 1960's and the 1970's. Because at that time, rimmed steel was mainly used, in which nitrogen could not be controlled. A forming defect of stretcher strain could not be avoided without the control of dissolved elements. After the 1973 oil crisis, the use of high strength steel in car body production accelerated due to the growing demand for fuel-efficient cars. A great deal of research has been carried out on high strength steel [1-3].

The concept of bake hardening has become the center of attraction again. After much research work on manufacturing and application of bake hardenable steel, it has been commercially used since the beginning of the 1980's. The reason its commercial application has been made possible in recent times is that aluminum-killed steel and vacuum degassed steels are available at reasonable cost. The use of aluminum steel can eliminate a forming problem of stretcher strain and dissolved carbon content can be controlled by vacuum degassing or continuous annealing processing. Various improvements were also made in die design and stamping technologies [3].

The success of bake hardenable steel application to outer panels has led to significantly increased usage for all outer "difficult to form" panels. Recently, automotive industries are requiring the bake hardenable steel sheets to reduce the weight of car bodies, and to apply these materials to certain structural parts to improve the crush resistance of the car bodies. As demand for the weight reduction is increasing, researchers are laying more stress on IF steels to develop formable high strength steel sheets [1-4].

1.2 BAKE HARDENABLE HIGH STRENGTH STEEL FOR CAR BODIES

In the automotive industry, the complexity of design and manufacturing requirements has constantly increased in the past years. Aspects such as active and passive security are as important as weight, quality and cost. Hence, the design of future cars will be more and more influenced by a material mix to optimize these facets. The amount of steel integrated in auto bodies will depend on developments of new steel grades with improved properties. For exposed panels, key issues are the development of high strength steels with excellent formability, an increase in dent resistance and weight reduction in down-gauging.

Bake hardening steels initially have a low proof stress and good formability, making them suitable for the more complex forming operations encountered during fabrication of outer body parts. During forming and paint baking, the steel will age significantly, resulting in the return of discontinuous yielding accompanied by an increase in the yield strength.

Figure 1.1 illustrates how this strength increase compares with that achieved with a formable IF steel and high strength rephosphorised steel. It can be seen that the use of bake hardening steel can result in both good shape fixabilty and improved dent resistance in the final component [1].

Since the strength increase occurs after the component has been formed, thinner material can be used for components such as fenders, bonnets, boot lids and door outers, resulting in a weight saving of ~7kg per car. Components such as boot lids and bonnets that experience relatively small deformations during forming benefit particularly from the use of a bake hardening steel, as the relatively small strength increase produced by work hardening can be improved with a larger bake hardening increase. Resistance to small dents caused by stones and other debris is also of importance, with parts such as bonnets and outer door skins being the most susceptible. Bake hardening steels can offer superior dent resistance to both static and dynamic denting, compared with other steel grades, because of their increased strength after baking [1-3].

High strength steel now accounts for about 30-40% of the total weight of car bodies.

1.3 BAKE HARDENABILITY TEST

The change of the properties by the thermal treatment of the paint-baking process, especially the increase in yield stress, is now established as the bake hardening effect.

In the processing of the panels during the bake hardening step, the cold rolled steel sheets are given a pre-strain of 2% in the interrupted tensile test. They are then assembled, phosphated and then electro-painted and paint baked several times. The total time for the baking treatment is approximately 20 minutes at 180° C. These steels exhibit a unique property of an increase of yield strength when subjected to the paint-baking step. Therefore, bake hardenability is defined as the difference between the flow stress at 2% tensile strain and the lower yield (or 2% offset) strength after a heat treatment at 180° C for 20 minutes, as shown in Figure 1.2. The bake hardening response measured via this procedure is referred to as the "bake-hardening index", (referred to as BH or BH1) [1-15].

1.4 MECHANISMS OF BAKE HARDENING

The term "aging" generally stands for a time dependent, often undesirable, mutation in the properties of materials and organisms. Concerning low carbon steels, aging results in an increase of yield strength, tensile strength and hardness with a corresponding decrease in ductility and the appearance of discontinuous yielding. The process depends on time and temperature and results from segregation, clustering and precipitation of supersaturated interstitial atoms such as carbon and nitrogen [1-5, 13-16].

The mechanism of bake hardening in low and ultra- low carbon steels is static strain aging as schematically shown in Figure 1.3. Static strain aging is defined as the increase in yield strength and/ or yield point elongation (YPE) that occurs through the interaction of interstitial solute atoms (e.g. C and N) and dislocations generated by plastic deformation. Static strain aging can be harmful, but when controlled carefully, it can be a valuable approach to strengthen the steel.

Bake hardening of steel is "supposed" to be controlled by the same mechanism responsible for strain aging. In this mechanism, solute nitrogen and carbon diffuse and interact with the strain fields of mobile dislocations and hence form atmospheres around them. These atmospheres are known as

Cottrell atmosphere, which has been named after Alan Cottrell, who proposed his famous theory in 1948 [4-5, 16].

These atmospheres would constitute regions in which the elastic strain field of the dislocation was partially relaxed, and hence its energy reduced, so that the solutes would effectively lock the dislocations. Hence they work either to increase the stress required for unlocking and subsequent dislocation movement or immobilize the dislocations. This will either increase the stress required to unlock and move dislocations, or immobilize dislocations and thus require generation of new dislocations for subsequent plastic flow. Either mechanism results in an increase in strength and a return of discontinuous yielding. The latter mechanism is thought to be more likely. This results in the return of discontinuous yielding behavior during the tensile test [1-4, 16-18].

In order for measurable static strain aging to occur, several criteria must be simultaneously met [5, 16-19]:

- The material must contain mobile dislocations (which are usually introduced by cold working, panel forming or by temper rolling of the steel).
- Sufficient concentrations of solute must be present in the ferrite.
- The solute must be mobile at the temperature of aging.
- Dislocation recovery processes must be sufficiently sluggish to avoid significant softening.

While the above mechanisms typically control static strain aging, the bake hardening process may be more accurately characterized as occurring in three or two (the first step is too fast and hence is ignored) steps. The step process mechanism of bake hardening is schematically illustrated in Figure 1.4 [1-5, 14-20].

1.4.1. Snoek Rearrangement or Ordering

This is a short time process. In fact it is too fast to be measured. Snoek rearrangement is a form of local rearrangement or short-range migration of interstitial solute atoms to favored octahedral sites under stress. The activation energy for this process is reported to be 59 $\pm$ 9.6 to 62.4 $\pm$ 2.1 KJ/ moles [5]. It is reported that this stage is complete in about the time required for a single jump between two interstitial sites in the stress field of a dislocation and thus occurs very rapidly at normal paint baking

temperature. This step causes an increase in yield strength, but not the ultimate tensile strength, by pinning the dislocations.

The first stage of strain aging, attributed to Snoek rearrangement of interstitials in the stress field of dislocation, can be described as follows. Initially, there is a random distribution of interstitials in the matrix. After an applied deformation, the interstitials in the stress field of a dislocation attempt to minimize the strain energy in the region of the dislocation by moving from random to minimum energy site positions. Only a minute amount of interstitials takes part in the Snoek rearrangement process and the time required is less than the time required for a normal interstitial jump [4-5, 16-19].

1.4.2. Cottrell Atmosphere Formation

The second and slower stage, which is the formation of Cottrell atmospheres by long-range diffusion of interstitial solutes from outside the strained region, follows $t^{2/3}$ kinetics. It is a form of long-range diffusion of interstitial solute atoms to dislocation cores, which immobilize the dislocation, and results in increase in both the yield strength and ultimate tensile strength. Hence, a solute atmosphere is formed which modify the dislocation stress fields. The consequent decrease in strain energy increases the stress required for subsequent dislocation movement. This movement requires separation of the dislocations from their solute atmospheres under applied stress. The activation energy for the second stage is 87.1 $\pm$ 10 KJ/ mole, in agreement with the activation energy for bulk diffusion of carbon [5].

Cottrell's model (in its original form) of atmosphere formation around dislocations, extended by Harper, only describes the kinetics of the change of carbon content in solution in the bulk due to diffusion of dislocations. The increase in yield stress caused by the formation of carbon atmospheres around dislocations rises with the number of atoms that gather in an atmosphere. But the interaction and the pinning effect decrease with the distance between the dislocation and the carbon atom.

Cottrell also mentioned that the first atoms, which arrive at a dislocation, ought to be more effective in anchoring it than those that arrive later. Thereby, it is obvious that for the later stages of aging, the direct proportionality between the numbers of carbon atoms around a dislocation and the yield stress cannot be valid. Hence, a new equation, considering the back diffusion, needs to be properly formulated [1-30].

1.4.3. Precipitation of Coherent Carbides

The last stage of the bake hardening process is the precipitation of ε-carbides. Carbide particles are nucleated by segregation of solute atoms to the core regions of dislocation, which causes an increase in yield strength and ultimate tensile strength. Hence, with continued solute segregation to dislocation cores, the increased local solute concentration leads to the formation of clusters and then precipitates which can eventually saturate the dislocation sites [1-30].

1.5 DRIVING FORCE FOR PINNING

The driving force for pinning is a reduction in lattice energy. Both impurity atoms and dislocations induce lattice strains in the iron matrix and these strains can be relaxed if the interstitial atoms diffuse to the vicinity of dislocations [1].

Cottrell and Bilby noted that the hydrostatic and shear stresses produced when carbon is introduced to the lattice, could be reduced by atomic diffusion to edge and screw dislocations, leading to the formation of solute "atmospheres" from which the dislocations must be torn before plastic flow can occur. This leads to the characteristic upper yield point seen in aged steels, followed by flow at a lower yield point when new dislocations are generated and can move under a smaller stress. It was suggested that segregation would continue until a state of saturation was reached, at which point the atmosphere could be visualized as a central row of dislocations situated just below the dislocation line, surrounded in the lower-half crystal by a dilute carbon atom distribution of the Maxwell-Boltzmann type [1-5, 13, 16, 21-22].

Once atmosphere formation has occurred, strengthening is associated with the formation of clusters of solute atoms, probably at close intervals along dislocations. Continued aging is then thought to coarsen these clusters, increasing tensile strength and eventually leading to classical precipitation hardening.

The maximum in strength was found to increase with increasing pre-strain. The availability of more nucleation sites on dislocations as the density increases would lead to the formation of smaller

particles, which would be expected to increase the yield strength. This is true initially, after which the observed decrease in strength was attributed to the formation of coherent particles that can more easily be cut by dislocations. Decreasing particle size would then represent less of a barrier to dislocation movement.

1.6 STRAIN AGING DUE TO NITROGEN

Bake hardening is understood to be a kind of strain aging and is caused by dissolved nitrogen and carbon.

When nitrogen is used to produce bake hardening, a forming defect of stretcher strain emerges frequently because of its diffusion coefficient being several times larger than that of carbon at ambient temperature. Nitrogen has a faster diffusion rate (1.34×10^{-16} cm^2 s^{-1}) at room temperature than carbon (2.8×10^{-17} cm^2 s^{-1}), which allows it to diffuse through the ferrite matrix and pin dislocations during storage of the steel at ambient temperatures [1].

Room temperature aging of this kind leads to the formation of stretcher strain markings (Lüder's Bands) when the steel is pressed, resulting in a "streaky" finish, which is not acceptable for exposed automotive applications.

Nitrogen produces larger yield point elongation than carbon when the concentration of dissolved nitrogen is equal to that of dissolved carbon. It is considered that nitrogen has larger pinning force of dislocations than carbon at ambient temperature. Today, bake hardenable steels are produced from aluminum-killed steel, in which nitrogen can be easily precipitated as AlN. It is important to know that nitrogen is more stable in AlN than it is near the core of dislocations, whereas carbon is more stable near the core of a dislocation than it is in Fe_3C. Therefore, the manufacturing method of bake hardenable steels is nothing but the control of dissolved carbon.

The slower diffusion rate of carbon allows the steel to remain at storage temperatures for up to six months without aging. At paint baking temperatures, however the diffusion rate is significantly increased (2.24×10^{-12} cm^2 s^{-1}), increasing the probability of dislocation pinning [1-5, 13-22, 24-30].

1.7 METALLURGICAL FACTORS IN THE MANUFACTURING OF BAKE HARDENABLE STEELS

The main factors of microstructure influencing the hardening effect are the solute carbon content, ferrite grain size and the amount of pre-strain. A discussion of these factors is presented below.

1.7.1 Effect of Solute Carbon on Bake Hardening Steel

The amount of carbon obviously controls the possibility for pinning mobile dislocations. Consequently, with more solute carbon, more dislocations can be pinned and a higher hardening effect can be obtained.

As mentioned earlier, strain aging and subsequently the bake hardening effect, are very sensitive to the amount of dissolved interstitial atoms, primarily carbon and nitrogen. In rimmed steels of the past, the bake hardening phenomenon was mainly due to dissolved nitrogen. Modern automotive steel sheets are aluminum-killed, which means all nitrogen atoms are combined as aluminum nitride. Hence, the bake hardenability in low and ultra low carbon steels is exclusively caused by dissolved carbon. To maximize the strength increase associated with bake hardening, it is necessary to have as much free carbon as possible [1-15, 18-20, 22-30].

However, as the amount of solute increases, the resistance to room temperature aging decreases. Room temperature aging prior to forming is not acceptable for exposed automobile panels because it can result in stretcher strain markings on formed panels. To determine the amount of free carbon that may be used in bake hardenable steel, it is necessary to examine room temperature aging resistance. It is generally considered that if yield point elongation is 0.2% or less in a uniaxial tensile test, stretcher strain problems will not arise during panel forming.

The times and temperatures of room temperature aging depend on the time and temperature at which the steel is stored between production and forming. Resistance to aging at 30°C for 90 days is commonly used as a guideline for the upper limit of room temperature aging.

Figure 1.5 schematically illustrates the effect of free carbon on bake hardenability. It shows that to avoid ambient aging of bake hardenable steels prior to forming, the maximum concentration of

dissolved carbon is to be restricted to about 10 to 25 ppm, which can be achieved by a proper control of chemistry and processing and which may exhibit strength increase up to about 40 or 50MPa [31]. As a part of the present study, the solute carbon concentrations and the corresponding bake hardenability in the experimental bake hardenable steels under different annealing conditions will be measured.

1.7.2 Effect of Grain Size on Bake Hardening Steel

The stable processing of bake hardening steels require proper grain size control as grain boundaries provide low energy sites for interstitial species.

Contradictory information about the effect of ferrite grain size on bake hardenability is reported in the literature. Some authors do not find any correlation between grain sizes and bake hardening. Others found an increase in the bake hardening effect with a decrease in grain sizes [3].

A variation of the grain size influences the distribution of carbon between the grain interior and the grain boundary by changing the number of segregation sites at the grain boundary. With an increase in grain size the grain boundary area decreases and the total amount of carbon that can be stored in the grain boundary decreases compared to that in a fine grain structure. In the case of a fine grain size, interstitials from the grain boundaries can move faster to dislocations in the middle of a grain due to the shorter distances.

Bake hardenability depends on the grain size as well as the concentration of carbon and nitrogen. Figure 1.6 shows the effect of grain size as well as C and N on bake hardenability more clearly. As the concentration of dissolved C becomes very high, the increase in bake hardenability reaches a saturation point. The grain size appears to determine the maximum bake hardenability attainable. The smaller the grain size becomes, the higher the bake hardenability. But a maximum of ~98 MPa of bake hardenability is obtainable because the grain size could be reduced to as small as eleven in grain size number [3, 30-32].

The reason why bake hardenability depends on grain size is not clear, but it is inferred that the influence of dissolved carbon on bake hardenability differs depending on the location of carbon. Different effect of dissolved carbon was reported on the bake hardenability depending on its location,

at grain boundary and inside grains. For a given carbon content, the bake hardenability increases with a decrease in grain size and the dependence on grain size increases with an increase in solute carbon, is schematically shown in Figure 1.7 [31]. While the explanation of this effect is not complete, data suggests that free carbon located near grain boundaries, which is not detectable by internal friction measurements, has a more profound influence on strength than free carbon located within the grain interior.

The effect of ferrite grain refinement on increase of bake hardenability is associated with the location of solute carbon. It is assumed that during cooling, the carbon atoms diffuse to the grain boundaries. Solute carbon positioned at the grain boundaries, so called "hidden" carbon atoms, cannot be detected by internal friction measurement, but it is supposed that this carbon makes a contribution to the BH effect. The smaller the grains are, the more carbon should be in the grain boundaries because of shorter diffusion paths. Thus, although the same overall solute carbon content can be measured, the "contributed" carbon content as well as bake hardenability can be higher in case of fine grains as the "hidden" carbon is more in finer grains [1-5, 26, 30-34].

The characteristic feature of the influence of ferrite grain size can be described by the scheme of Figure 1.8. Ferrite grain size controls the diffusion distance between intragranular solute carbon and the grain boundary area with higher density of mobile dislocations [32].

In the case of low solute carbon, the difference in gain size contributes only a little to the hardening effect because the diffusion distances for carbon atoms (arrows 1) are practically equal for the large and small grains.

For higher solute carbon, the difference in grain size essentially affects hardening. If it is assumed that arrow 1 is the most distance contributed to hardening, in this case only the diffusion distances marked by arrows 2 are significant for a hardening effect. Intragranular solute carbon atoms located in "black" positions in grain bodies of large grains are fairly far from the boundaries (arrow 3 is longer than 1) and do not contribute to the hardening effect [32].

Since bake hardenability is higher in steels with fine grains for the same solute carbon content, the efficacy of solute carbon content has to be higher the finer the grain size. The explanation seems to be not in the activity of carbon located at the grain boundaries, but in the shorter diffusion distances between intragranular solute carbon and the grain boundary area. During straining, grain boundaries are the major sources of mobile dislocations and with a smaller grain size, the intra-granular solute carbon is more readily available to block these mobile dislocations, thus producing a higher BH-effect.

1.7.3 Effect of Temper Rolling and Pre-Strain on Bake Hardening Steel

The amount and type of strain in the steel also has an effect on the bake hardening behavior. Strains introduced into bake hardenable steels come from two sources: temper rolling and tension deforming. These strains produce different dislocation structures and affect bake- hardening behavior differently.

Temper rolling is a necessary step in the production of BH steels because it eliminates the discontinuous yielding behavior of the as- annealed material. The effect of temper rolling on the stress – strain behavior is shown schematically in Figure 1.9. The Lüder's strain is completely eliminated by temper rolling. Due to the small grain size of most bake hardenable steels, relatively high amounts of temper rolling are necessary to eliminate discontinuous yielding. Usually, it has been observed that a TR of 1% completely eliminates discontinuous yielding [31].

Aging of temper- rolled steel is more sluggish than for tension-deformed steel. The reason is the difference in the aging behavior is two fold. First, the dislocation density of the temper- rolled steel is less than that of the tension- deformed material. Therefore, the average distance between dislocations is greater for the temper rolled steel than for the tension deformed steel. Hence, the distance carbon atoms must diffuse to dislocations to promote aging is greater for the temper rolled steels. Second, a strain aging suppression effect peculiar to temper rolling has been observed. TR produces regions of high and low strains in the sheet, as shown in Figure 1.10. The inhomogeneous strain distribution is believed to be the cause of the strain aging suppression effect associated with temper rolling [4, 31].

Hence, to get the maximum benefit of temper rolling and pre- strain, the sample should be pre-strained such that it crosses over the yield point elongation. This is because complications arise if the sample is pre- strained such that it does not overcome the YPE. The regions inside and outside the Lüder's strain undergo different levels of strain and this causes complications in the stress-strain curve after re-loading. The details are yet to be understood.

This factor controls the density of mobile dislocations as well as the dislocation structure (different slip systems and cell substructure). The dislocation density increases with increasing pre-strain and hence a higher pinning potential for solute carbon exists.

After temper rolling (without pre-strain), ferrite grains exhibit a heterogeneous dislocation structure in such a way, that the areas near the grain boundary contain some mobile dislocations but their density decreases sharply with the increasing distance from the boundary. Pre-strain of 2% generates a considerably higher mobile dislocation density but the heterogeneity of dislocation structure remains [31-39].

1.7.4 Effect of Alloying Elements on Bake Hardenability

Bake hardenable IF steels commonly contain small amounts of solid solution strengthening elements, such as P, Si and Mn. A straightforward way to increase the strength in these steels would be to increase the amounts of these solid solution elements. However, each of these elements has characteristics, which limit their additions.

1.7.4.1 Effect of Manganese

Manganese has an affinity for carbon and forms a dipole with carbon. It is, however, not clear whether the Mn-C dipole decreases BH. Dissolving of manganese into cementite accelerates the precipitation of cementites, which reduces dissolved carbon content resulting in lower bake hardenability. The formation of MnC clusters also reduces the amount of carbon available to move to dislocations. Manganese has another disadvantage because it reduces plastic strain ratio.

But on the other hand, proper control of Mn can enhance aging index and bake hardening index. Without Mn, only Ti (C, N) and $Ti_4C_2S_2$ were observed. With Mn at the 1.00-wt-pct levels, MnS and TiS replace $Ti_4C_2S_2$ as the precipitates, which combine with S and C. As a result, less C is combined as $Ti_4C_2S_2$, and more C is available to go into solution and contribute to aging and bake hardening [3, 17-19, 29-30].

1.7.4.2 Effect of Silicon

Silicon enhances the bake hardenability. It repels carbon. Silicon delays the precipitation of cementites because it enhances the activity of carbon around the cementites. Therefore, higher bake hardenability is obtained as silicon content increases. But Si causes higher yield point elongation as compared with its strengthening capability. Silicon is not used for bake hardenable steels as long as the BH steels can be strengthened by other elements [3, 17-19].

However, no more than 0.5% of Si should be added to avoid poor surface quality due to SiO_2 formation.

1.7.4.3 Effect of Phosphorous

Phosphorous increases bake hardening. It is reported that this is due to the fact that P segregates to the grain boundaries, which are favorable sites for C to precipitate. Less C segregating to grain boundaries results in greater intra-granular solute C and therefore greater bake hardenability. A possible contributing factor is that, by adding P, some Ti may be removed through the formation of FeTiP, which is more stable than $Ti_4C_2S_2$ and TiC.

Phosphorous also contributes to the increase in bake hardenability by reducing the grain size. Phosphorous has the advantage that it does not deteriorate the plastic strain ratio. Hence, it is used mainly as the strengthening element of bake hardenable high strength steel of drawing quality [3, 17-19].

Although phosphorous is the most effective solid solution strengthening element, not more than 0.1% phosphorous causes strain induced brittleness and welding problems. With respect to casting higher strength steels, one major concern is the possible appearance of “ghost lines” in the formed part. These lines are traceable to P segregation. As P is added for strength, special casting precautions are needed to insure that the high strength and good bake hardenability are obtained without loss of surface quality. Improved castability of higher strength BH steels is generally desired.

Except for steels with P additions, pickling presents no difficulties. For the P bearing steels, ease of over-pickling can lead to poor cold-rolled and annealed surface.

1.7.4.4 Effect of Boron and Vanadium

Boron is known to enhance the bake hardenability of the ULC steels. Though the reason is still not clear, it can be inferred that boron has an affinity for carbon and exists mainly at grain boundaries. Therefore, it attracts the carbon into the grain boundary, which is considered to be a more effective location for carbon existence in bake hardenability than inside the grain.

Vanadium is a weaker carbide former than Ti or Nb. Hence, it is expected to dissolve easily during annealing and, as a result, increases the amount of solute carbon, thus enhancing the bake hardenability of the steel [3, 17-19].

1.8 HARDENING BEHAVIOR OF BAKE HARDENABLE SHEET STEEL

Dislocations play an important role in a plastic deformation of metals. It is defined as the line defect in the crystalline structure. The deformation proceeds with the nucleation and propagation of dislocations. Work hardening can be explained microscopically as follows. The necessary stress required to move the dislocations increases gradually due to a tangle of dislocations induced by plastic deformation.

On the other hand, C and N in Fe exist as interstitial atoms, which cause a strain field around themselves. Solute C and N diffuse fast in steel and tend to relax the strain energy by moving adjacent to the core of dislocations, which also produces a strong strain field. The immobilized dislocations increase the flow stress when the steel is deformed. This phenomenon is called “strain aging” and the cause of stretcher strain, which is detected as a high yield elongation in a tensile test.

Cottrell assumed that the stress concentration produced by a pile-up in one grain activated dislocation source in the adjacent grain. J.C.M Li’s theory is widely established which considers the grain boundary to be a source of dislocations. Li suggested that the grain-boundary ledges generated dislocations, “pumping” them into the grain. These dislocations act as forests in regions close to the boundary. The dislocations emitted from the grain boundaries undergo cross-slip.

Extensive cross-slip and the generation of dislocation locks will result in a localized layer with high dislocation density. The plastic flow of the grain boundary region attenuates the stress concentration; geometrically necessary dislocations accommodate these stresses [1-6, 40-48].

1.9 GRAIN BOUNDARY CHARACTER DISTRIBUTION (GBCD)

Grain boundaries are characterized by differences in their structure, and as a result, in their properties. This phenomenon is termed the grain boundary character distribution.

The differences in the structure of individual grain boundaries are usually described quantitatively in terms of the distribution of their mis-orientation parameters. The distribution function of the mis-orientation parameters has attracted a great deal of interest since it has been postulated that this parameter controls the diffusivity, especially of interstitial species and other properties of grain boundaries. Experimental studies have shown that their mis-orientation parameters correlate with the strengthening effect of individual grain boundaries [40-52].

1.9.1. The Grain Boundary Mis-orientation Angle

The GB mis-orientation angle is the simplest description of the GB structure. It is the minimum rotation angle, (θ), between the two grains. Using this parameter, grain boundaries are classified the in simplest case as low angle boundaries if $\theta \leq 15°$ and as high angle boundaries if $\theta > 15°$. High angle boundaries are always more sensitive to segregation [40-52].

It is noticed that the degree of segregation increases with increasing tilt angle of the mis-orientation. The main source of the variation was found to be related to the difference of the grain boundary structure. The amount of segregated C appeared to increase with the tilt angle of the grain boundary mis-orientation.

1.10 COMMERCIAL PRODUCTION OF BAKE HARDENABLE STEELS

Bake hardenable steels have entered the main stream of auto production. Several kinds of bake hardenable steels are now in production at the various auto companies like Nippon, Toyota, Ford and Daimler-Chrysler, to name a few [35-36].

Figure 1.11 shows an example of the application of bake hardenable steels to automobile parts at Toyota Motor. Bake hardenable steels account for about 45% of high strength steels at Toyota Motor. High strength steels with tensile strength below 392MPa are largely used in exposed panels moderately drawn such as hoods, doors and trunk lids, and also to inner panels such as cowls, floors and side sills. High strength steels with tensile strength above 392MPa are applied to structural parts such as structural members. These steels with tensile strength above 588MPa are applied to reinforcements such as bumpers and door impact bars [53].

Bake hardenable steels are mainly applied to the exposed panels because of the advantage in reduction of gauge and dent resistance. The other application of bake hardenable steel is for structural members, which need higher resistance against an impact load. Bake hardenable steels are also applied to the structural parts such as members in order to obtain high deformation starting strength [1-12, 51-64].

2.0 STATEMENT OF OBJECTIVES

Paint bake hardening is essentially the strain aging increment found after forming and aging for 20 minutes at 180°C. It is commonly assumed in the steel industry that the carbon and nitrogen in solution in the ferrite at the time of paint bake hardening is responsible for the bake hardening strengthening increment observed. However, numerous studies have shown that there is little correlation between the interstitial solute level and the measured paint bake hardening response. The goal of achieving a large and consistent paint bake hardening is impossible at this time due to lack of a basic understanding of the paint hardening mechanism.

The main purpose of the program is to develop ultra low carbon steel that can provide a consistent BH increment of 100MPa, while retaining good formability. It is to maximize the paint bake hardening increment in ultra low carbon, high strength steel sheets in a consistent and reproducible manner and hence to obtain cost savings in steel plants from improved product yield. This will be accomplished by gaining insights into the mechanisms of flow strength increment, as well as specific factors and processing conditions that influence strain aging via the dislocation content and its overall mobility.

This is important for improving product quality and consistency as well as saving resources and energy, since a higher degree of consistency means fewer rejects, less scrap and re-melting, and fewer failures during the fabrication process. The program will investigate the BH mechanism in ULC steels and use the better understanding of this mechanism to design and process a new generation of bake hardening steels for automotive applications. These new steels will be thoroughly characterized in terms of their microstructures, formability, BH response, and tensile properties to develop a consistent baseline of properties for further improvement.

The focus would also be to develop criteria for bake hardening based on the fundamental understanding of the interaction between the strain sources- temper rolling and pre- strain, interstitial character and content, and the bake hardening time-temperature response. Along with the above, the

program would also try to characterize the grain boundary distribution, and hence to establish a correlation between the grain boundary hardening, segregation of interstitial solutes and the grain boundary mis-orientation. This will tend to improve our understanding of the nature of the ferrite or final microstructure on the BH response.

Another purpose of this research is to study the processing condition dependence of the segregation of carbon in low carbon bake hardenable steel, taking account of the variation of the segregation on the individual grain boundaries and to elucidate the relation between the grain boundary segregation and the crystallographic orientation of grain boundaries.

The successful completion of this program will result in large energy savings for steel plants and in the transportation sector.

3.0 EXPERIMENTAL PROCEDURE

3.1 MATERIALS SELECTION AND PROCESSING

This study used a commercially produced, typical low carbon, batch-annealed, automotive grade sheet steel as well as two sets of laboratory produced ULC sheet steel, respectively. The chemical composition of the commercially produced low carbon steel (phase1) confirmed through spectro-chemical analysis, is shown in Table 3.1. Obtaining bake hardenability depends on having a small amount of solute carbon in the steel. The amount of free carbon in solution in the as-received condition, determined by a spreadsheet program- TOOLBOX II, is schematically shown in Figure 3.1. The level of aluminum is in lot excess of nitrogen to prevent the presence of free nitrogen in the as-annealed condition.

Figure 3.2 illustrates the mill process variations in the steel samples [21]. All sheets were obtained from the same coil after three successive processing steps: batch annealing, temper rolling, and electro-galvanizing. During processing, the sheets were reduced in thickness by approximately 1.0%, resulting in the final sheet thickness of 0.9 mm.

The aim and the actual chemical compositions of the laboratory produced, ultra-low carbon bake hardenable steels (phase2), are shown in Table 3.2._ and Table 3.3 respectively. The steels were designed to have sufficient amounts of solute carbon in solution in the as- received condition, which was again determined by the spreadsheet program- TOOLBOX II. The amount of free carbon in solution in the as-received condition (for both the above compositions), determined by TOOLBOX II, is also mentioned in Table 3.2 and Table 3.3, respectively.

The design also takes into account the difference in the level of carbon in solution, ranging from as insignificant as 0ppm to as high as 120ppm respectively, keeping all the other alloying

elements constant. The steels are Ti-Nb stabilized and have sufficient amounts of Al to eliminate free nitrogen completely from solution.

The major difference in the composition is also the amount of boron and molybdenum added in the six steels; the first 3 being plain ULC with traces of them and the other 3 being multi-phase ULC steels with significant amount of them, respectively.

Cast ingots of the experimentally produced ULC steel were reheated to 1250°C and hot rolled to a final thickness of 0.2" or 5 mm, approximately, on a commercial hot strip mill. The hot rolling was conducted in two stages. The first stage involves reducing the thickness to 1" and allowing the rolled slab to air cool to room temperature. Then the slab is cut into lengths of between 6 and 12" and rolled again, this time properly controlling the temperatures, reductions and cooling rates.

The steel was finish rolled above 920°C and then water sprayed to the coiling temperature of 714°C. In order to avoid complications due to chilling, scaling and decarburization, a practice of finishing at a thickness substantially greater than the final thickness and grinding the surface off, was adopted. Hence the actual final thickness of 0.15" was achieved by sending the 0.2" pieces out for grinding down to 0.15", carefully removing equal amounts from both sides.

The hot bands were then cold rolled to 0.04" (1.0 mm) to obtain the cold reduction ratio of 73 %.

3.2 EXPERIMENTAL TECHNIQUES

3.2.1 Metallographic Analysis

Metallographic analysis of the as-received samples as well as samples from various processing and conditions was performed by sectioning the samples parallel to the rolling axis, and mounting them in bakelite. The samples were then rough polished using standard metallographic abrasive grinding papers ranging from course (180) to fine (600). The final polishing was done using 1.0μm and 0.05μm alumina, respectively. The microstructure was developed for optical analysis by etching with 2% Nital for 8 to 15 seconds, depending on the steel and condition.

Grain size measurements were evaluated with the aid of a computer controlled, image analysis Bio-Quant IV System. The measurement of the equivalent grain diameter was done on at least 200 grains from different areas of the sample.

3.2.2 Electron Back-Scattered Diffraction Analysis (EBSD)/ Scanning Electron Microscopy (SEM)

The EBSD technique is now widely used to collect crystallographic data from surface analysis. It is used in various fields of materials science such as re-crystallization, phase transformation, and deformation mechanisms, to link macroscopic metallurgical and/or mechanical properties with local crystallographic properties. The technique is almost exclusively used in SEM and only scarcely in TEM. The advantages in using SEM are simple specimen preparation and the possibility to study wide areas on the same specimen, giving statistically reliable data sets [65-67].

The EBSD technique along with the SEM was used to obtain the relation between the fraction of the grains and their mis-orientation which would reveal the nature of the ferrite (polygonal, non-polygonal or mixed) or the final microstructure with the Grain Boundary Character Distribution (GBCD) and hence on the bake hardening increment response. The relation between the carbon segregation (from Nano-hardness technique) and the grain mis-orientation would also be revealed.

The sample preparation for EBSD analysis was quite similar to the optical microscopy except for the last stage where the samples are electro-polished. The electro-polish was done using a solution of 90% acetic acid and 10% Perchloric acid at around 36 volts for 2 to 3 seconds. The samples were not mounted when introduced into the Philips XL30 FEG SEM chamber. Spot size of four with an acceleration voltage of 15kV was used, respectively.

3.2.3 Transmission Electron Microscopy (TEM)

TEM microscopy was performed to do the fine detailed analysis of the ferritic microstructure, including the measurement of the dislocation density present in the materials. It was also used to try to reveal the existence of Cottrell Atmospheres or barriers. The foils to be tested were prepared from various annealing conditions and also before and after the bake-hardening test in each condition.

Thin foils were prepared by mechanical thinning until a thickness of 75μm was reached, and 3mm diameter discs were punched out of it, followed by twin jet polishing at room temperature with an electrolytic solution of 85% acetic acid and 15% perchloric acid at 25 volts and 50mA.

Rough grinding to 0.38mm was done from where the samples were chemically thinned to 0.125mm by immersing in a solution containing 50ml H_2O, 50ml H_2O_2 (30%) and 7ml HF. Thinning of the samples to a final thickness of 75μm was obtained by immersion of the samples in the second solution comprised of 50ml H_2O, 30ml HNO_3, 15ml HCL and 10ml HF.

Electron microscopy examination of materials was conducted in various TEM instruments. Most of the examination was conducted in a CM-30 Philips electron microscope operated at 300kV, as shown in Figure 3.3 at ORNL (Oak Ridge National Laboratory) [68]. Some of the foil examinations were also done using a JEM- 200CX electron microscope operated at 200kV. Analysis included bright field, dark field, CBED (Convergent Beam Diffraction Pattern) and selected area diffraction studies.

3.2.4 Nano-Hardness Technique

Materials with fine microstructures, such as thin films, nano-crystals, and fine-grained ferritic steels, are of great interest and importance. The fine microstructures can be observed by various means including optical, electron beam and scanning probe microscopy. However, only a few options are available on a sub-micron scale for observing the mechanical properties of microstructures.

The Nano-indentation technique is one such technique that can provide information about local elastic and plastic deformation as a “strength probe”. It has the potential to be the standard testing tool or materials with fine microstructures.

This new technique, capable of measuring the mechanical properties of a small volume of material, is the nano-indentation technique. As the name applies, nano-indentation is an indentation technique, which measures mechanical properties by making indentations on a nanometer scale. Nano-indentation is performed by an instrument such as the Nanoindentor II^{TM}, which continuously records the applied load, P, and the penetration depth of the indenter, h, into the specimen [68-70].

A schematic drawing of the Nanoindentor II^{TM} at Oak Ridge National Laboratory (ORNL) is shown in Figure 3.4. It consists of an indenter shaft with a diamond indenter mounted at a bottom and a loading coil at the top. The loading coil consists of a copper wire wrapped around a hollow cylinder. A permanent magnet is attached to the casting of the indenter head. The loading force is controlled by adjusting the amount of dc current to the load coil. The normal displacement of the indent is measured by a capacitance gage.

The Nanoindenter II^{TM} load and displacement resolutions are $\pm$ 75nN and $\pm$ 0.04nm respectively. The indenter shaft is supported by 2 leaf springs, one located at the top and the other at the bottom of the shaft. Specimens are mounted on an x-y-z motorized table, which has an x and y positioning resolution of less than 1μm. The ability to accurately position indentations is one of the most valuable features of the Nanoindenter II^{TM} [68-70].

The measurement of mechanical properties such as hardness, H, and elastic modulus, E, by nano-indentation methods has been conducted largely with indenters having the Berkovich geometry. Of the many sharp indenters, the Berkovich has proven the most useful in nano-indentation work. This is because the three-sided pyramidal geometry of the Berkovich naturally terminates at a point, thus facilitating the grinding of diamonds, which maintain their sharpness to very small scales.

3.2.5 Internal Friction Technique

This technique provides an indirect measurement of the amount of interstitial solutes that are present in the matrix of the material.

Now in bcc α-Fe, we know that the interstitial atoms such as C and N prefer to sit in the octahedral interstices. These sites are located at the centers of the cube edges and at the centers of the cube faces. When a stress is applied in the direction [001], the octahedral interstices expand in that

direction and shrink in size along the other two directions ([100] and [010]). This is because direction [001] becomes the favored interstitial sites. This short-range, stress induced, migration of interstitial atoms is called the Snoek effect. These short-range motions can cause the strain to lag behind the stress, giving an inelastic effect. In these materials, the strain takes time to totally recover on removal of the applied load, and if set into vibration, the vibrations die away or damp out. This damping of vibration is due to internal friction [32, 61, 71].

Snoek peaks of internal friction were measured by the torsion vibration method with the test pieces of 4mm wide and 30mm long, keeping the same sheet thickness of ~1.0mm. These samples were carefully cut, avoiding any heating or distortions of samples that could affect pinning/unpinning of dislocations. The frequency was nearly 1Hz and Q^{-1} was measured between -40 to 100°C. The temperature dependency of internal friction was analyzed by subsequent computer-aided background subtraction and separation of carbon and nitrogen Snoek peaks.

The short range, stress induced migration of interstitial atoms, known as the Snoek effect, can cause the strain to lag behind the stress, giving an inelastic effect. In these materials, the strain takes time to totally recover on removal of the applied load, and if set into vibration, the vibrations die away or damp out. This damping of vibration is due to internal friction.

The common measures of internal friction are as follows:

$$Q^{-1} = \tan\phi = \ln (A_n / A_{n+1}) / \pi$$

Where,

ϕ = angle by which strain lags behind stress and,

A_n / A_{n+1} = ratio of successive amplitudes

The greater the number of atoms that jump, the larger will be the value of Q^{-1}.The maximum internal friction is attained when the period of application of stress equals the jump rate. Since the Snoek effect is a thermally activated process, there is a temperature at which the diffusion jump frequency of the interstitial in the iron lattice is of same order of magnitude as the frequency of applied stress. At lower temperatures, the atoms cannot move rapidly enough for any an-elastic strain to develop in a cycle, and at higher temperatures, the atoms move so rapidly that the inelastic strain develops instantaneously. In both cases, no stress-strain lag occurs [61].

3.2.6 Micro-Hardness Measurements

Micro-hardness measurements were done on various annealing conditions of the commercially produced low carbon steel to verify the conditions for the elimination of the effect of temper rolling on the steel. Micro-hardness was taken in a Leco micro-hardness tester using a small 20 and 50g load. In general, approximately 6 indents were taken along each thickness line perpendicular to the rolling direction and results of various lines were averaged to get the final results.

3.3 MECHANICAL PROPERTIES EVALUATION

3.3.1 Bake Hardenability Tests

Bake-hardenable high strength steels show a relatively low yield strength and good formability associated with bake-hardenability, which provides a capacity for yield strength improvement after paint baking of approximately 20% of the initial yield strength.

For all experiments with the 2 phase steels, sub-size ASTM tensile specimens as shown in Figure 3.5, were used, the thickness being the final steel sheet thickness of ~1mm. All the samples were machined with the tensile axis parallel to the rolling direction/ deformation axis.

The as- received commercial bake-hardenable low carbon steels (with temper rolling of ~ 1%) were pre- strained to 2% and 5% and then subjected to the BH test as shown below:

0% pre-strain – unload - 180°C/ 20 minutes - ACRT.

0% pre-strain – unload - 180°C/ 30 minutes - ACRT.

0% pre-strain – unload - 180°C/ 60 minutes - ACRT.

2% pre-strain – unload - 180°C/ 20 minutes - ACRT.

2% pre-strain – unload - 180°C/ 30 minutes - ACRT.

2% pre-strain – unload - 180°C/ 60 minutes - ACRT.

5% pre-strain – unload - 180°C/ 20 minutes - ACRT.

5% pre-strain – unload - 180°C/ 30 minutes - ACRT.

5% pre-strain – unload - 180°C/ 60 minutes - ACRT.

After the paint baking step and ACRT (air cool to room temperature), all the samples were reloaded and re-strained until they fractured. Load, extension, stress, strain, and time were collected with a computer based data acquisition system. From the stress-strain data, the yield strengths (YS), ultimate tensile strengths (UTS), yield point elongations (YPE), total elongations (e_t) and Hollomon work hardening exponent (n) were determined. For each of the above conditions, 3 tests were conducted and then the results were averaged.

For the second phase laboratory heats, the samples were pre-strained to 2% and then paint bake-hardened.

3.3.2 Baking Treatment

To simulate the steps during the production of automotive parts, the tensile specimens were pre-strained in a tensile testing machine followed by a subsequent baking treatment in an environmental chamber of 180°C for 20 minutes. Re-straining in tension provides data for a complete stress-strain curve. Figure 1.2, shown earlier, schematically presents the influence of pre-strain and baking treatment on a stress-strain curve. The most common property to describe the bake-hardening behavior is the increase in the lower yield stress, ΔYS, as illustrated in the above figure. In the present investigation, the bake-hardening index was defined as the difference between the flow stress after pre-strain and the lower yield strength after baking [1-20, 66-76].

The baking simulation was carried out in an agitated oil bath. It ensured a good thermal flux and a constant temperature. Regardless of the baking condition, all materials and samples were stored in a freezer prior to testing at approximately -10°C to prevent any room temperature aging occurring in any of the samples. The untested materials were not left outside the freezer for any longer than was necessary for sample preparation, i.e., sample machining at the machine shop.

3.3.3 Pre-Straining and Tensile Test

The strengthening mechanisms of bake hardening induce a strong dependence on the paint-baking conditions and on the dislocation microstructure created by temper-rolling and/ or pre-straining.

After stamping, the strained areas of the steel sheet are hardened and offer more dent resistance than the un-deformed areas. For the BH steels the baking treatment effect is added to the work hardening effect and is especially useful in unstrained areas.

Standard tensile properties (yield strength, tensile strength, % elongation, % reduction in area, n-value) were determined according to ASTM standards, by performing tension tests in a MTS 880 servo-hydraulic machine. Some of the conditions of the commercial low carbon steel were also tested on a screw driven Instron machine at US steel, Monroeville. For all the specimens in both the machines, a constant crosshead velocity of 1.5mm/min (~0.06”/min), a 2 metric ton load cell was used.

Since the data of interest in this study always fall into the initial strain range, extra care was taken to ensure that each sample was properly aligned in the grips prior to the start of each test.

4.0 RESULTS

In this study, a large amount of data has been collected. In order to present and discuss these data in a reasonable and organized fashion, the presentation and the discussion of the results will be divided in two sections. In this section, all of the experimental results will be presented. However, the interpretation of the data will be limited which will be done in detail in the discussion section. Also, the results have been presented in 2 phases, each based on the study of different type of steels; the low carbon commercial bake-hardenable steel and the two sets of laboratory experimental heats.

4.1 PHASE 1: COMMERCIAL LOW CARBON BAKE-HARDENABLE STEEL

Characterization of the as-received microstructure and of the various processing conditions of the same steel, interstitial content and mechanical response was done to develop a consistent baseline of properties for further improvement.

4.1.1 Processing Treatments

The as-received, low carbon steel (CR_AR*)* was processed under different conditions to enhance our understanding of the initial property database. The bake-hardening property is a consequence of strain aging due to interstitial atoms segregation towards dislocations. In the present alloy design of bake-hardening steels, only carbon is in solid solution, since nitrogen is combined with aluminum or titanium. In these conditions, bake-hardening depends strongly on the solute carbon content.

Hence, to maximize the amount of carbon in solution, the as-received steel was given a heat treatment of 715°C for 30 minutes and then ice-water quenched to room temperature as shown in Figure 4.1. The excessive fast cooling rate causes the steel to have insufficient time for precipitation, segregation or even cluster formation and hence maximum amount of the bulk carbon is found to be in solution in the matrix. Henceforth, this condition would be denoted as CR_AR_MAX.

In the second treatment, the as-received steel was taken to 750°C for 10 minutes and then air cooled slowly to room temperature. This processing cycle resulted in removing the temper rolling effect in the as-received steel and hence this condition is labeled as CR_NTR.

The above annealing treatment was confirmed through the micro-hardness measurements as is schematically shown in Figure 4.2. It was noted that there was very insignificant change in the hardness level across the sheet thickness for the CR_NTR condition, unlike the as-received (CR_AR) steel which showed lower hardness at the mid-thickness. The measured hardness values for the non-temper rolling steel showed a fairly low scatter, the maximum Vickers's hardness (VHN) being 138.5 and minimum being 136, respectively. On the other hand, for the temper rolling condition, the fluctuation in VHN was significant, ranging from as low as 135 (at the mid-thickness) to as high as 148 (near the surface).

4.1.2 Mechanical Properties

4.1.2.1 Commercial Steel: CR_AR Condition

The tensile properties of the as-received sheet steel are summarized in Table 4.1. The results shown are based on the average of 3 tests for each condition. As seen in the table, the results also include the standard deviations indicated against each data point. The annealed conditions revealed the round-house curve phenomenon. On the other hand, the annealed and paint baked samples had YPE, the amount of which increased significantly with increase in pre-strain. The bake hardening and the work hardening response of the CR_AR condition are schematically shown in Table 4.2. The comparison of the increment in flow stress (BH0, BH2 and BH5) due to the paint baking treatment, with paint-baking test time at various pre-strains, is shown in Figure 4.3.

The bake hardenability test was conducted at annealing times of 20, 30 and 60 minutes, keeping the test temperature constant at 180°C. For the same condition, the dislocation density and, hence, its mobility, was varied by changing the pre-straining from as low as 0% (no strain increment except initial 1% temper rolling) to as high as 5% (maximum strain increment). The results, as clearly seen in Figure 4.3, indicate that the maximum increment in bake hardenability is at 2% pre-strain and 20 minutes of BH test time.

The variation of bake hardening increment (BH), work hardening increment (WH) and "total strength" increment (WH+BH) with pre-strain at BH time of 20 minutes is schematically shown in Figure 4.4, respectively. The bake hardening increment is seen to be at its maximum at 2% pre-strain and 20 minutes of baking time. On the other hand, the work hardening increment keeps on increasing with increase in pre-strain. The rate of increment in work hardening with pre-strain is seen to be more than the rate of decrease in bake hardening after 2% pre-strain and hence, the total strength increment is seen to be increasing with pre-strain.

4.1.2.2 Commercial Steel: CR_AR_MAX Condition

In the same fashion, as for the as-received steel condition, the tensile properties are summarized in Table 4.3. Here also, the results are based on the average of 3 tests for each condition. As seen in the table, the results also include the standard deviations indicated against each data point. The baking response as well as the work hardening response effect is summarized in Table 4.4. The effect of the annealing times with the pre-strain on the paint baking is schematically presented in Figure 4.5. As clearly seen in the above figure, the maximum bake hardening increment is seen at 2% pre-strain and 20 minutes of BH test time.

Analogous to the as-received condition, the variation of the increase of BH, WH and total strength after 20 minutes of the BH test, was also studied at various pre-strains, as shown in Figure 4.6. The variations of all the strength increments were shown at the time of maximum optimum bake hardenability, hence 20 minutes was the time chosen. The bake hardening increment is maximum at 2% pre-strain, after which it is seen to be increasing. On the other hand, the work hardening keeps on increasing with pre-strain.

4.1.2.3 Commercial Steel: CR_NTR Condition

The tensile properties of this annealing treatment are shown in Table 4.5. Similarly here also, the average of 3 test data is shown for each condition. As seen in the table, the results also include the standard deviations indicated against each data point.

The baking response as well as the work hardening response effect is summarized in Table 4.6.

The comparison of the increment in flow stress (BH0, BH2 and BH5) with BH test time at various pre-strains is shown in Figure 4.7. Like the previous conditions, it also clearly indicates that the maximum increment in bake hardenability is at 2% pre-strain and 20 minutes of BH test time, though the actual increment varies.

The tests with variations of BH test time and pre-strains in the above 2 conditions clearly showed that the annealing time and pre-strain for "maximum effective" bake hardening increment is 20 minutes and 2%, respectively. To confirm the above, the same tests were carried out for the non-temper rolling condition also (see Figure 4.7 and 4.8).

4.1.3. Optical Analysis

Optical microscopy of the commercial steel under different annealing conditions clearly characterized the steel in all conditions to be essentially purely ferrite. The as-received microstructure (CR_AR) is shown in Figure 4.9. The micrographs of the non-tempered rolled steel (CR_NTR) and the condition of maximum carbon in solution (CR_AR_MAX) are shown in Figure 4.10 and 4.11, respectively.

In general, the structure of the ferrite in all three processing conditions of the same steel chemistry is seen to be essentially polygonal. The nature of the grain boundary is mostly regular, and is comprised of the mixture of high and low angle boundaries, though the fraction of the high angle boundaries increases significantly in the CR_AR_MAX condition. The above is confirmed in the EBSD analysis (shown later) where the relationship between the fraction of the grains and their mis-orientation was analyzed.

The grain size measurements of the polygonal ferrite in all three conditions are shown in Table 4.7, where the diameters of more than 200 grains were recorded and averaged. The results also include

the standard deviations indicated against each grain size. The grain size for the as-received steel (CR_AR) was measured to be 15μm. On the other hand, it was 9.8μm for the CR_AR_MAX condition and 14.5μm for the CR_NTR condition, respectively.

4.1.4. TEM Analysis

TEM microscopy was performed to do the fine detailed analysis of the ferritic microstructure, including the measurement of the dislocation density present in various processing conditions.

The TEM bright field micrographs of the as-received (CR_AR) condition are shown in Figure 4.12. The dislocation density is seen to be rather strongly heterogeneous with both long, single dislocations as well as tangles seen in the matrix, though the density of the tangles increases in and around the grain boundary region. The dislocation density as seen in the above figure, seem to be high due to the fact that the steel was 1% temper- rolled initially.

With the CR_AR_MAX condition, the dislocation density increases both in the matrix and grain boundary leading to the development of a homogeneous dislocation substructure (see Figure 4.13). The tangles seen earlier seem to be more structured, usually in the helical form to minimize the equilibrium core diameter and hence minimize the total core energy.

A subdivision of grains into regions characterized by a relatively homogeneous dislocation density is also observed in the as-received steel with no temper rolling (CR_NTR condition), as shown in Figure 4.14. Such regions are seen to be separated by rather narrow transition (deformation) bands, which may extend in length over a significant part of the grain and may carry a cumulative mis-orientation across them. The dislocation density is seen to be high and fairly homogeneous in nature, both in the boundary region as well as inside the grain.

4.1.5. EBSD/ SEM Analysis

The EBSD technique, along with the SEM, was used to obtain the relation between the fraction of the grains and their mis-orientation, which would explain the Grain Boundary Character Distribution (GBCD) and hence the bake hardening increment response. Many sets of experiments were carried out; the results of only those experiments are shown where the Confidence Index (CI) was not less than 0.8, indicating the very high accuracy of the data.

Figure 4.15 shows the EBSD results of the phase1 steel in the as-received (CR_AR) condition, maximum carbon in solution (CA_AR_MAX) condition and removal of temper rolling effect (CR_NTR) condition. Comparison of the theoretical, random mis-orientation with the actual mis-orientation in the above 3 conditions is also shown there. It is not clearly understood as to why only evidence of high substructure is seen on CR_AR condition though high dislocation density is noticed generally in all the three conditions.

The fraction of the high angle boundaries significantly increase with the condition of maximum carbon in solution. High angle boundaries are more sensitive to segregation which is later confirmed by the relation between the carbon segregation (from Nano-hardness technique) and the grain mis-orientation (from EBSD).

4.1.6. Nano-Hardness Measurements

The variation of hardness across a grain boundary, observed from a sequence of nano-hardness impressions, is a well documented effect. Nano-hardness measurements for all the 3 processing conditions of phase 1 steel were done. Figure 4.16 shows the hardness measurement as a function of the constant depth of indentation for all the indents in the as-received (CR_AR) steel. The sample was not etched at the time of indentation to minimize its effect on the hardness profile. The sample was indented randomly in straight lines at 2 different regions (named position 1 and 2, respectively). The length of the line chosen was significantly larger than the grain diameter such that at least some grain boundaries are traversed as shown in Figure 4.17 (the sample was later slightly etched to reveal the

regions of indent). The hardness profile is generally seen to be pretty uniform in this case (see Figure 4.16).

Two different tests were done for the condition to maximize the carbon in solution (CR_AR_MAX) as this steel revealed significant increase in hardness across some regions (as much as increment of 3.3 GPA) which were later revealed to be near the grain boundary. The indent depth was significantly reduced for accuracy (60 nm as compared to 100 nm in earlier cases). The Nano-hardness data is shown as a function of the depth of indentation in Figures 4.18 and 4.20 (position 1 and 2 respectively as shown in Figure 4.22). There is a clear indication of the increase in hardness across the grain boundary, as seen in Figure 4.18 till Figure 4.21, respectively. The increment is seen to be more in position 2, where the sample was deliberately etched before the test, than position 1.

Position 2 indents were carried out after slight etching to deliberately traverse a grain boundary region unlike the position 1 experiment, which was done on the un-etched sample. To clearly demonstrate the grain boundary hardness increment (being as high as 3.3 GPA), the hardness results are shown as a function of the number of indents, which the hardness variation with the depth of indentation being revealed (see Figure 4.19 and 4.21 for position 1 and 2 results, respectively).

One set of nano-hardness measurement was also carried out for the CR_NTR condition, where the hardness was measured as a function of the constant depth of indentation, as revealed in Figure 4.23. The sample was not etched to minimize its effect on the hardness profile and the position of indent is revealed in Figure 4.24, respectively. It is clearly noticed that there is no significant variation in hardness across the indents (see Figure 4.23) in this steel condition.

The mis-orientations of the grains traversed were later determined by EBSD analysis to examine the correlation of the degree of segregation (reflected through hardness increment) with the mis-orientations.

4.1.7. Internal Friction Measurements

This technique was used to get an indirect measurement of the amount of interstitial solutes that are present in the matrix of the material. Snoek was the first to report that cold worked iron containing C

or N exhibited an internal friction peak near 200°C at a frequency of 0.2Hz. A few years later Koster confirmed these observations and hence the peaks are commonly known as Snoek-Koster peaks (S-K).

The phase 1 steel in all the 3 conditions was sent for the internal friction measurements. Due to the effect of mill processing in the as-received CR_AR steel, i.e., temper rolling and electro galvanizing, there was difficulty in measuring the amount of interstitial elements in solution, as shown in Figure 4.25. The peaks were not at all significant and so the diffused peaks could not be analyzed.

The amount of carbon in solution was found to be very high (80.4 ppm) for the processing cycle with very fast cooling rate to maximize the carbon (CR_AR_MAX) as again the slow cooling of CR_NTR condition (27.9 ppm) done to remove the temper rolling effect from the as-received steel. Figures 4.26 and 4.27 clearly show the above. Since the phase 1 steel is aluminum-killed, the amount of nitrogen in solution in each condition was found to be insignificantly less and almost the same (~1ppm) in each processing conditions.

4.2 PHASE 2: PLAIN CARBON STEELS AND ALLOYED (MO-B) STEELS

4.2.1 Processing Conditions

A more advanced understanding of the role of carbon in the bake hardening increment in ferritic steels was done using 2 sets of laboratory heats; plain carbon, low alloyed steel (mentioned as 24CA in Table 3.2) and Mo-B alloyed steel, brought about by addition of 2000 ppm of molybdenum and

53 ppm boron (mentioned as 25CA in Table 3.3). In each of the above laboratory sets of steels, the heats with maximum bulk carbon were used, keeping the amount of bulk carbon same in both sets. These were then given different annealing treatments to reveal different ferritic conditions (polygonal, non-polygonal and mixed). The processing condition is shown schematically in Figure 4.28 and briefly explained in Table 4.8, respectively.

Both the steels were initially annealed at 820°C for 140 minutes from which it was slowly air cooled to room temperature. The above processing condition (time, temperature and cooling rate) was found to be the most effective in obtaining a fully re-crystallized ferritic structure.

In the second treatment meted out to the above steels, they were heated to 870°C and held there for 30 minutes and then immediately ice-water quenched to room temperature. In the final treatment,

the steels were annealed at 920°C, a little above the AC_3 temperature (AC_3 is 916°C as revealed from the Thermocalc software). After a hold of 30 minutes at that temperature, they were immediately cooled to room temperature by ice-water quenching medium.

4.2.2 Strength Increments

Description of the bake hardening and the work hardening increments at 2% pre-strain for the plain carbon (24CA) steel is shown in Table 4.9 for all the 3 heat treatments mentioned above. The individual contributions of the work hardening and the bake hardening increment along with the total strength increment (WH+BH) at 2% pre-strain for the plain carbon steel is schematically shown in Figure 4.29. It was earlier confirmed from the phase1 commercial steel that maximum optimum increase in the bake hardenability is seen at 2% pre-strain and 20 minutes of paint baking time. Hence, only that combination of BH test time and strain was chosen for the phase 2 steel to reveal the strength increments.

Analogous to the above, the individual strength increments were also determined for the Mo-B steel (25CA) under different heat treatments, as mentioned in Table 4.10 and schematically shown in Figure 4.30.

The results clearly indicate that the increase in bake hardening was significant by just changing the annealing temperature, by increasing it, and by a fast cooling rate. Both the bake hardening and the work hardening component seem to follow the above trend, with the bake hardening ranging from as low as 18 MPA at low annealing temperature of 820°C and air cool to as high as 60 MPA at 920°C and water- ice quench for the plain carbon (24CA) steel. For the Mo-B (25CA) steel, the above ranges from as low as 24 MPA at 820°C to the maximum of 72 MPA at 920°C, respectively.

The bake hardening increment was also found to be more in Mo-B steel (25CA) than in plain carbon steel (24CA), for the same processing condition, with the maximum of 72 MPA for Mo-B steel and 60 MPA for plain carbon steel at the same annealing temperature of 920°C and fast ice- water cooling rate.

4.2.3 Optical Analysis

Optical microscopy of the laboratory heats; plain carbon steel (24CA) and Mo-B steel (25CA); under different annealing treatments clearly revealed the microstructure to be essentially ferrite though the nature of the ferrite varies with the processing conditions.

Figure 4.31 reveals the base microstructure of the plain carbon steels at different annealing conditions. It is well known that the final ferritic microstructure will show morphological characteristics which are dependent on the metallurgical condition of the parent phase (either two-phase or fully austenite) prior to its transformation. In accordance with above, it is known that the nature of the ferrite changes as we anneal from the ferrtic region to the two-phase region and finally to the austenitic region; from fully polygonal ferrite structure to the non-polygonal structure, the mixture of both being in the two-phase region.

It is observed that as the annealing temperature increases traversing the different phases, the percentage of "polygonal", equiaxed ferrite decreases, being supplanted by "jagged"-like grains in the microstructure. Hence, depending on the transformation of low annealing temperature to high annealing temperature and also on cooling rate, the percentage of polygonal ferrite decreases and non-polygonal ferrite increases.

Except for the slight variations in grain size; the same observations are noted when the Mo-B steel is treated under different processes, as revealed in the optical micrographs shown in Figure 4.32. The grain size measurements for both the plain carbon steel and Mo-B steel under different conditions are shown in Table 4.11. The measurements are the mean of the grain diameter measurements of more than 200 grains. The results also include the standard deviations indicated against each grain size. In both the steels, the high annealing temperature and fast cooling rate condition revealed the larger grain size than the intermediate and low annealing temperature (26.1μm and 17.2μm grain sizes for the 25CA and 24CA steel at 920°C and ice- water quench where as 12.2μm and 14.0μm for same steels but at 820°C and air cool).

4.2.4 TEM Analysis

TEM microscopy was performed to do the fine detailed analysis of the ferritic microstructure, including dislocation density present in both the plain carbon (24CA) and Mo-B steel (25CA), under various processing conditions. Each steel type was analyzed in TEM at two different processing treatments, as mentioned in Table 4.8. For each of the processing treatments, TEM foils were analyzed under two experimental conditions. For the first condition, the steel was given a processing heat treatment and then pre-strained. The foils under the second condition were first annealed then pre-strained to 2% and finally given a paint baking treatment at 180°C for 20 minutes.

Figures 4.33 and 4.44 reveal the bright field micrographs of the plain carbon steel in the as-annealed and pre-strained condition as well as in the paint baked condition done after anneal and pre-strain. The micro-structural developments from the "tangled" array of dislocations to cells occur. As observed, with increasing strain, dislocations start to cluster inside individual grains, and these clusters eventually join together to form a cell structure. The tangled network is seen to increase in the as-annealed and pre-strained condition before the paint-baking treatment when the annealing temperature is increased from 870°C to 920°C, as revealed in Figure 4.35. It also shows a decrease in the carbide fraction with increasing annealing temperature. At this temperature, with increasing amount of deformation (after pre-strain and paint baking) the cell walls become more sharply defined and tend to align themselves into certain crystallographic directions, as observed in Figure 4.36.

Similar trend is seen to be followed by the Mo-B steel, except for the basic difference in the dislocation density, which increases sharply as we go from as-annealed and pre-strained condition, to paint-baked condition. Before the baking treatment, the density of dislocations is mostly heterogeneous, being more in the grain boundary region and single, long-straight dislocations sparsely within the matrix, as seen also in Figures 4.37 and 4.39, respectively.

On the other hand, the strained and paint baked foils seem to reveal a very dense homogeneous dislocation density uniformly spread within the boundary and the matrix, as seen in Figures 4.38 and 4.40, respectively. Well defined cell walls are observed after pre-straining in the Mo-B steel annealed at 920°C and also at 870°C, though here, the cell structure is not as much sharp and well defined as that from 920°C treatment (see Figures 4.38 and 4.40, respectively). At 920°C, the cell walls are clear, and the interior of the cells are essentially dislocation free. The average size of the cells seems to have

decreased more than those observed in the plain carbon steels under same annealing conditions, indicating higher dislocation densities.

4.2.5 EBSD/ SEM Analysis

The EBSD technique along with the SEM was used to obtain the relation between the fraction of the grains and their mis-orientation, which would reveal the nature of the ferrite (polygonal, non-polygonal or mixed) or the final microstructure with the Grain Boundary Character Distribution (GBCD) and hence on the bake hardening increment response.

Figure 4.41 and Figure 4.42 show the EBSD results of the plain carbon steel and Mo-B steel as a function of the various annealing treatments, respectively. The actual grain boundary mis-orientations at all the annealing conditions were also compared to the theoretical, random mis-orientation.

In both cases, many sets of experiments were carried out; the results of only those experiments are shown where the Confidence Index (CI) was not less than 0.8 indicating the very high accuracy of the data. High angle boundaries are more sensitive to segregation, which is later confirmed by the relation between the carbon segregation (from Nano-hardness technique) and the grain mis-orientation (from EBSD).

4.2.6 Nano-Hardness Measurements

The purpose of this study was to understand the variation of the interstitial segregation in the Mo-B steel (annealed at 920°C for 30 minutes and then water quenched) on the individual grain boundaries and to elucidate the relation between the grain boundary segregation and the crystallographic orientations of grain boundaries.

Figure 4.43 reveals the hardness measured as a function of the number of indents for varying depths of indentations. The sample was intentionally partially etched to reveal the grain boundaries. A significant increase in hardness is observed around the 4th indent, the increase being as high as 2.1 GPA from the average hardness level. The increment in hardness is more clearly revealed in Figure 4.44, where the hardness is shown to be measured as a function of the constant depth of indentation and is shown for all the indents. The hardness profile for the 4^{th} indent is consistently seen to be above the rest throughout the varying depths of indentations. Later on EBSD analysis was used to reveal the mis-orientation between the grains giving significant hardness variations.

5.0 DISCUSSION

In this section, a discussion of the results obtained in this project is presented in a reasonable and organized fashion. In the earlier section, all of the experimental results were presented. However, the interpretation of the data will be performed in detail in this section.

5.1 EFFECTS OF TENSILE PRE-STRAIN ON THE BAKE HARDENING RESPONSE

The amount and type of strain in the steel also has an effect on the bake hardening behavior. The relationship between the bake hardening responses with the paint-baking time as a function of pre-strain has been shown clearly in Figures 4.3 (as-received, CR_AR), 4.5 (as-received processed to maximize the amount of carbon in solution, CR_AR_MAX) and 4.7 (as-received processed to remove the effect of temper rolling, CR_NTR) of the phase 1 commercial steel respectively. The results of the above have also been summarized in Tables 4.2 (CR_AR), 4.4 (CR_AR_MAX) and 4.6 (CR_NTR), respectively.

It is clearly concluded that, irrespective of the processing treatment, the maximum bake hardening increment is found to be at 20 minutes and 2% pre-strain, though the actual increments may vary. This is best revealed in Figure 5.1, which reveals the comparative results of the BH2 (Bake hardening increment after 2% pre-strain and baking) increments at all the heat treatments.

The Bake hardening index (BHI) is measured as the increase in the flow stress from the pre-strained condition (0%, 2% or 5% in our case) to the “paint-baked” condition at the same strain. The increase in the flow stress due to work hardening (WH) is measured as the maximum strength during the pre-straining step minus the initial yield strength. The total strengthening increment (WH+BH) is

the difference in flow stress between the as-received (i.e., temper-rolled) condition and the pre-strained and paint-baked condition.

The fraction of the bake hardening increment to the total increment (WH2 + BH2) is at its maximum at 2% pre-strain and 20 minutes of baking time.

Several possible explanations for the decreasing bake hardening increment with increasing pre-strain levels in steels have been proposed. Most bake hardenable steels are designed to have an optimal solute content for good bake-hardenability and good aging resistance. Normally aging resistance decreases as the bake hardening potential increases. This is no surprising since both properties are determined by the same mechanism- interstitial diffusion to mobile dislocations. To address this dichotomy, a balance must be struck with the solute content. Too large a solute carbon content can lead to poor aging resistance, and too small a solute content can lead to poor bake-hardening potential.

The rate at which solute atoms move through the iron lattice, depends on both the mobility of the solutes and the driving force for migration (strain aging). Pre-strain serves to increase the driving force for migration.

If a small pre-strain is applied to the material, there is a driving force for strain aging, and the solute atoms will diffuse to the dislocations if given enough time at a certain temperature. As mentioned earlier, the diffusion velocity of carbon increases significantly at the baking time at 180°C, from 2.8 x 10^{-17} cm^2 s^-1, at room temperature to as high as 2.24 x 10^{-12} cm^2 s^{-1} respectively. A number of the mobile dislocations introduced from the pre-straining will, therefore, be effectively pinned by the carbon solutes. If the material is now re-strained, more mobile dislocations must be created to continue plastic flow; thus, the effective flow stress is raised. If the pre-strain is large, the mobile dislocation density will be higher, and the solute carbon may not be enough to pin as many dislocations as in the case of the small pre-strain [58]. Hence, it is seen in our study of all phase 1 steel conditions, that though the "total strength" increases with pre-strain due to the continuous generation of high mobile dislocation density, though at higher strains, the fraction is greatly dominated by the work hardening increment rather than the bake hardening increment.

Thus, the "pining effect", or the BH increment, will not be as strong, even though the driving force for strain aging may be higher. Therefore, it is seen that with the pre-strain, the bake hardening increment initially increases and then decreases steadily as a function of the increasing pre-strain. The BH peak at its maximum is seen around 2% of pre-strain in all conditions respectively.

The tensile properties for all the conditions of the phase 1 steel shown in the Tables 4.1 and 4.3 (for as-received and condition for C maximum in solution) shows that increasing the pre-strain result in an increase in the UTS (ultimate tensile strength). This behavior is believed to be related to the effect that pre-straining has on the work hardening increment. It follows from the definition of work hardening that increasing pre-strain causes an increase in the work hardening capacity of the steel.

Since the WH increment in the as-received, non-tempered, rolled steel (CR_NTR), is negligible, (see Table 4.6), the above effect of increase in UTS is also less, thus confirming the above dictum.

The current interest in the sheet material has emphasized the need of a more accurate understanding of the significance of ductility. This is especially true of elongation, which is the most common and, frequently, the only means used for accessing ductility of sheet materials. Unfortunately, elongation values depend on such geometrical factors as specimen thickness and width in addition gage length and the inherent ductility of the material itself. Normally for convenience, the ASTM standard sheet size specimen [72] is used.

Since all our results are based on the geometries of ASTM subsize E-8 specimens (see Figure 3.5); the actual tensile elongations for the standard ASTM size have also been found for effective comparisons. In brief, under some conditions, it is a good approximation for rectangular bars, which follow this comparison [72]:

$$L_1 / \sqrt{A1} = \quad L_2 / \sqrt{A2}$$

Hence for comparison, a tensile elongation of 52% in our case (ASTM subsize E-8 tensile specimens) reduces to 47% when comparing to a standard ASTM (8” gage length).

The tensile properties revealed in the above tables also show that the total elongation (TE %) decreases with increasing pre-strain (as seen in the tensile properties of all the steel conditions). This behavior was expected because aging at 180°C for 20, 30 or 60 minutes will not eliminate the cold work that the tensile pre-strain put in the steel.

5.2 EFFECTS OF TEMPER ROLLING ON MECHANICAL PROPERTIES AND AGING BEHAVIOR

The examination of the as-received steel (CR_AR) having 1% temper rolling with the other 2 conditions with no temper rolling, especially the CR_NTR condition steel designed specifically to remove its effect, clearly indicates its importance in the final step of steel processing particularly to bake hardening steels.

The yield point elongation (YPE %), shown in the properties of the steels shows that temper rolled steels have insignificant YPE (see Table 4.1) as opposed to non-temper rolled steels (see Table 4.5). YPE occurs when carbon is in solution, the yielding behavior of the steel is discontinuous, i.e., a sharp yield point accompanied by a yield point extension will be seen on the stress-strain curve. Successive micro yielding leads to the formation of Lűder's bands, which manifests as stretcher strain marking in pressed sheets. These markings, once formed, cannot be disguised by painting or other surface treatments and are highly undesirable in exposed applications. Temper rolling can prevent discontinuous yielding by imparting a small strain in the strip. The yield point elongation is exceeded by this strain and further yielding is continuous as seen in Figure 1.9. Over time, interstitial elements will diffuse to the mobile dislocations produced during temper rolling and the yield point will reappear.

Very low YPE in temper-rolled steels is primarily a consequence of the ease with which yielding is nucleated at very many points on the surface of the sheet, generally at the interfaces between the bands of deformed and un-deformed material in the temper rolling pattern. It is suggested that the low yield stress, hence the small Lüder's strain, is principally a strain-rate effect, resulting from the simultaneous operation of very numerous microscopic band fronts during yield propagation. Macroscopic residual stresses are unlikely to exert any important influence once yielding is initiated, but they may play a part in promoting the widespread nucleation of yield [37].

A rolling reduction of about 1% is sufficient to eliminate the sharp yield point. Thus the initial reduction in ductility, directly due to pre-straining, is very small and the potential loss of ductility, due to aging, is also appreciably less than that of a sheet stretched in excess of YPE. A second important advantage of temper rolling is that the sharp yield point returns more slowly during strain aging. Non-

aging steel, considered to be stable at room temperature for three months, can be achieved by temper rolling a bake hardening steel in the range 0.8-1.4%.

Hence temper rolling (also called skin passing) is a process to produce good flatness and low surface roughness in sheet samples in order to achieve a high "glossiness" in the finished product after painting. A small reduction is usually employed to satisfy the above and also not to change the mechanical properties too much [2-4, 15-17, 37].

5.3 EFFECTS OF CARBON IN SOLUTION ON THE BAKE HARDENING RESPONSE

Internal friction is a technique was carried out to provide the measurement of the amount of carbon within the grains (matrix).

The effect of cooling rate from the annealing temperature is clearly noticed in the steel conditions of CR_AR_MAX (water-ice quench from 715°C) and CR_NTR (air cool from 750°C). Figures 4.26 and 4.27 shows the corresponding effect of the cooling rate on the de-convoluted Snoek-Koster peaks shown, indicating that fast cooling rate produced by water quenching results in the greatest carbon Snoek peak height (80.4 ppm), while slow air cooling results in the lowest carbon Snoek peak height (27.9 ppm).

The reduction of the carbon Snoek peak height with slower cooling rate is attributed significantly to the high proportion of solute carbon segregating to the grain boundaries in the as-annealed condition and to a lesser degree to carbide precipitation. On the other hand, in the as-annealed condition of the CR_AR_MAX (measured by internal friction tests), the maximum amount of carbon is in solution due to the fast quenching medium and hence, insufficient time for segregation. This later is involved in segregation to grain boundaries and pinning of dislocations during the paint baking treatment resulting in a much higher pinning and hence a high BH increment.

The above is confirmed from all the tables and figures summarizing the work hardening and bake hardening increments in each condition (Tables 4.1, 4.3 and 4.5 and Figures 4.3, 4.5, 4.7 and later the self explanatory figure of 5.1). The indirect confirmation of the internal friction results is also seen through the yield point elongation results, which are indicative of the amount of carbon in solution. The non-temper rolled steel condition (CR_NTR) has very less YPE (average around 2.1) as

opposed to the high YPE (average around 3.6) noticed in the steel condition having maximum amount of carbon in solution (CR_AR_MAX).

The nitrogen Snoek peaks, as seen in the results of every condition, are found to be insignificant (~2ppm) due to the precipitation of stable aluminum nitrides (AlN).

5.4 ANALYSIS OF NANO-HARDNESS MEASUREMENTS ACROSS GRAIN BOUNDARIES

The detection of hardening from sub-surface boundaries, and the detailed understanding of nano-hardness data which has been demonstrated, indicate that the grain boundary hardening observed in low carbon BH steels is a well established phenomenon, which may well be an important feature in the interpretation of bulk mechanical properties.

5.4.1 Orientation Dependence of the Amount of Segregation

The crystallographic orientations of the grains of both the phase 1 (all conditions- see Figures 4.16-4.24) and phase 2 (alloy steel with maximum BH- see Figures 4.43 and 4.44), were determined by EBSD analysis in order to examine the correlation of the degree of segregation (from nano-hardness results) with the crystallographic orientation of the grain boundary plane or the mis-orientation of two grain boundaries (from EBSD). The relation between the increments in nano-hardness level at the grain boundary region with the mis-orientation of the grains for different steel conditions, is shown in Table 5.1. As observed, there appears to be systematic dependence of the rotation angle on the amount of segregated carbon.

In our study, carbon was found to tend to segregate more on grain boundaries with higher tilt angles, as summarized in Table 5.1. The result showed that the amount of segregated carbon varied among the different grain boundaries to a substantial degree.

The distribution function of the mis-orientation parameters has attracted a great deal of interest since it has been postulated that this parameter controls the diffusivity especially of interstitial species and other properties of grain boundaries. Experimental studies have shown that their mis-orientation parameters correlate with the strengthening effect of individual grain boundaries [40-52].

The main segregation mechanisms by which solute interstitial atoms can reach surfaces or interstitial interfaces like grain boundaries are the equilibrium (Gibbs type) segregation (ES) and non-equilibrium (NES) [74]. Mis-fitting interstitial atoms have their energies reduced by location at regions of bad crystalline arrangement in the solid. These regions are mainly surfaces and grain boundaries. Hence, a monolayer of interstitial carbon might be expected to form if enough solute carbon were present and if sufficient energy (like the paint baking treatment) were fed to the segregating atoms to allow them to reach the boundary.

High angle boundaries, in general, have higher bad crystalline arrangements and hence the higher tendency of segregation is expected as the interstitials can significantly reduce their energy in those high misfit regions. The segregating species is mainly seen to be carbon as the bulk nitrogen has been precipitated in the form of AlN. The fact that only carbon is the segregating species and, hence, in solution, has been confirmed through the internal friction tests earlier described where the Snoek-Koster peak for nitrogen was significantly low. On the other hand, the carbon species was found to be highly in solution, though the amount of which differed with the processing conditions.

NES mechanism relies on the formation of interstitial-vacancy complexes in matrices where there is a substantial matrix-interstitial atom misfit. If the material is subjected to a heat treatment where non-equlibrium condition prevails, i.e., a quench, then the vacancy super-saturation varies in different localized regions of microstructure. The grain boundaries are good vacancy sinks and, therefore, the vacancy concentration becomes rapidly reduced in grain boundaries during quenching. On the other hand, in the grain centers, there is nowhere for the excess vacancies to go and so the grain remains supersaturated with vacancies. This results in a concentration gradient for vacancies between the grain centers and boundaries.

Naturally, the vacancies move down this gradient towards the grain boundary. Some of the vacancies will be complexed with the interstitial atoms; in our case being the interstitial carbon atoms, and these atoms will be dragged towards the boundary with the vacancies. This produces an accumulation of solute carbon in regions within a few nanometers of the grain boundary, indicated through the increase in the grain boundary hardness.

This situation is not in equilibrium and the segregation will die away if the material is re-annealed to give enough energy for the interstitial atoms to diffuse back down the concentration gradients that the NES has produced [74]. Hence it is seen that the grain boundaries are characterized by differences in their structure, and as a result, in their properties.

5.4.2 Accuracy of the Nano-Hardness Measurements

The variation of hardness across a grain boundary, observed from a sequence of nano-hardness impressions, is a well-documented effect.

Indentation hardness can be defined as the resistance of a specimen to the penetration of a non-deformable indenter under the action of a force. It is generally expressed as the ratio of the applied force or load (P) to the total surface area (A) of the impression.

The influence of the microstructure on the load dependence and, in general, on the hardness, can be explained by the mechanism of penetration of the indenter into the material. The basic elements of the penetration mechanism are mobile dislocations and their mean free path. The generation of dislocations at a contact interface can be visualized as arising from a punching mechanism. When an indenter is strongly pressed against the surface of a metal it creates an impression by introducing loops of dislocations.

As the dislocation loops expand from the source, their movement may effectively be impeded by pinning and blocking by lattice defects, such as grain boundaries, vacancies, solute atoms, precipitates and similar imperfections. This is shown schematically in Figure 5.2 where the dislocations generated by the indenter are blocked by the obstacles [46]. Obviously the true mechanism is much more complex, but this rather simplified model can, nevertheless, adequately describe the effects of various lattice imperfections on the indentation hardness [46].

One aspect of the phenomenon which is the cause of some concern, is whether the measured grain boundary hardening is a property of the grain boundaries throughout the bulk of the steel and hence can be understood on the same basis as “normal” hardness, or whether it is really a property of the metallographic surface of the specimen introduced into the surface (near the grain boundaries) during the metallographic preparation or, perhaps, actually an intrinsic surface contribution to the nano-hardness measurement which differs from the grain interior to the vicinity of the grain boundary.

If the observed grain boundary hardening can be interpreted as a "surface" effect, then whilst it still has interest and could be of significance, it would not necessarily have the same significance for the bulk mechanical properties of the steel. On the other hand, if the increased hardness at the grain boundaries, which can be as much as 30% of the grain hardness, is a property of the boundaries throughout the bulk of the specimen, then such inhomogeneity in the specimen would be an important feature to study. Hence, though the "actual" amount of increase in the nano-hardness may vary with the metallographic preparation (e.g., etched samples are found to be softer), the increase at the vicinity of the grain boundary is prominently observed.

Hence, any deviation from the basic form has to be considered as an anomaly, which, in the absence of experimental errors, should be explicable in terms of microstructure. Since the hardening occurring at a grain boundary causes the same distortion of the hardness curves as, say, surface hardening of a material, it is clear that this is a real hardening phenomenon. In other words, material in the boundary is indeed "hard" in the real meaning of the word.

The presence of such internal heterogeneities (or property gradients) in a material should have a significant influence on its bulk mechanical properties.

5.5 MICROSTRUCTURAL ANALYSIS THROUGH TEM

TEM microscopy was performed to do the fine detailed analysis of the ferritic microstructure, including the measurement of the dislocation density present in various processing conditions.

From the TEM bright field micrographs (see Figure 4.12 and 4.13) of the different conditions of phase 1 steel, it is clear that the dislocation density significantly changes as the processing treatments are varied. Evidence of very high homogeneous dislocation structure is observed in the condition when the maximum amount of carbon is in solution (CR_AR_MAX) and the long, straight dislocations seen in the as-received steel condition are absent.

During the as-received condition, the dislocation lines are fairly straight. The dislocation density is rather seen to be strongly heterogeneous with both long, single dislocations as well as tangles seen in the matrix, though the density of the tangles increases in and around the grain boundary

region. The amount of solute carbon in solution is less (as indicated through the internal friction results).

On the other hand, though the dislocation tangles are seen when maximum amount of carbon is in solution, they now tend to be more structured (see Figure 4.13), usually in the helical form. This is clearly understood as follows. The total energy of any dislocation is the sum of the energy stored in the long-range strain field and the energy of the dislocation core. The dislocation structure of minimum energy (the equilibrium core diameter) follows from the condition that the total energy of the long-range strain field (decreasing with growing core size) and the core energy (increasing with growing core size) is a minimum [2, 52, 74, 82].

There is an increase in dislocation density, as noticed, and to accommodate this, mutual trappings of the dislocations into low energy configurations occur. This follows from the LEDS (low energy dislocation structure) concept that particular dislocation microstructure forms, which minimizes energy per unit length of dislocation line, hence the spiral shape of the dislocation in the form of a helix.

When the as-annealed and 2% pre-strained foils for both the plain carbon and alloy phase 2 laboratory heats were paint-baked, it was generally noticed that the microstructural developments from the “tangled” array of dislocations to cells occur. Dislocations start to cluster inside individual grains, and these clusters eventually join together to form a cell structure after the baking treatment.

Most grains are sub-divided into well-defined cells whose walls consist of a tangled network of dislocations. Within each cell, the dislocation density is low. The cell walls become more sharply defined and tend to align themselves in certain crystallographic directions. A complex array of dislocations is seen consisting of two sets of parallel dislocations, which have formed short lengths of dislocations in a third direction at their point of intersection. These dislocation arrays are generally favored over a quasi-uniform three-dimensional distribution since for a given total dislocation density, the dislocation spacing is smaller in the arrays.

This network will probably have them immobile, giving stability to the whole system. Hence, the “pinning effect”, or the bake hardening increment by the interstitial species after their diffusion to these mobile dislocations during the baking treatment, is seen to be very strong (as much as 72MPA is seen in our study).

The micro-structural regions after the baking treatment seem to be very heavily dislocated, resulting in the homogeneous structure with dislocations uniformly distributed in the matrix as well as

within the grains as clearly seen in the micrographs. It was impossible to measure the dislocation density due to the heavy tangles and later cell structures. Before the paint-baking treatment, the density of dislocations is mostly heterogeneous, being more in the vicinity of the grain boundary and long, straight widely spaced dislocations within the matrix. Though evidence of atmospheres is yet to be seen, these dislocation- solute interactions are seen to be the driving force that causes huge bake hardening increments seen in our research.

6.0 CONCLUSIONS

From the results of the present study, the following conclusions can be drawn:

- The relationship between the bake hardening response with the paint baking test time as a function of pre-strain clearly indicates that irrespective of the processing treatment given to low and ultra-low carbon steels, the maximum optimum bake hardening increment is seen when the as-received steels are baked for 20 minutes pre-straining to 2%. The fraction of the bake hardening increment (BH) to the total strength increment (BH+WH) is in its maximum at 2% pre-strain and 20 minutes of baking time when annealed at 180°C.

- A small strain introduced due to temper rolling is a necessary step in the commercial production of bake hardenable steels because it eliminates the discontinuous yielding behavior of the as-annealed steel.

- To maximize the strength increase associated with bake hardening, it is necessary to have as much free carbon in solution before the paint-baking step.

- There appears to be a systematic dependence of the grain boundary mis-orientations on the amount of segregation of carbon. High angle boundaries are noted to be more sensitive to segregation. Carbon tends to segregate more on high angle boundaries.

- The dislocation density significantly increases after the paint-baking treatment under all processing conditions. Cell walls and helical structures are different ways to minimize the energy per unit dislocation line.

- Non-polygonal ferritic grain boundaries are indirectly observed to be more sensitive to segregation and hence, higher bake hardening response than polygonal ferrite.

- The grain boundary hardness is significantly higher than the grain interior when segregation occurs, as much as 30%, though the difference is significantly reduced when no segregation occurs.

.

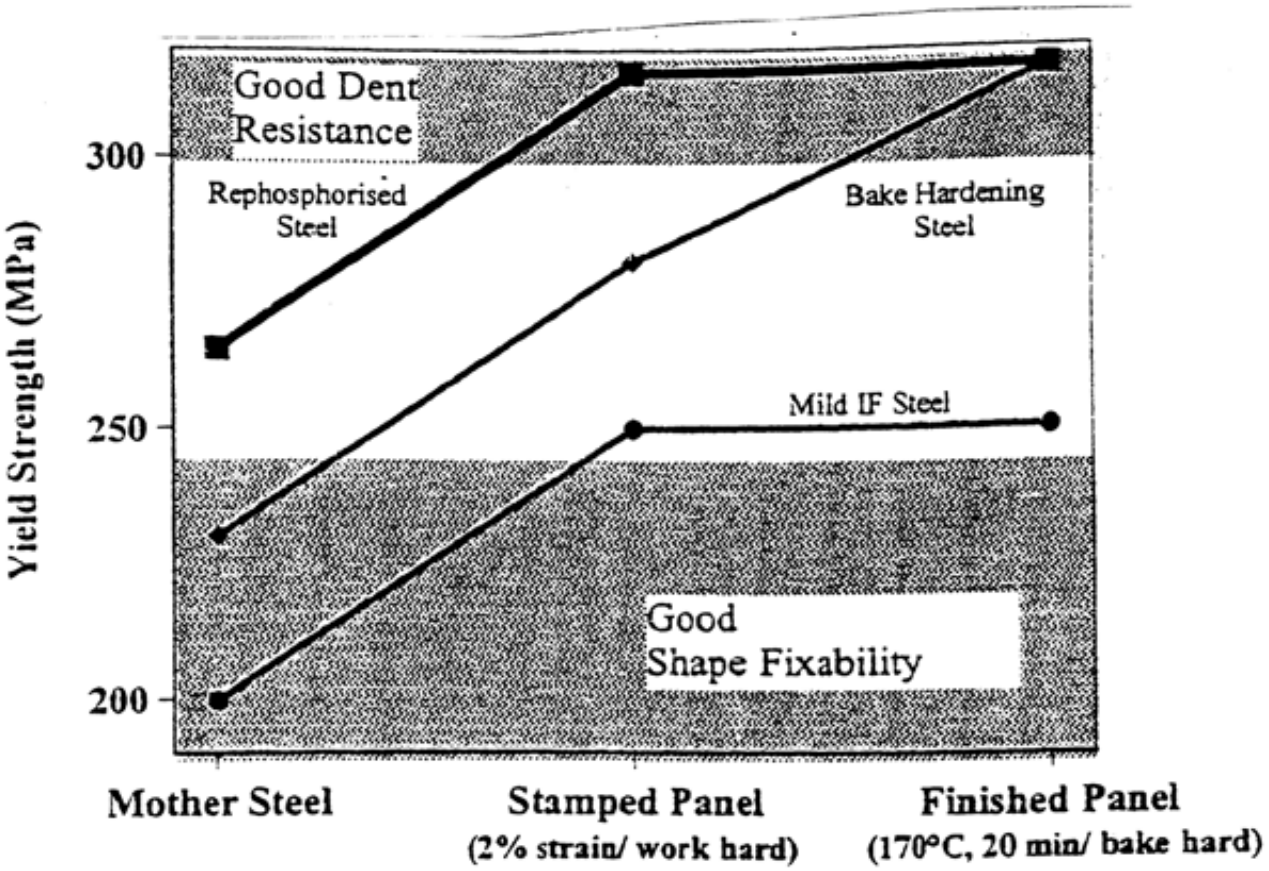

Figure 1. 1 Schematic illustration of the bake hardening concept in fabrication of automotive body parts [1].

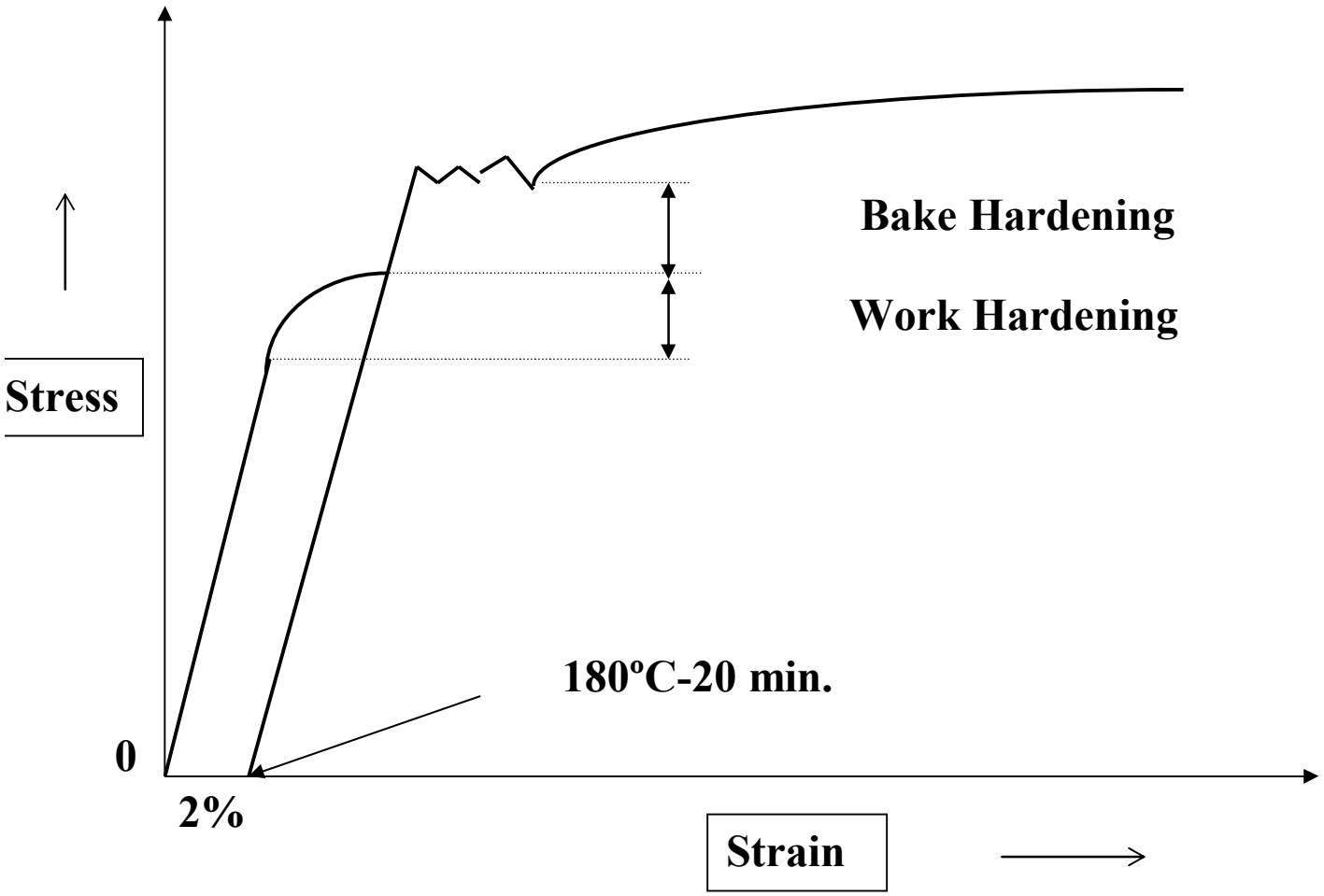

Figure 1. 2 Schematic illustration of the standard bake hardenability test.

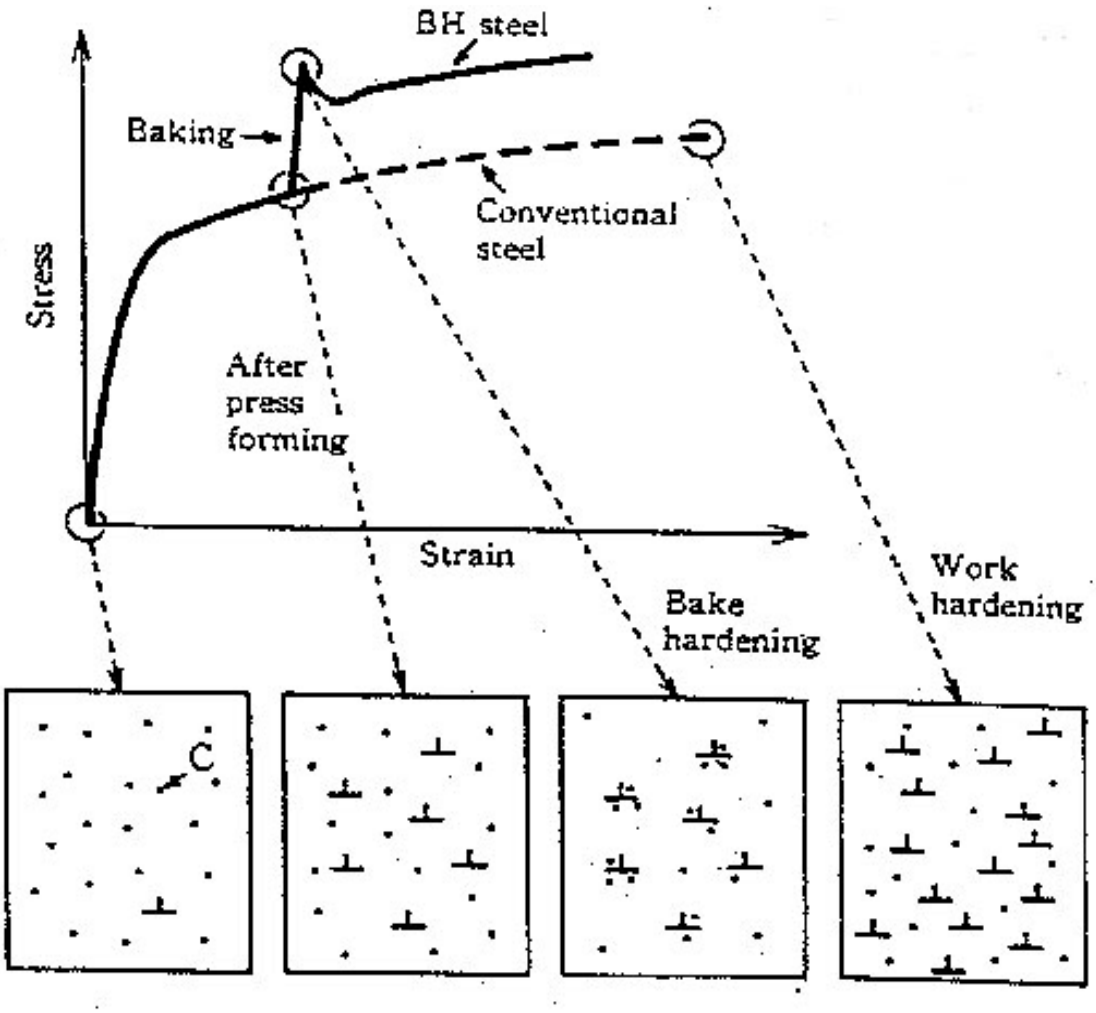

Figure 1. 3 Schematic illustration of the bake hardening mechanism in ULC steels.

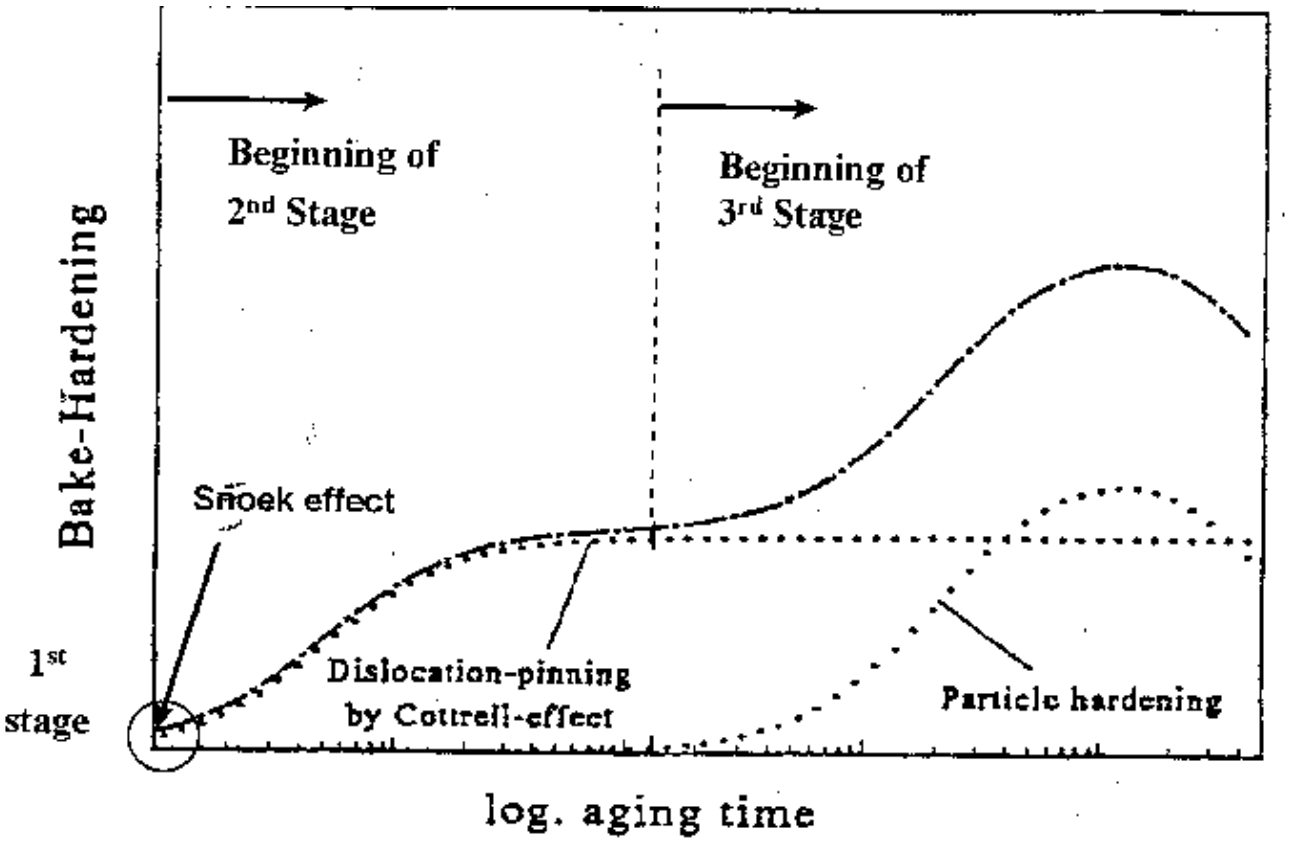

Figure 1. 4 Schematic presentation of the bake hardening mechanisms [5].

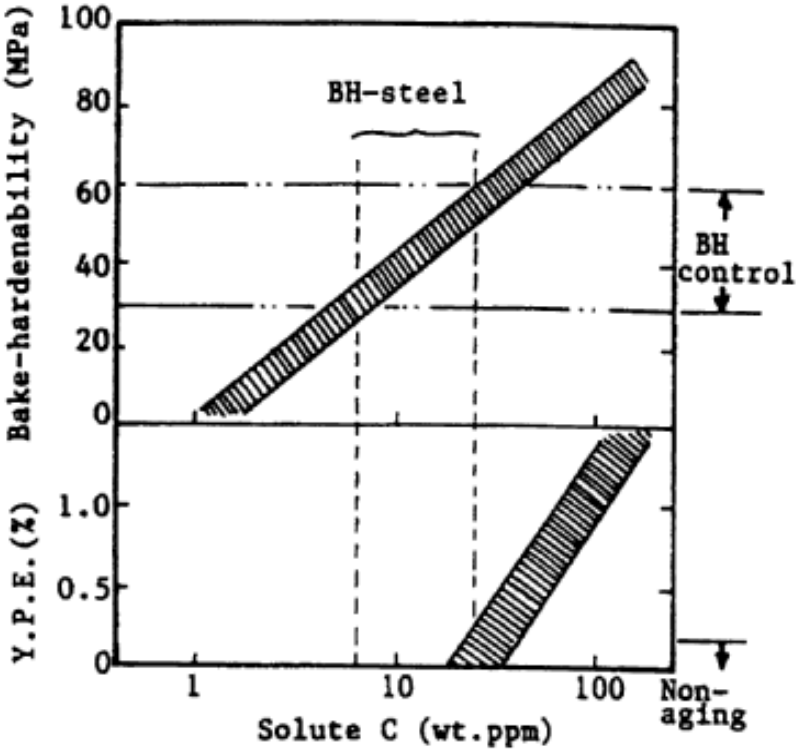

Figure 1. 5 **Bake hardenability and yield point elongation as a function of solute carbon content [31].**

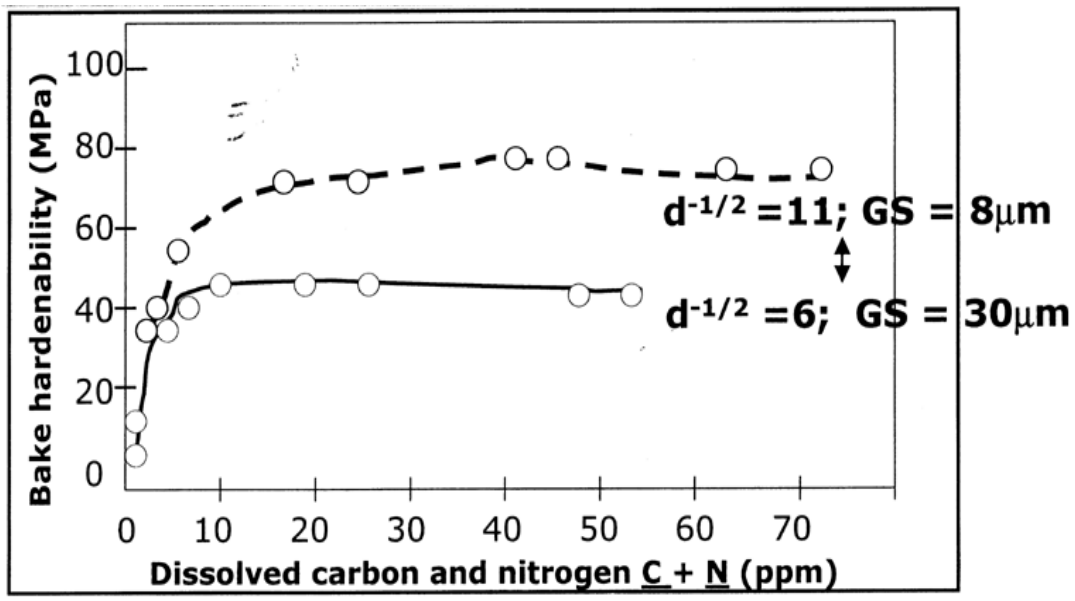

Figure 1. 6 **Bake hardenability as a function of solute carbon and nitrogen content for two different grain sizes [31].**

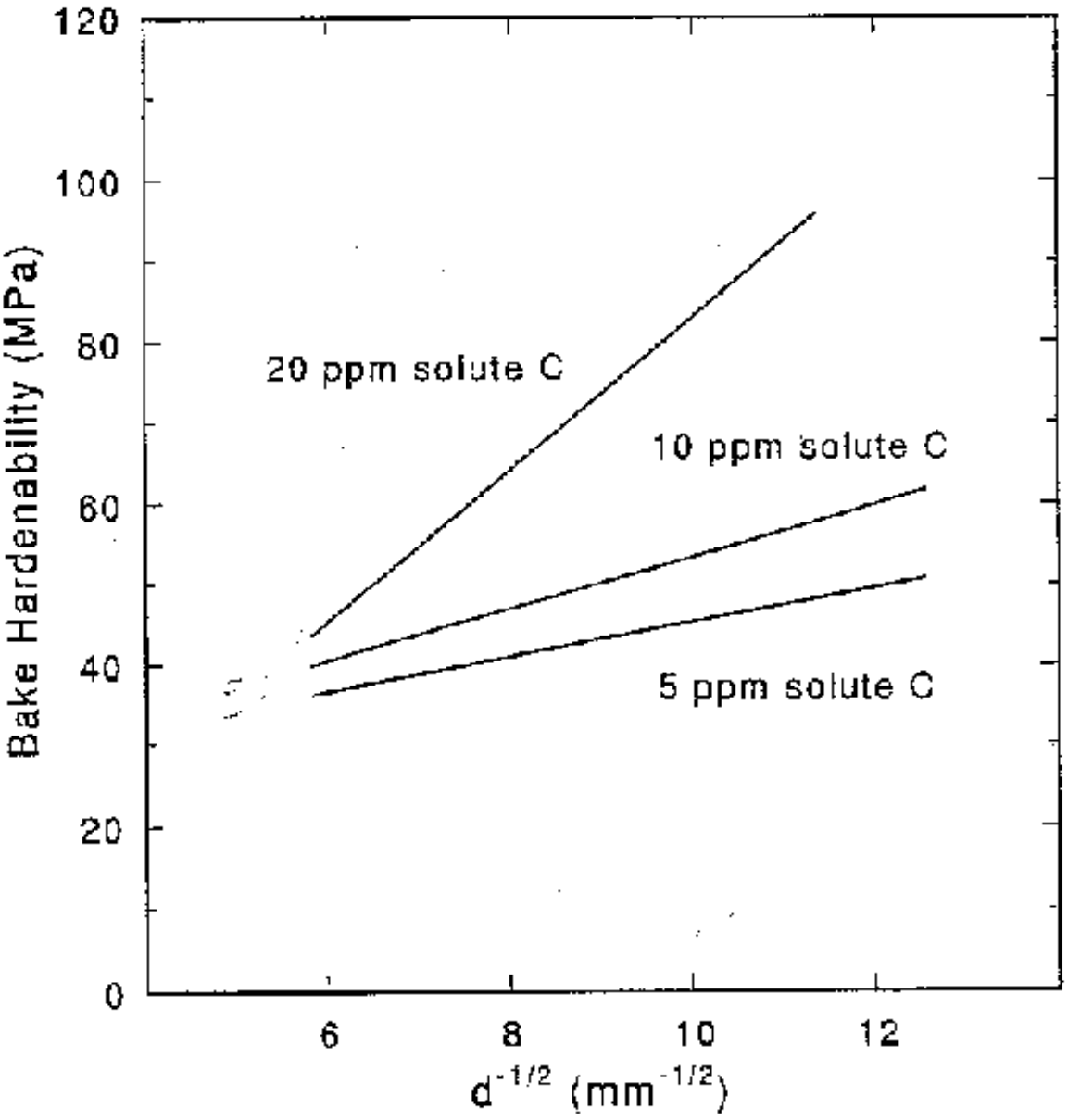

Figure 1. 7 Bake hardenability as a function of grain size for various solute carbon contents [31].

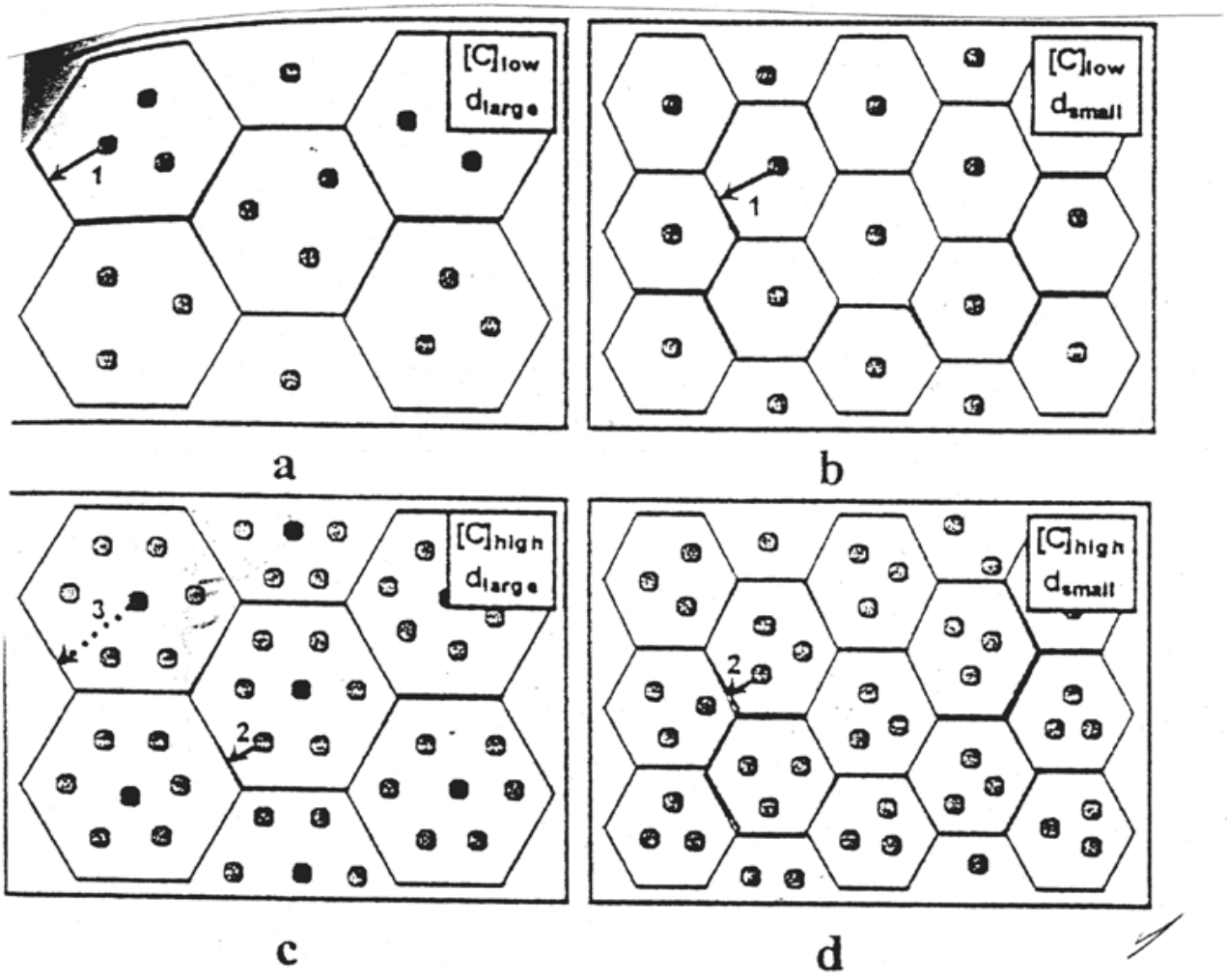

Figure 1. 8 Graphical description of factors influencing the bake hardenability effect [32].

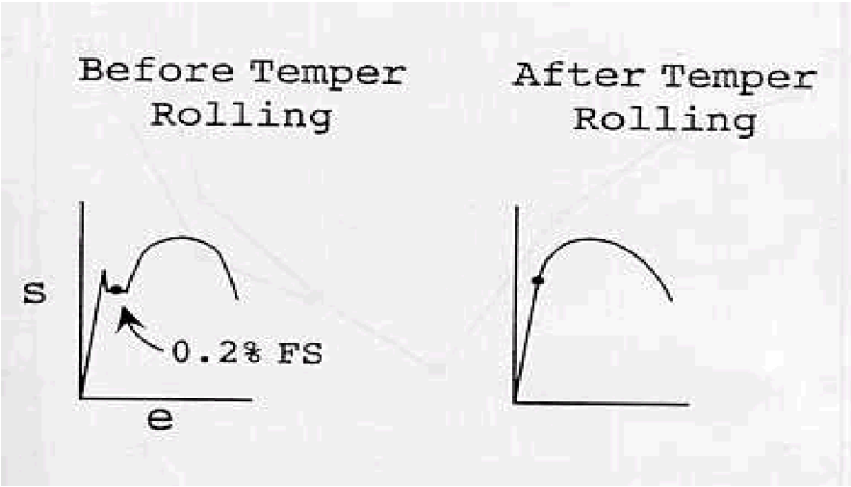

Figure 1. 9 Schematic drawing showing the effect of temper rolling on the stress-strain behavior of bake hardenable steel.

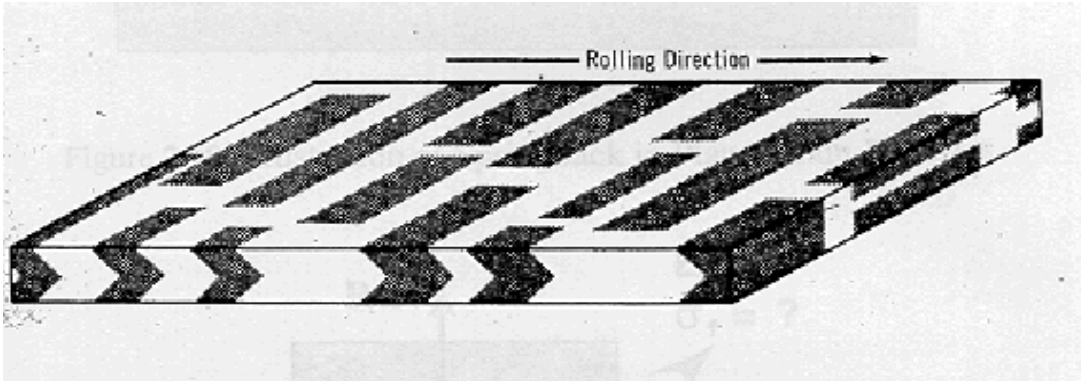

Figure 1. 10 Schematic illustration showing the inhomogeneous strain distribution associated with temper rolling.

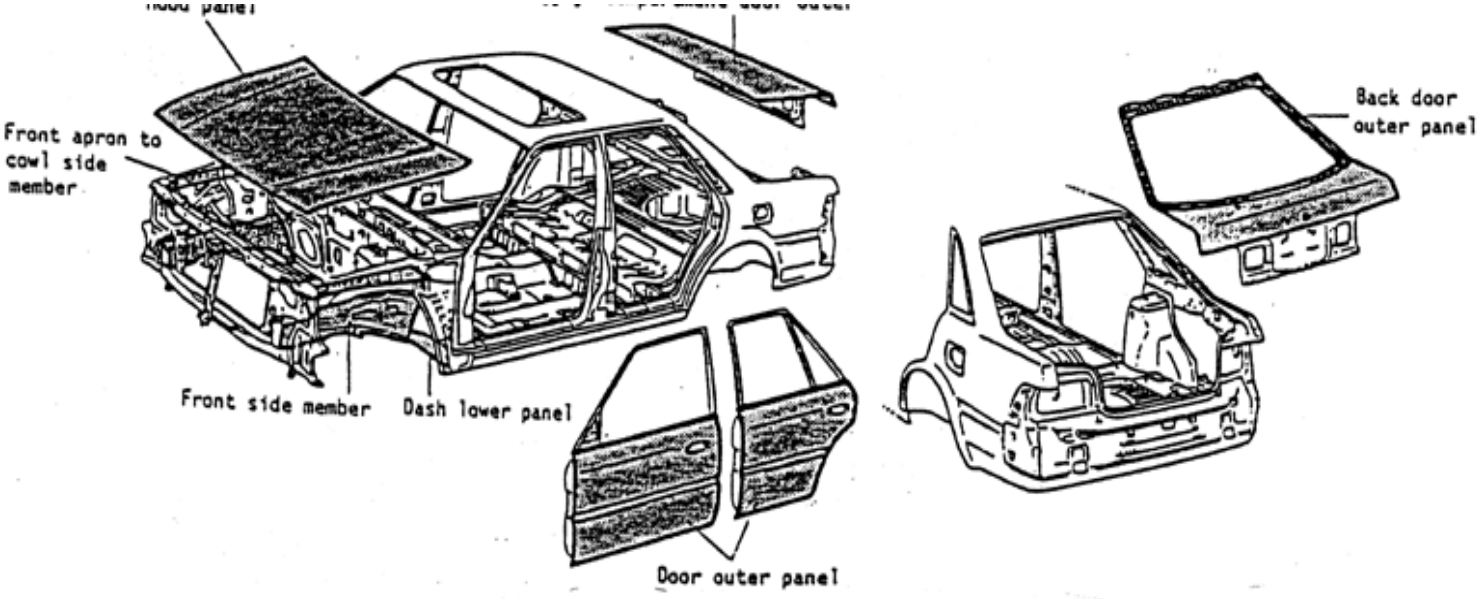

Figure 1. 11 Application of bake hardenable sheets to automotive parts.

Table 1: Chemistry of Steel Entered in Row 1 of the INPUT Table

Final C [ppm]	N [ppm]	S [ppm]	Ti [ppm]	Nb [ppm]	Mn [ppm]	P [ppm]	Si [ppm]	Al [ppm]	B [ppm]
270	50	50	50	0	1700			420	2
		0	0						
			0						

A = total, B = effective, C = equivalent

Table 2: Distribution of Principle Elements

	f x 10^4	Rel. Vol. Frac	M [ppm]	C [ppm]	S [ppm]	Mn [ppm]	Ti [ppm]	Nb [ppm]	
TiN	0.947	1.000	50	-	-	-	50	-	**Partition**
MnS	2.645	2.795			50	86			**Factor**
MC_f	0.000	0.000	0	0	-	-	0	0	-
Solution	-		0	**270**	0	1615	0	0	

III': MC_f + M + Mn Regions IV': III': MC_f + C + Mn

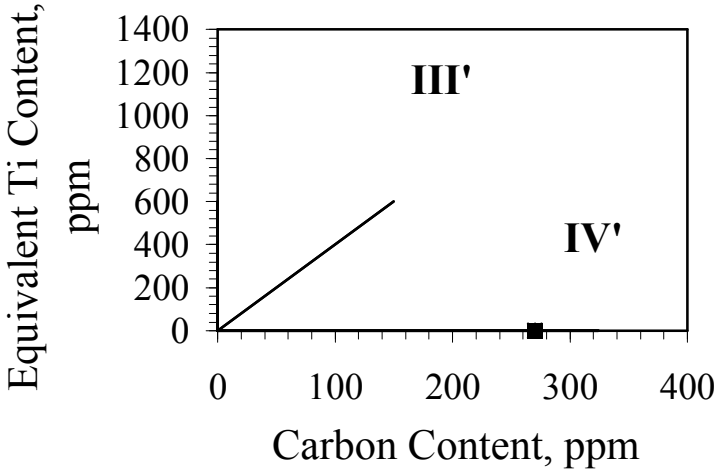

Figure 3. 1 Mass balance of commercial low carbon bake hardenable steel (phase 1: as-received), determined by TOOLBOX II

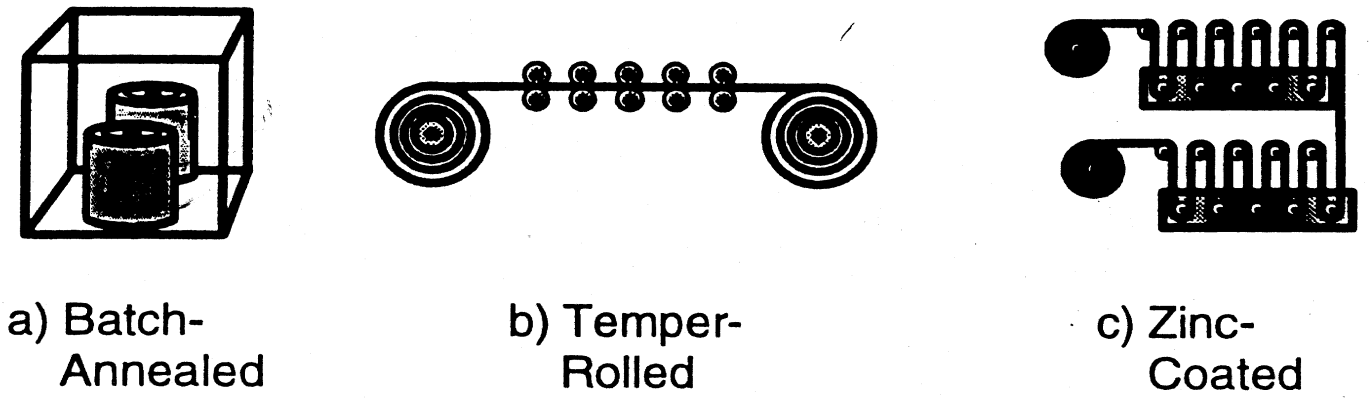

Figure 3. 2 **Mill processing condition of as-received samples, (a) batch-annealed, (b) temper-rolled, and (c) electro-galvanized [21].**

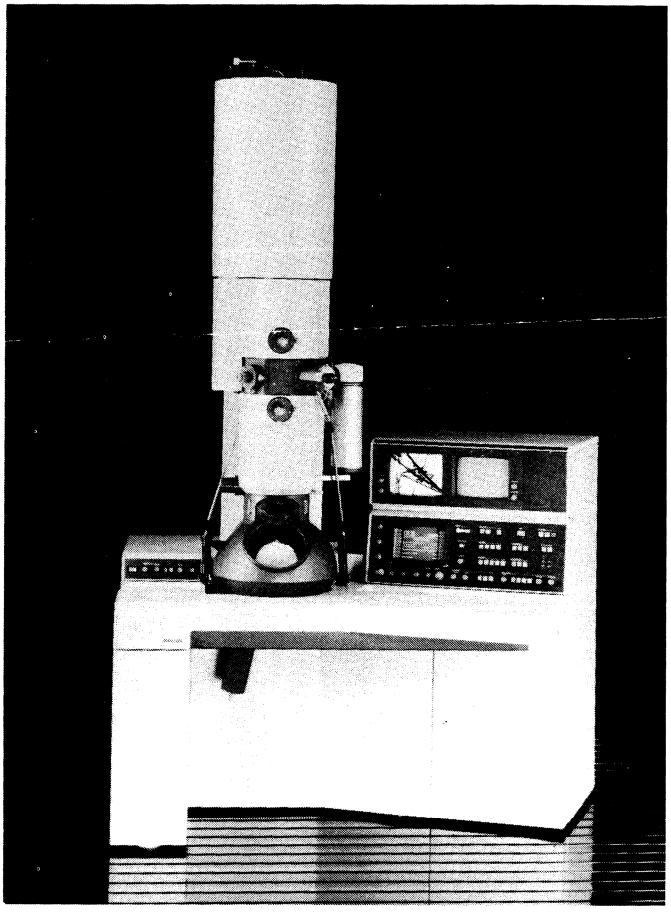

Figure 3. 3 **CM-30 Philips Electron Microscope at ORNL [68].**

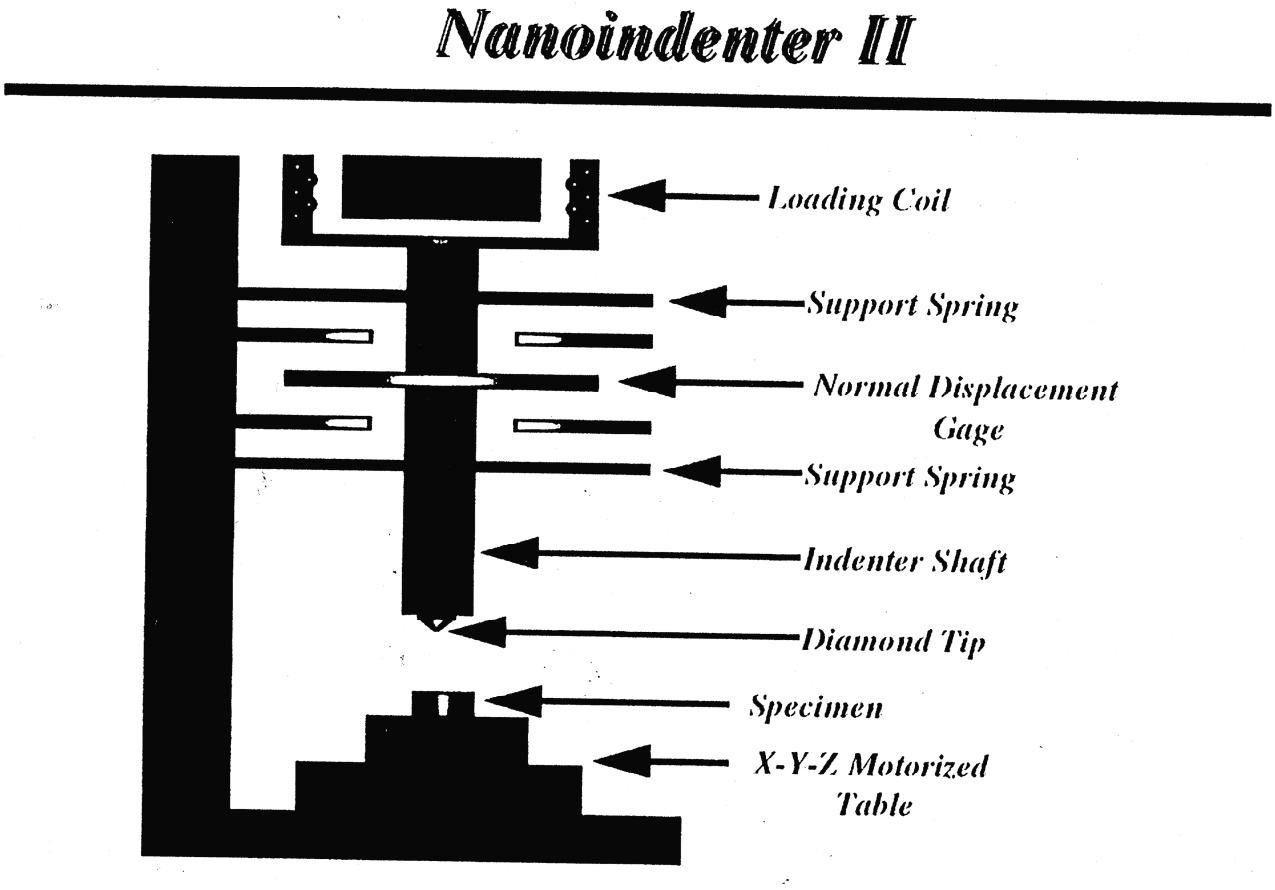

Figure 3. 4 Schematic drawing of a Nanoindenter II [68].

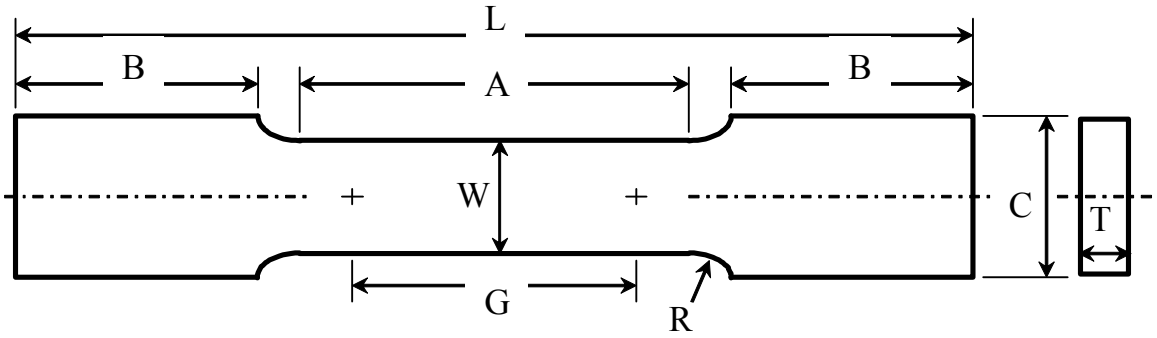

	Gauge length	1.0”
W	Width	0.25”
T	Thickness	Material
R	Radius of fillet	0.25”
L	Overall length	4”
A		1.25”
B	Length grip section	1.25”
C	Width of grip section	0.5”

Figure 3. 5 Geometries of ASTM subsize E-8 specimens used in this study [54].

Table 3. 1 Chemical compositions of the commercial low carbon bake hardenable steel (phase 1). Values given in ppm.

C	S	N	Nb	Ti	Al	B	P	Mn	Mo
270	50	50	-	50	420	-	-	1700	-

C 270ppm

C: Carbon in solution from TOOLBOX II

Table 3. 2 The aim and actual chemical composition of the laboratory produced ULC bake hardenable steels (phase 2: plane C condition referred as 24CA in study). Values given in ppm.

Heat	0102-8124A	0102-8124A	0102-8124B	0102-8124B	0102-8124C	**24CA** 0102-8124C
	Aim	Actual	Aim	Actual	Aim	Actual
C	**30**	**19**	**60**	**53**	**120**	**110**
N	**30**	**46**	**30**	**43**	**30**	**43**
Ti	**150**	**170**	**150**	**140**	**150**	**110**
Nb	**200**	**160**	**200**	**180**	**200**	**190**
Mo	**<150**	**<20**	**<150**	**<20**	**<150**	**<20**
B	**<2**	**<2**	**<2**	**<2**	**<2**	**<2**
Mn	**2000**	**1800**	**2000**	**1900**	**2000**	**2000**
P	80	110	80	110	80	110
S	80	83	80	84	80	82
Si	<150	111	<150	130	<150	380
Al	**420**	**310**	**420**	**200**	**420**	**100**
C	***0***	***0***	***22***	***30***	***82***	***80***

C: Carbon in solution from TOOLBOX II

Table 3. 3 The aim and actual chemical composition of the laboratory produced ULC bake hardenable steels (phase 2: multi-phase condition referred as 25CA in study). Values given in ppm.

Heat	0102-8125A	0102-8125A	0102-8125B	0102-8125B	0102-8125C	**25CA** 0102-8125C
	Aim	Actual	Aim	Actual	Aim	Actual
C	**30**	**17**	**60**	**51**	**120**	**110**
N	**30**	**33**	**30**	**33**	**30**	**31**
Ti	**150**	**190**	**150**	**190**	**150**	**210**
Nb	**200**	**170**	**200**	**180**	**200**	**180**
Mo	**2000**	**2000**	**2000**	**2000**	**2000**	**2000**
B	**50**	**52**	**50**	**51**	**50**	**53**
Mn	**2000**	**2000**	**2000**	**2100**	**2000**	**2100**
P	80	100	80	100	80	100
S	80	81	80	82	80	82
Si	150	180	150	280	150	350
Al	**420**	**530**	**420**	**470**	**420**	**470**
[C]	***0***	***0***	***22***	***9***	***82***	***88***

C: Carbon in solution from TOOLBOX II

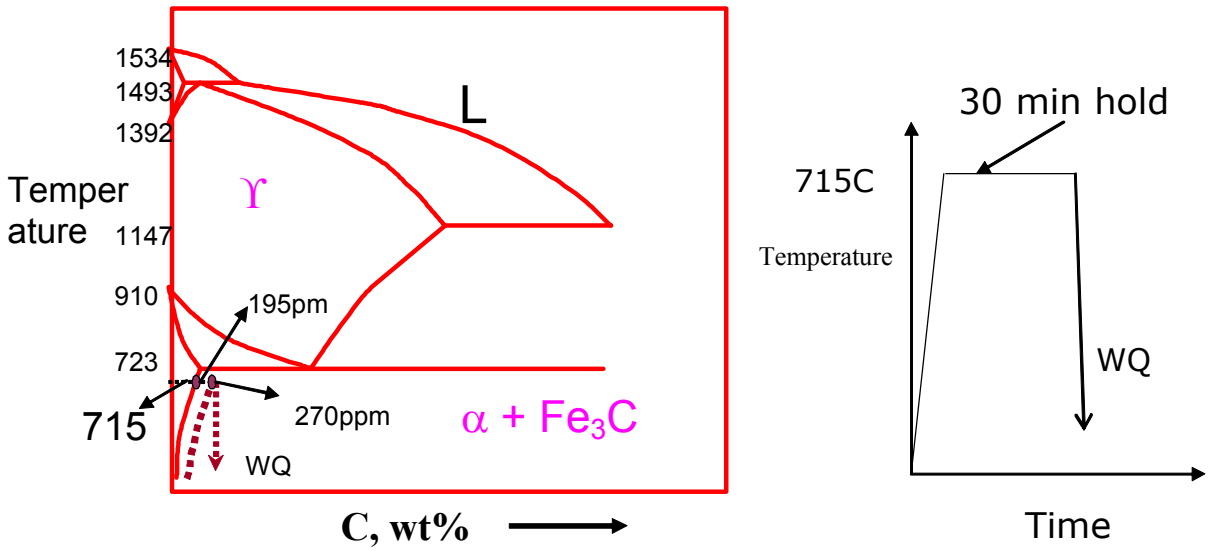

Figure 4. 1 Processing treatment employed to maximize the amount of carbon in the as-received phase 1 steel: CR_AR_MAX condition.

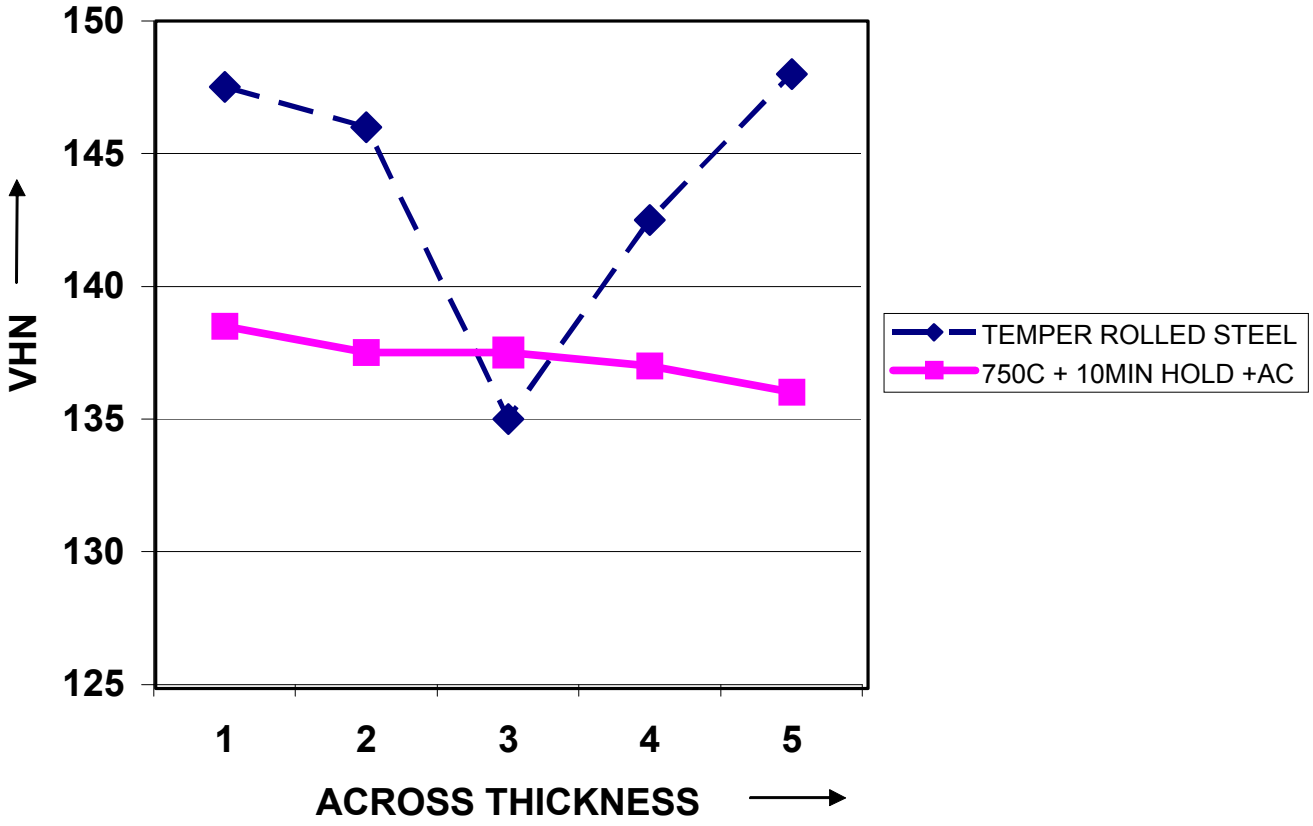

Figure 4. 2 Effect of temper rolling on the micro-hardness measurements in the as-received phase 1 steel: Confirmation of CR_NTR condition.

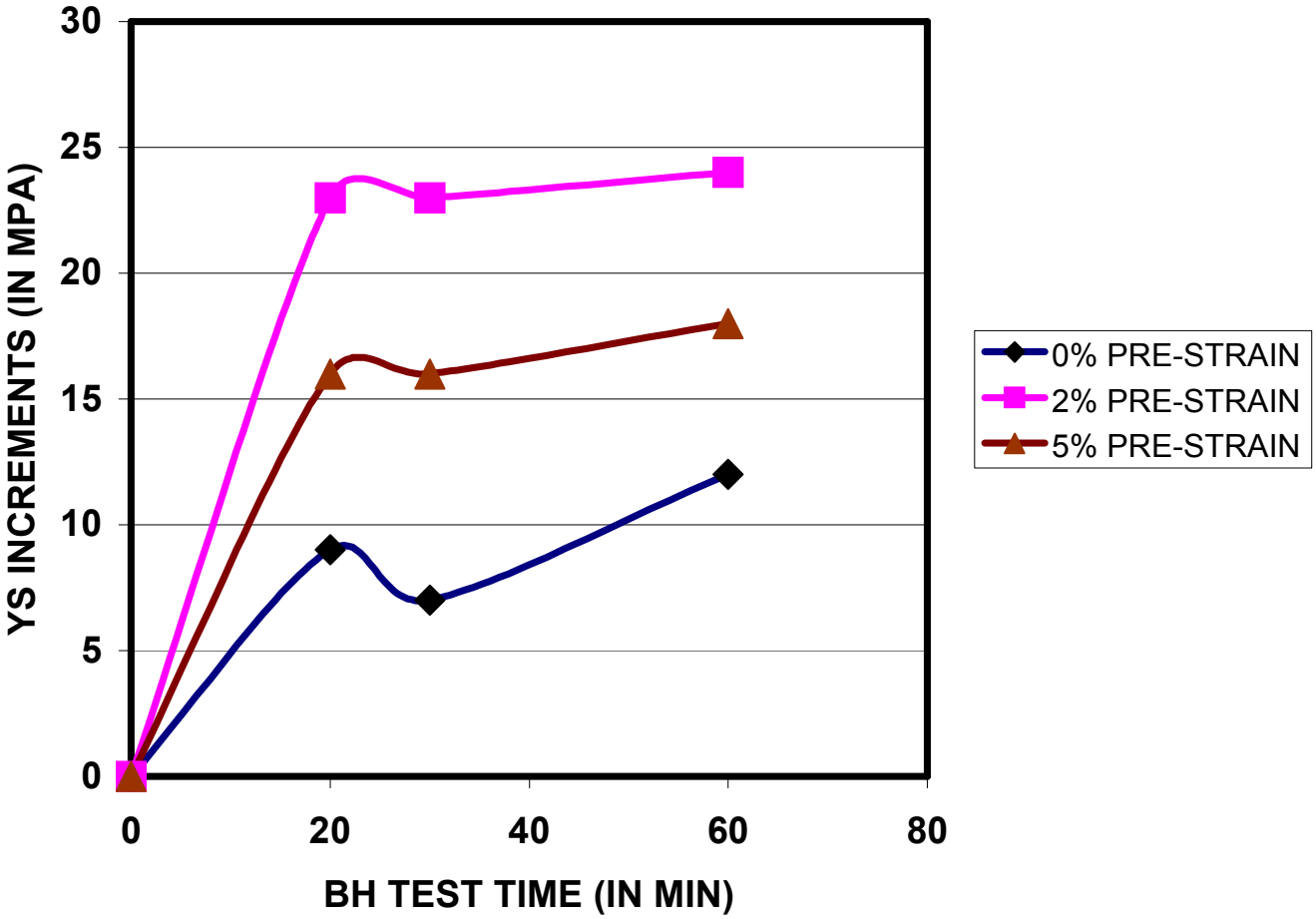

Figure 4. 3 Comparison of strength increments with BH test time at various pre-strains in as-received phase 1 steel: CR_AR condition.

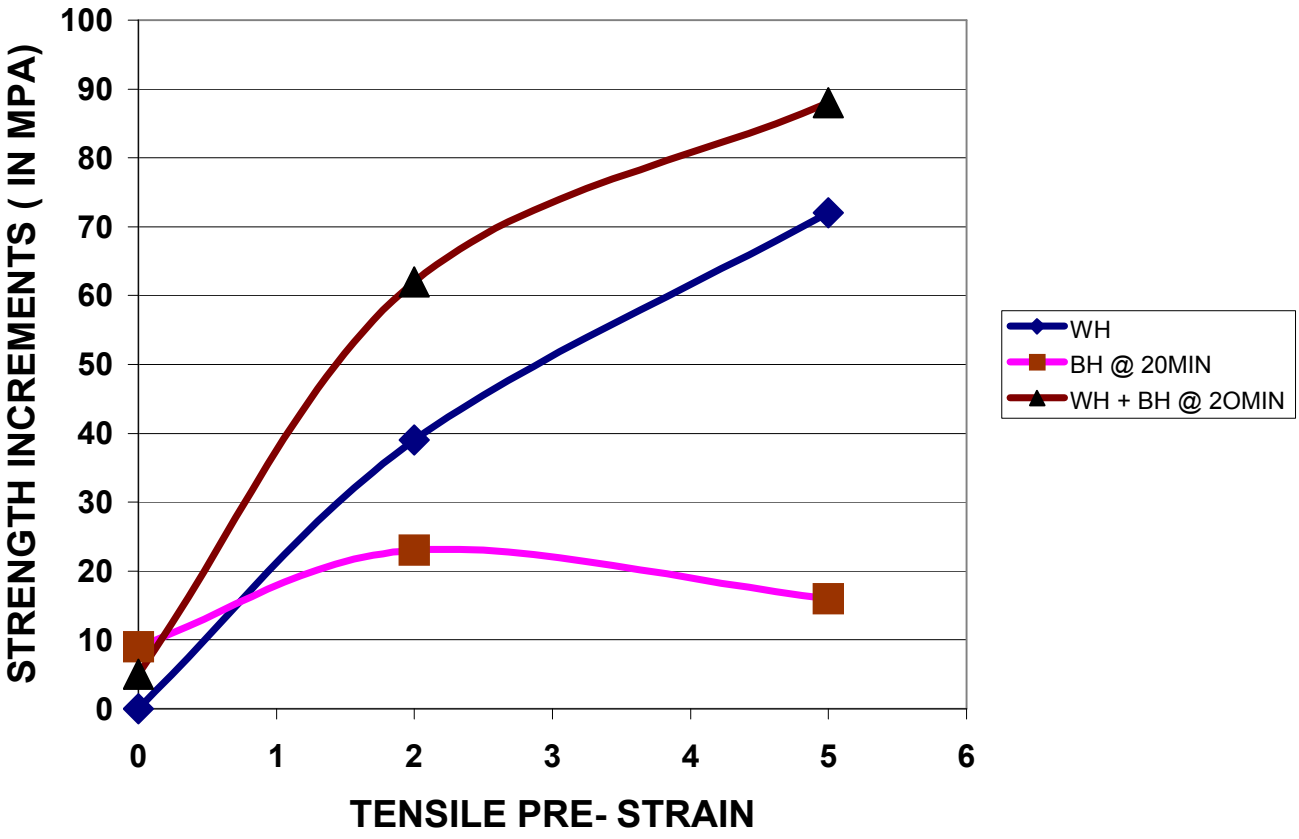

Figure 4. 4 WH, BH and total strength (WH+BH) increments at 20 minutes test time for the phase 1 CR_AR condition steel as a function of pre-strain.

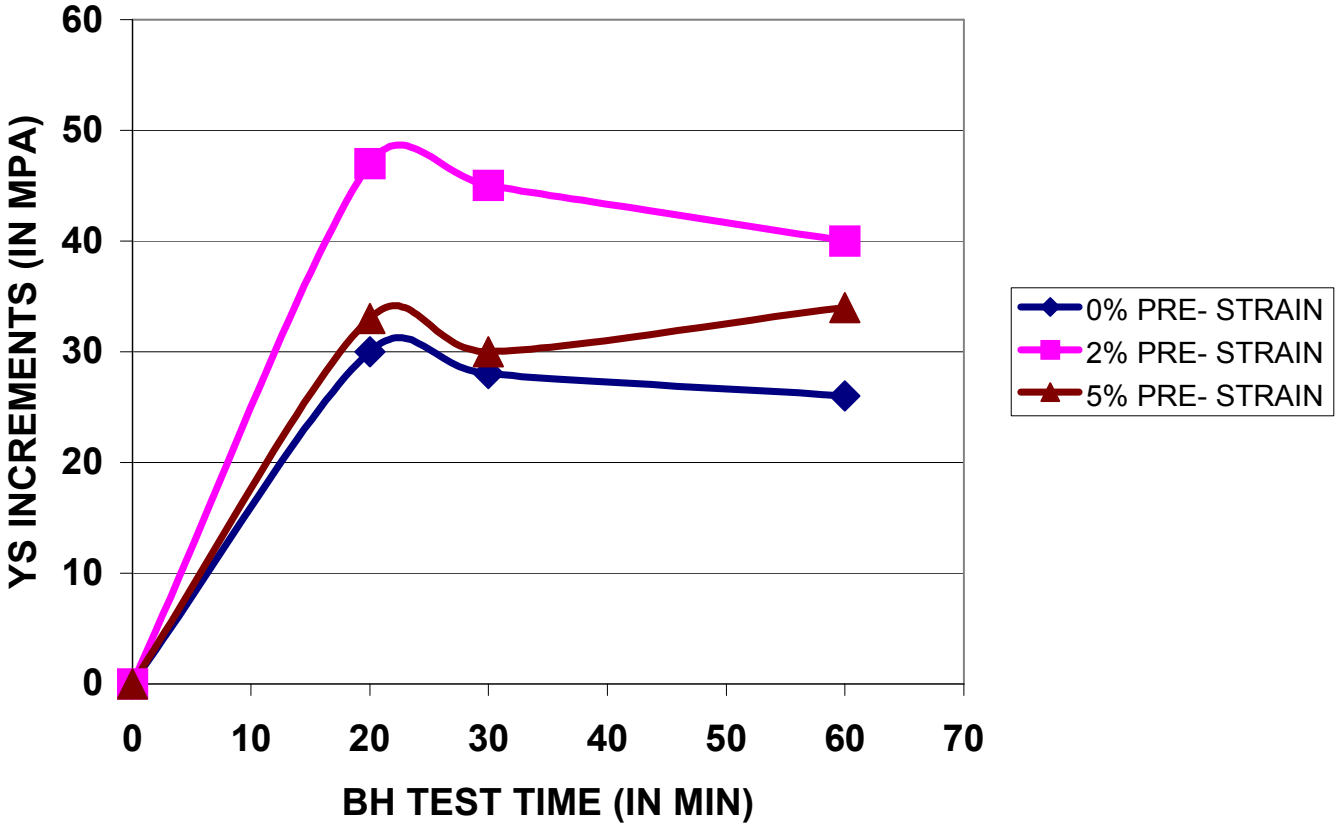

Figure 4. 5 Comparison of strength increments with BH test time at various pre-strains in phase 1 steel after additional heat treatment to maximize C in solution: CR_AR_MAX condition.

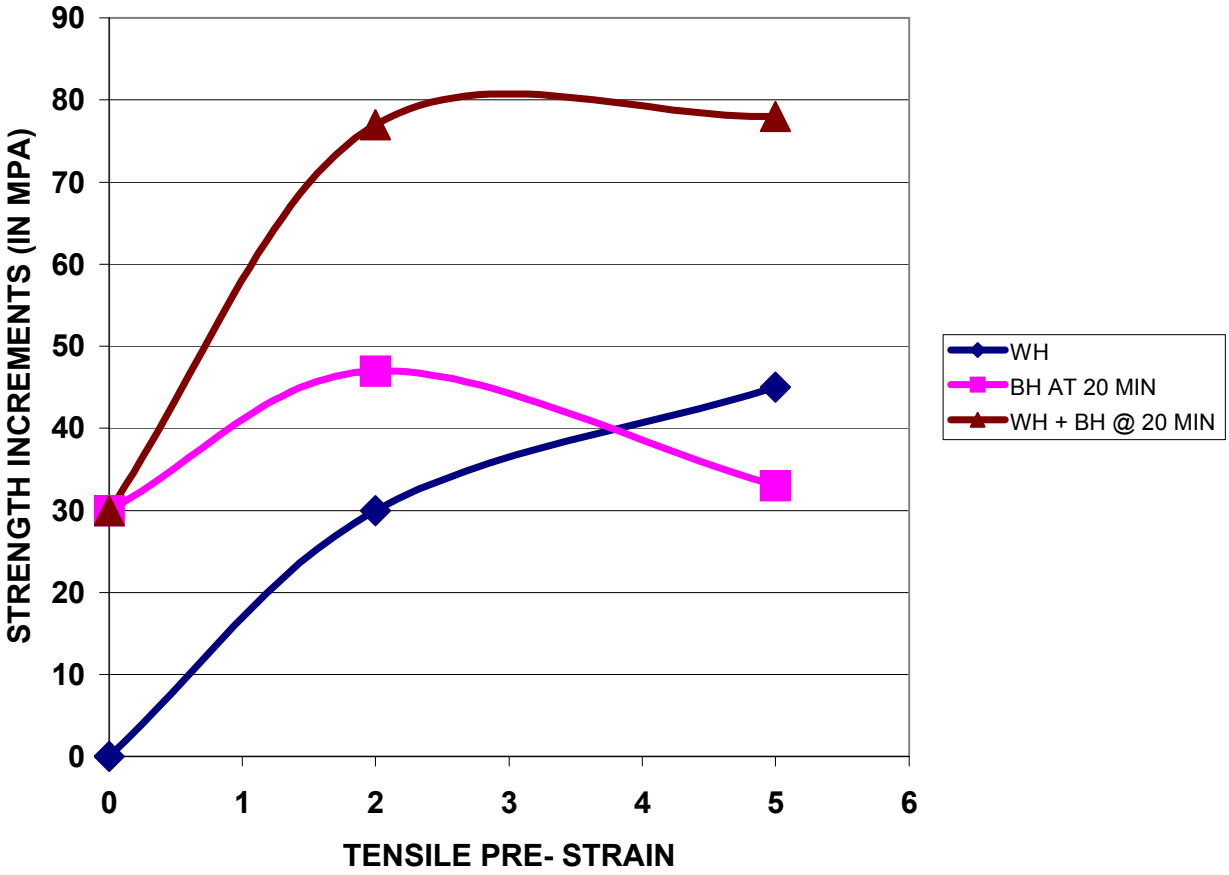

Figure 4. 6 WH, BH and total strength (WH+BH) increments at 20 minutes test time for the phase 1 CR_AR_MAX condition steel as a function of pre-strain.

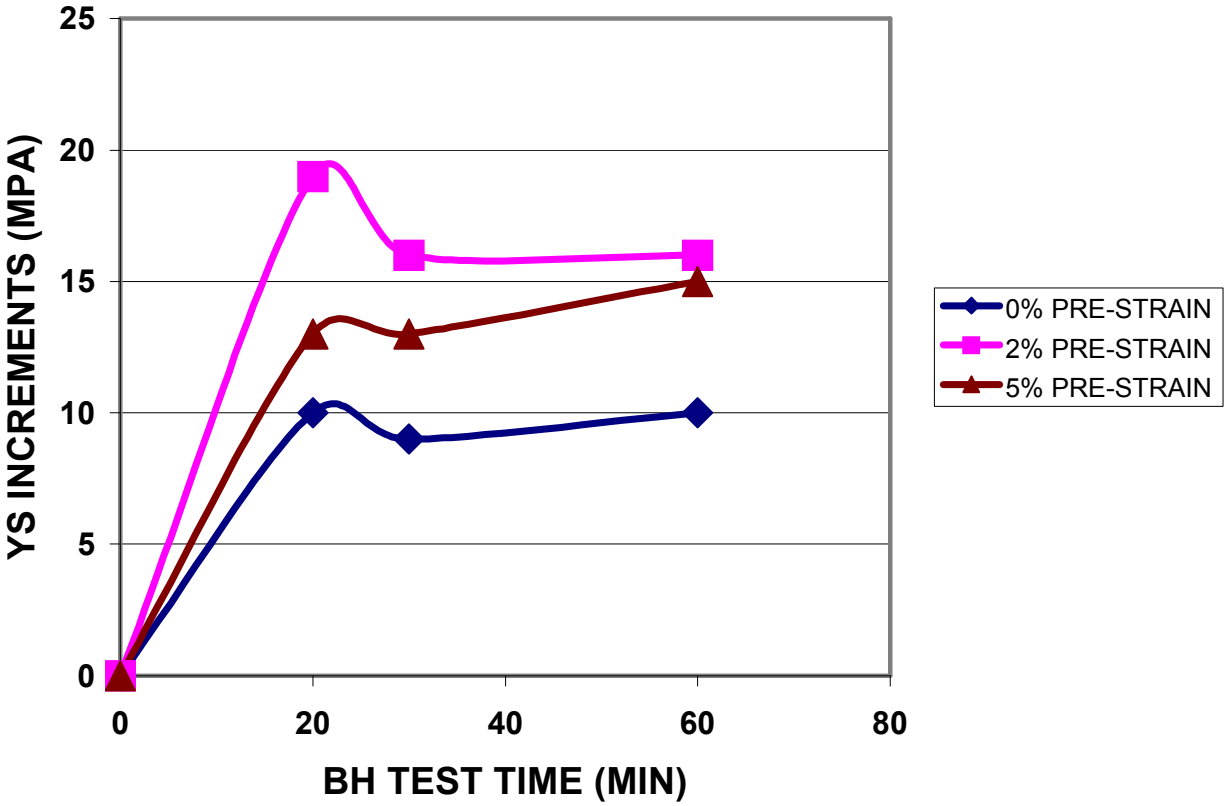

Figure 4. 7 Comparison of strength increments with BH test time at various pre-strains in phase 1 steel after additional heat treatment to remove the effect of temper rolling: CR_NTR condition.

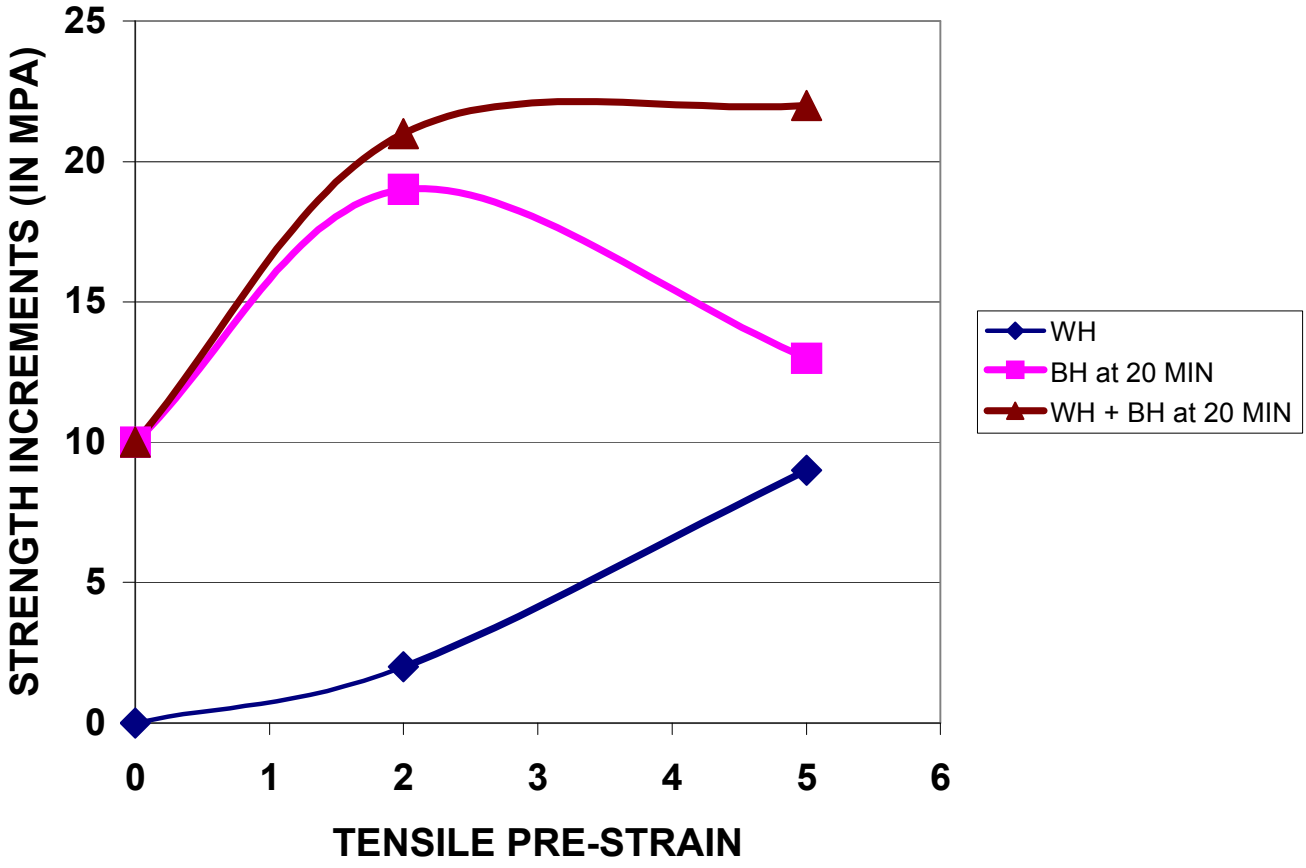

Figure 4. 8 WH, BH and total strength (WH+BH) increments at 20 minutes test time for the phase 1 CR_NTR condition steel as a function of pre-strain.

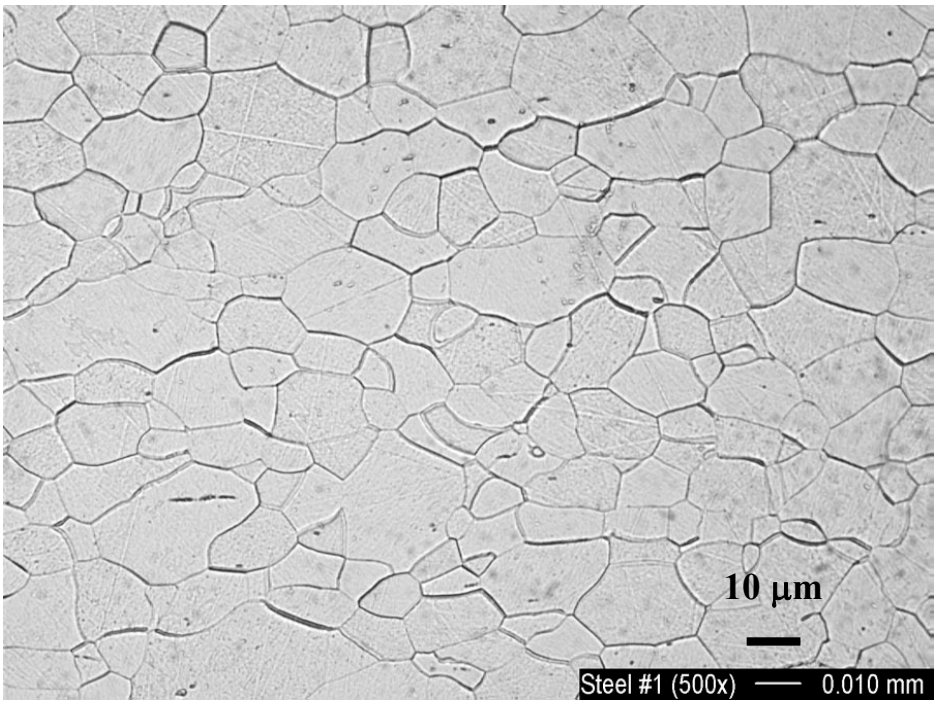

Figure 4. 9 Optical micrograph of the as-received phase 1 steel: CR_AR condition.

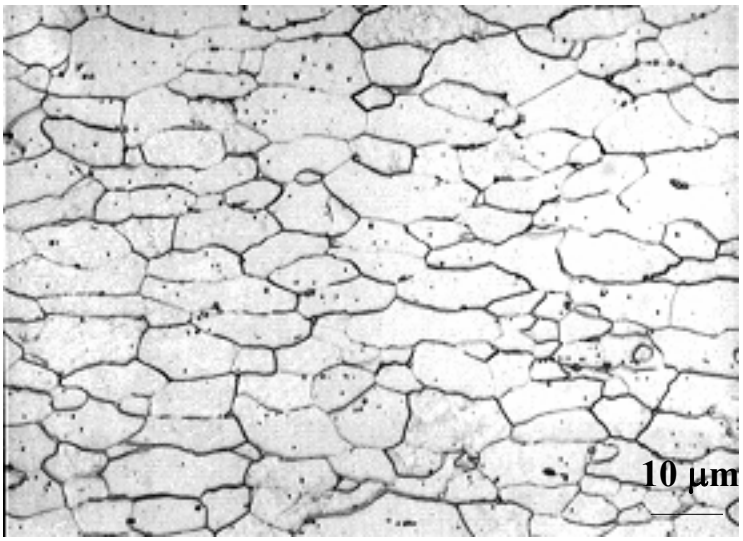

(A)

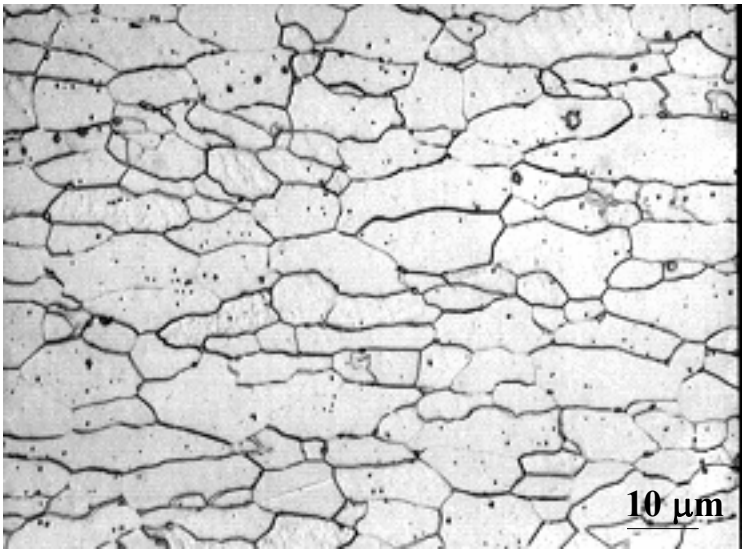

(B)

Figure 4. 10 Optical micrographs of the as-received phase 1 steel after additional heat treatment to maximize carbon in solution: CR_AR_MAX condition. (A) And (B) are different areas across the thickness.

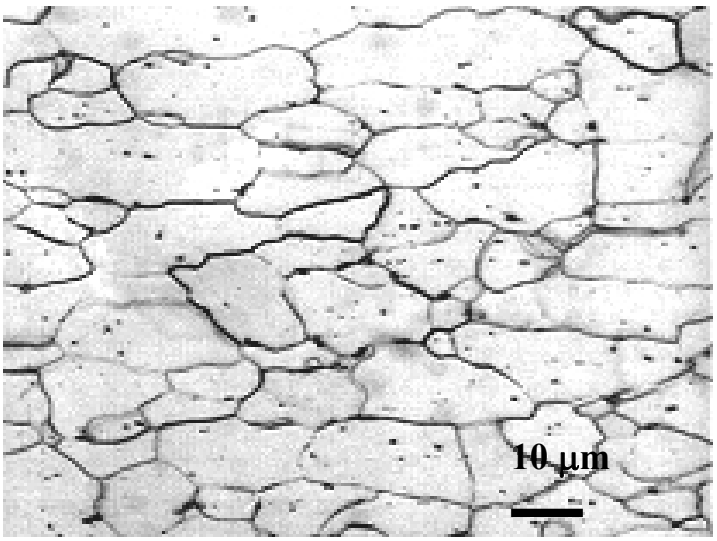

(A)

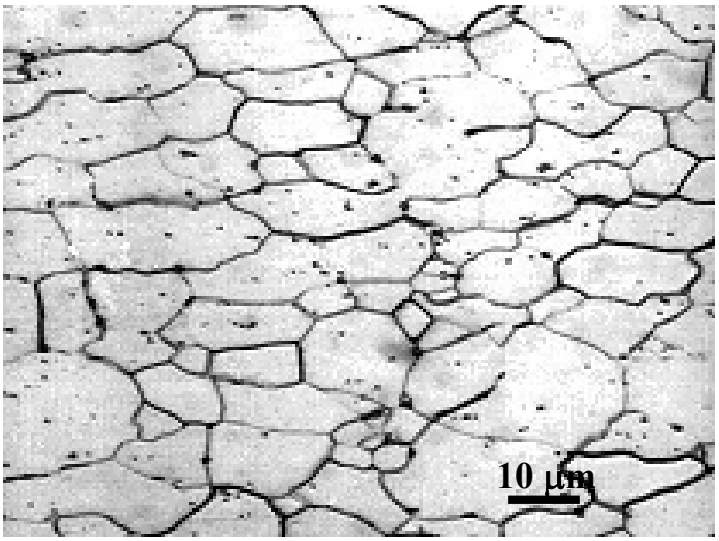

(B)

Figure 4. 11 Optical micrographs of the as-received phase 1 steel after additional heat treatment to remove the effect of temper rolling: CR_NTR condition. (A) And (B) are different areas across the thickness.

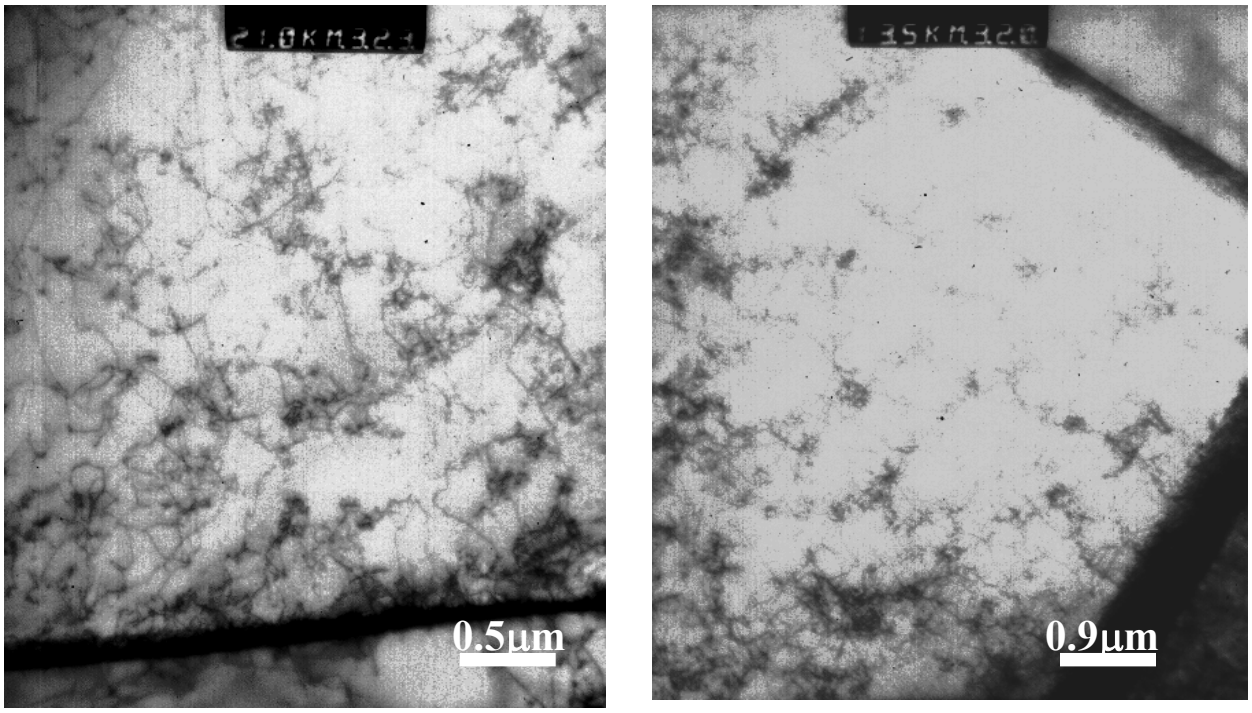

(A) (B)

Figure 4. 12 TEM bright field micrographs of the as-received phase 1 steel: CR_AR condition. (A) and (B) are the different (random) regions of the foil.

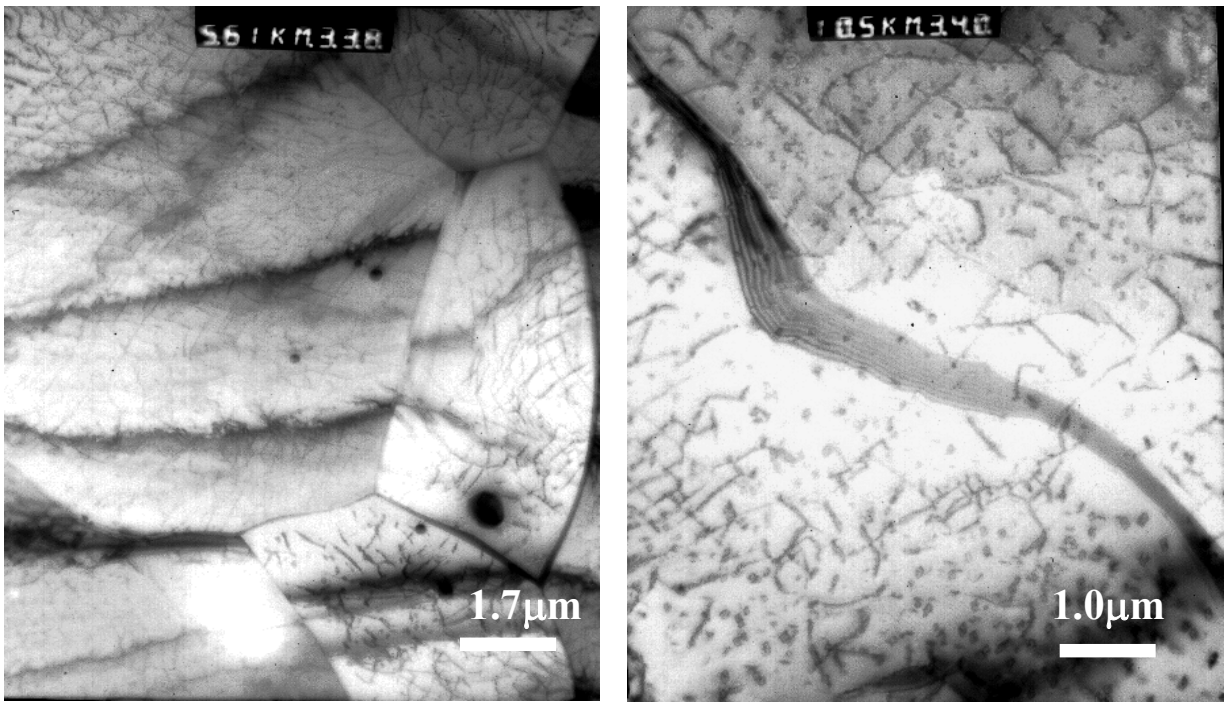

(A) (B)

Figure 4. 13 TEM bright field micrographs of the as-received phase 1 steel after additional heat treatment to maximize carbon in solution: CR_AR_MAX condition. (A) and (B) are the different (random) regions of the foil.

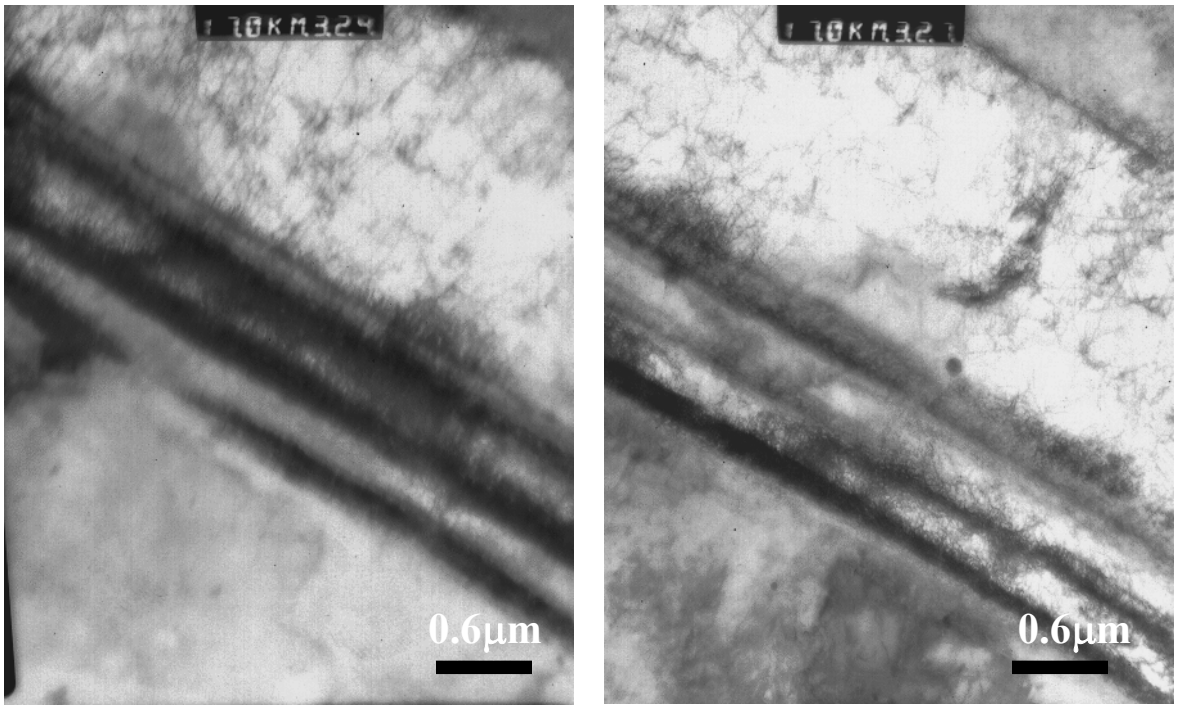

(A) (B)

Figure 4. 14 TEM bright field micrographs of the as-received phase 1 steel after additional heat treatment to remove the effect of temper rolling: CR_NTR condition. (A) and (B) are the different (random) regions of the foil.

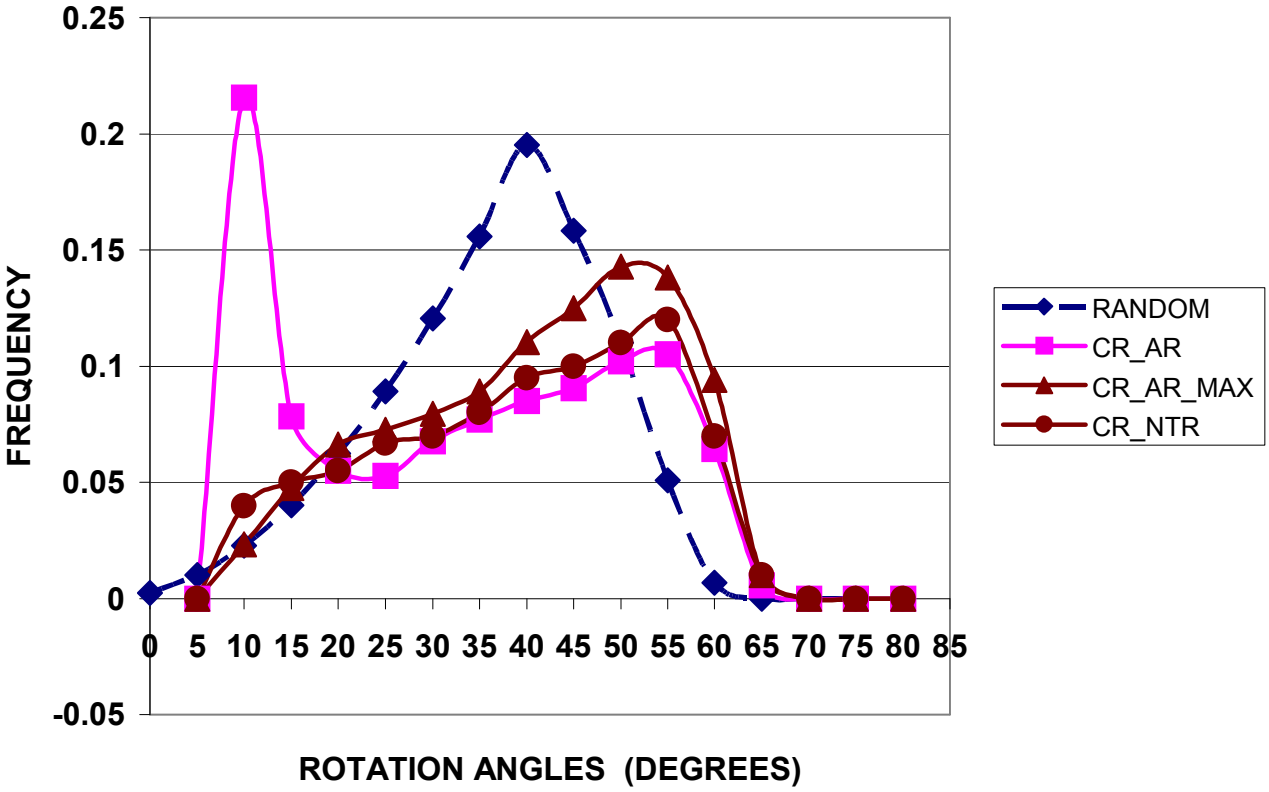

Figure 4. 15 EBSD results of the phase 1 steel in the as-received (CR_AR) condition, maximum carbon in solution (CA_AR_MAX) condition and removal of temper rolling effect (CR_NTR) condition. Comparison of the theoretical, random mis-orientation with the actual mis-orientation in the above 3 conditions is shown here.

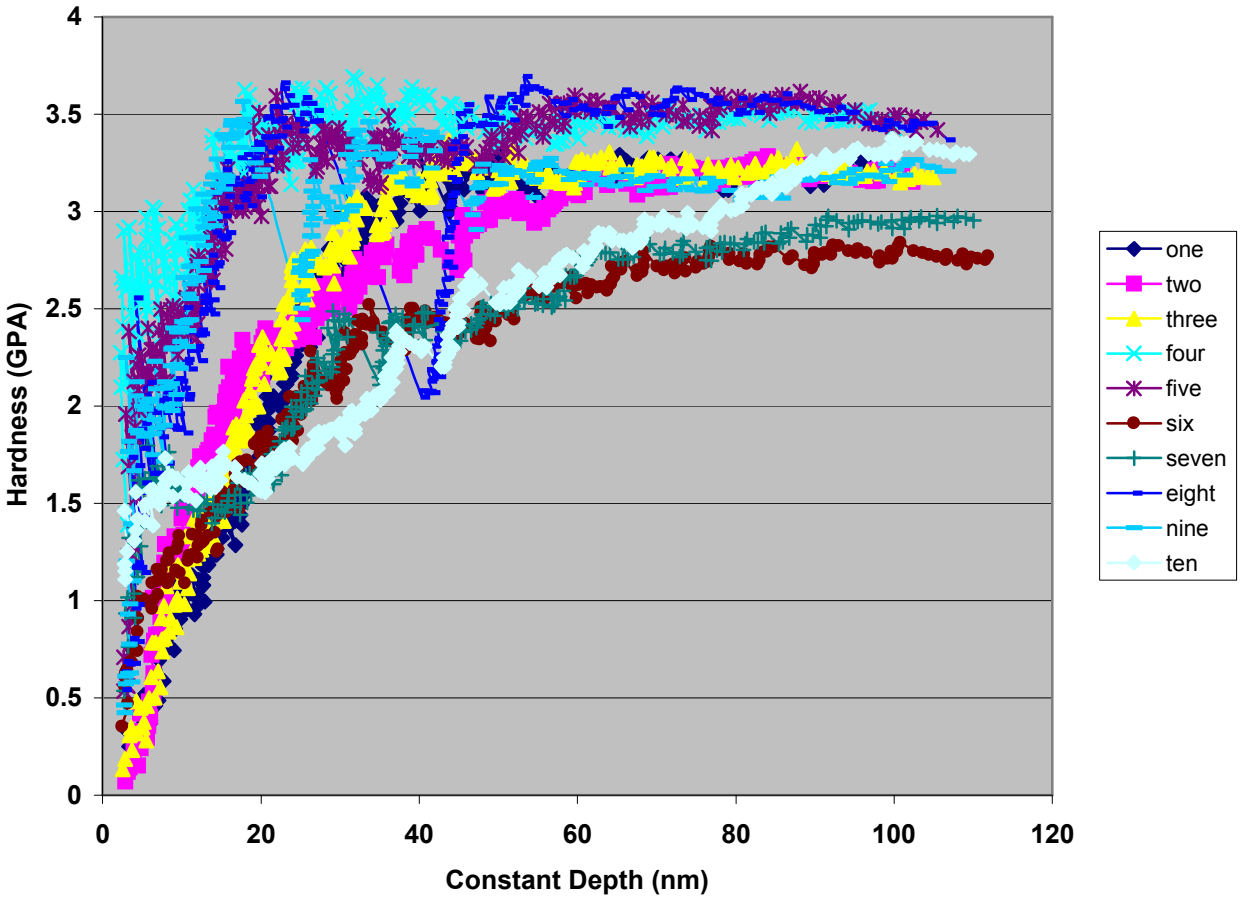

Figure 4. 16 Nano-Hardness measurement results of the as-received phase 1 steel: CR_AR condition. The hardness is measured as a function of the constant depth of indentation and is shown for all the indents at position 1. The sample was not etched at the time of indentation.

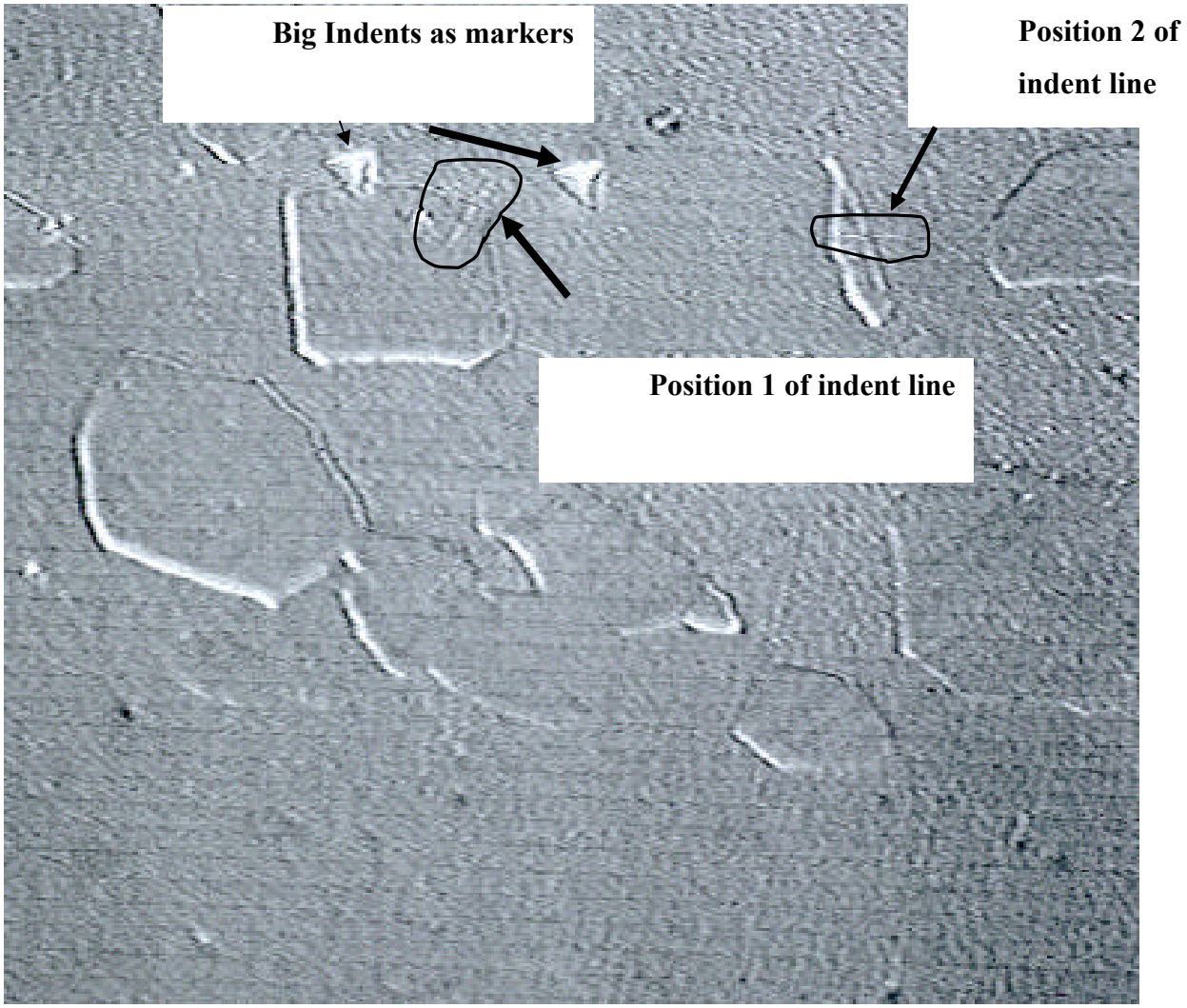

Figure 4. 17 Optical micrograph showing the 2 positions at which the indentations were taken for the as-received phase 1 steel: CR_AR condition. The sample was slightly etched after the test only to reveal the area of indentation.

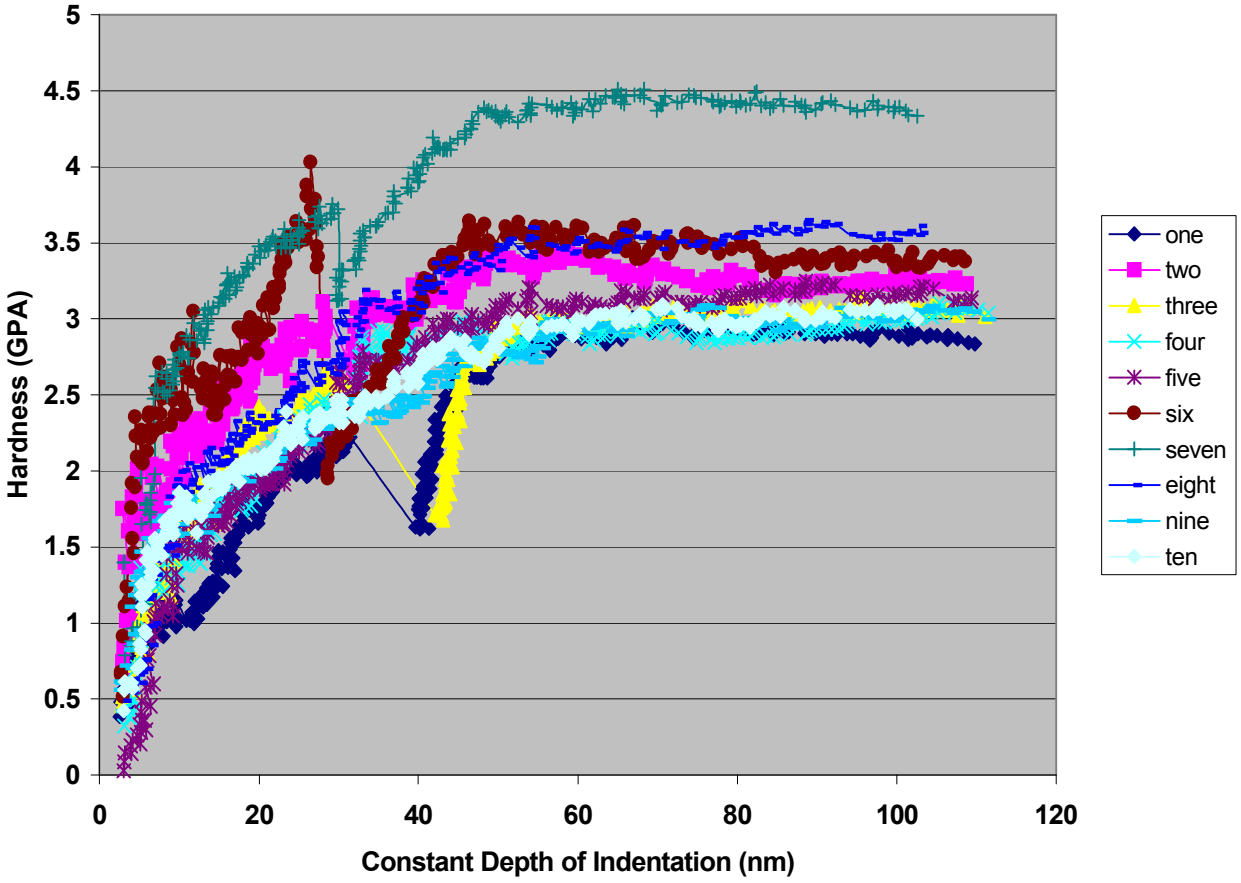

Figure 4. 18 Nano-Hardness measurement results of the as-received phase 1 steel after additional heat treatment to maximize carbon in solution: CR_AR_MAX condition. The hardness is measured as a function of the constant depth of indentation and is shown for all the indents. Shown are the results at position 1. The sample was not etched before the test.

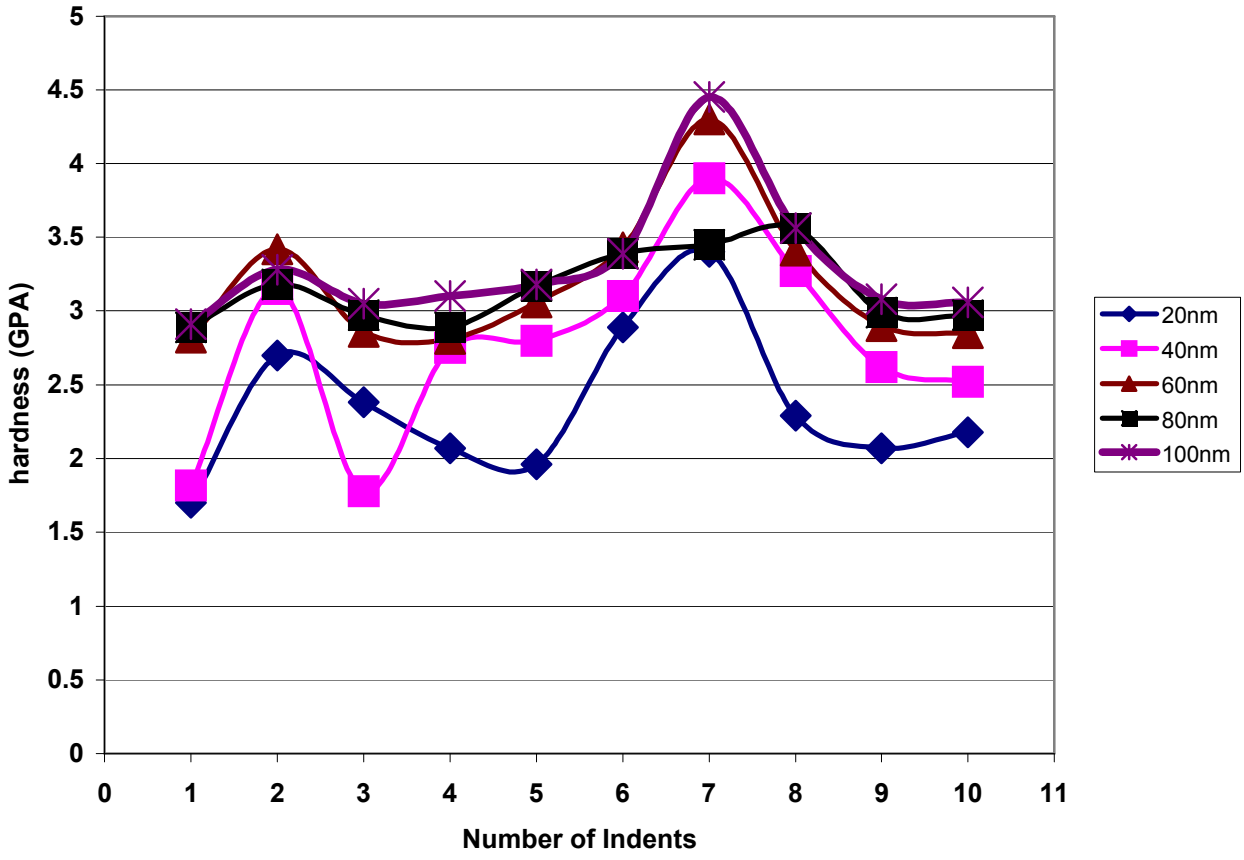

Figure 4. 19 Nano-Hardness measurement results of the as-received phase 1 steel after additional heat treatment to maximize carbon in solution: CR_AR_MAX condition. The hardness here is measured as a function of the number of indents and is shown for varying depths of indentations. Shown are the results at position 1. The sample was not etched before the test.

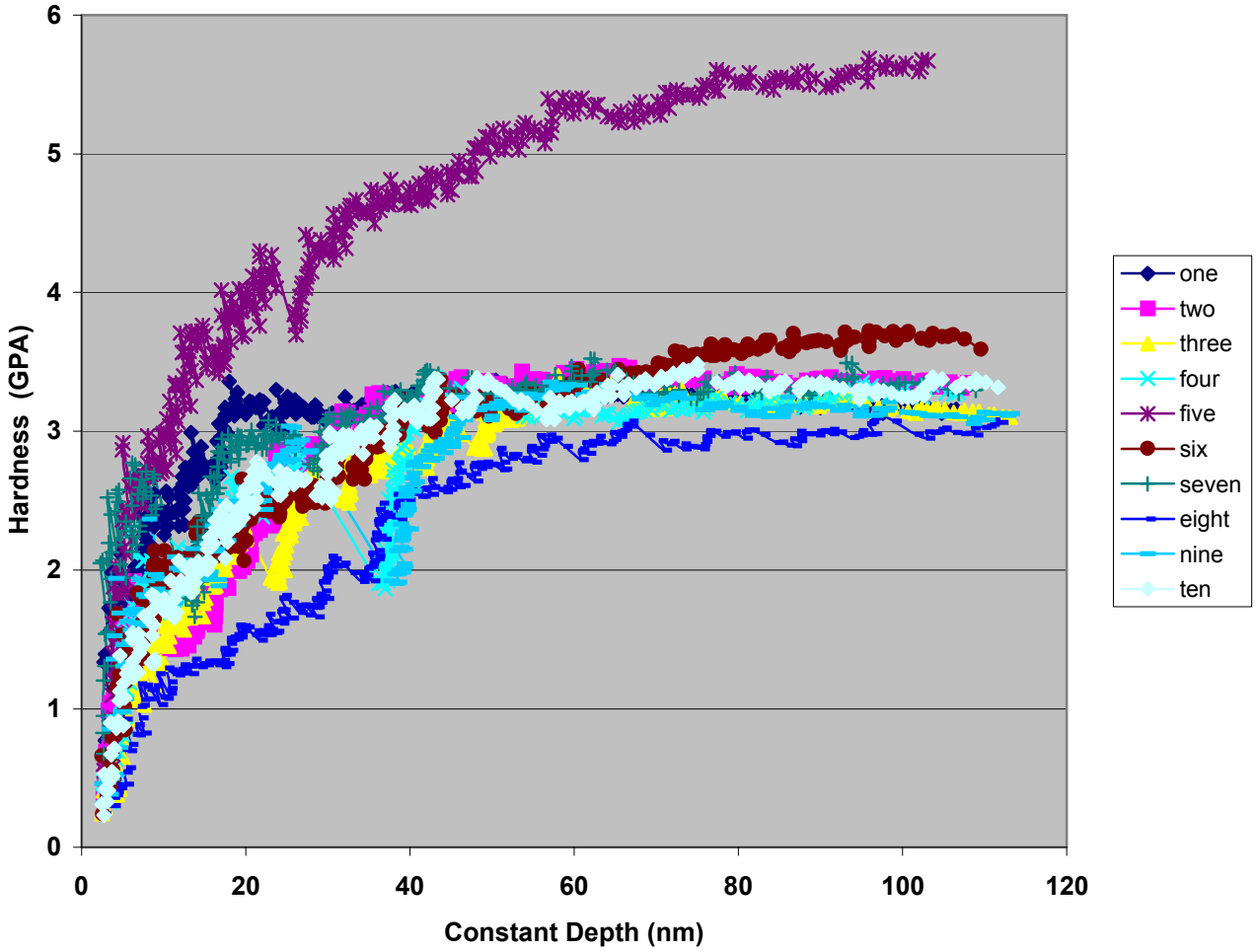

Figure 4. 20 Nano-Hardness measurement results of the as-received phase 1 steel after additional heat treatment to maximize carbon in solution: CR_AR_MAX condition. The hardness is measured as a function of the constant depth of indentation and is shown for all the indents. Shown are the results at position 2. The sample here was etched before the test.

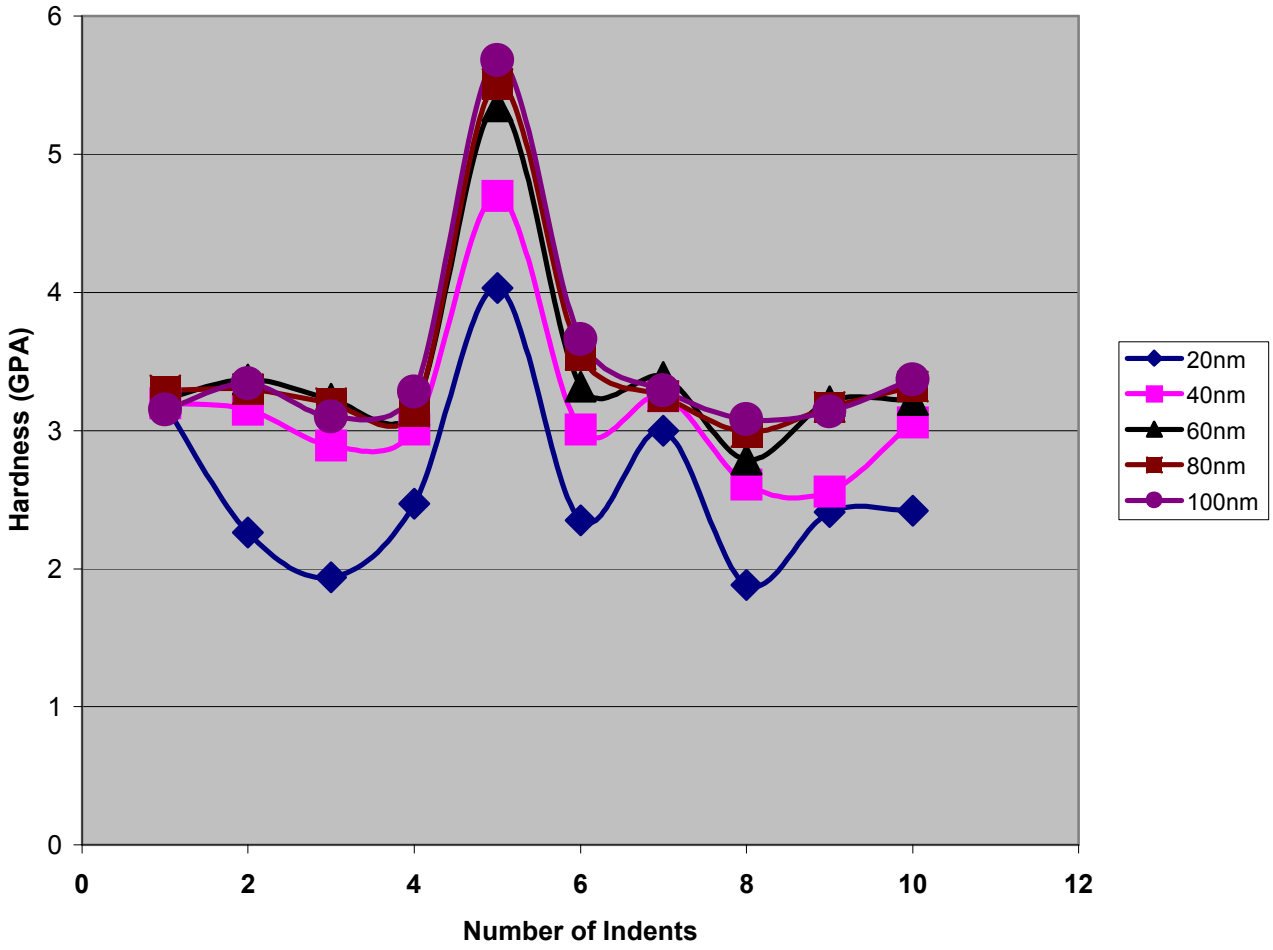

Figure 4. 21 Nano-Hardness measurement results of the as-received phase 1 steel after additional heat treatment to maximize carbon in solution: CR_AR_MAX condition. The hardness here is measured as a function of the number of indents and is shown for varying depths of indentations. Shown are the results at position 2. The sample here was etched before the test.

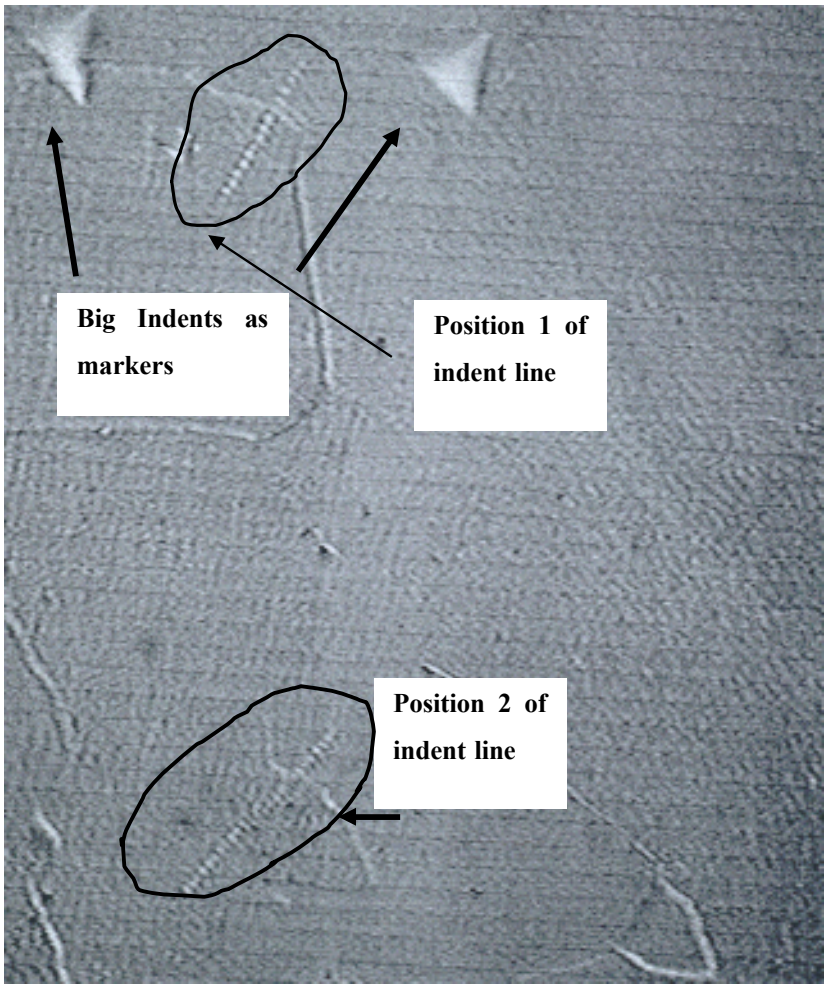

Figure 4. 22 Optical micrograph showing the 2 positions at which the indentations were taken for the as-received phase 1 steel after additional heat treatment to maximize carbon in solution: CR_AR condition. The sample was slightly etched after the test only to reveal the area of indentation.

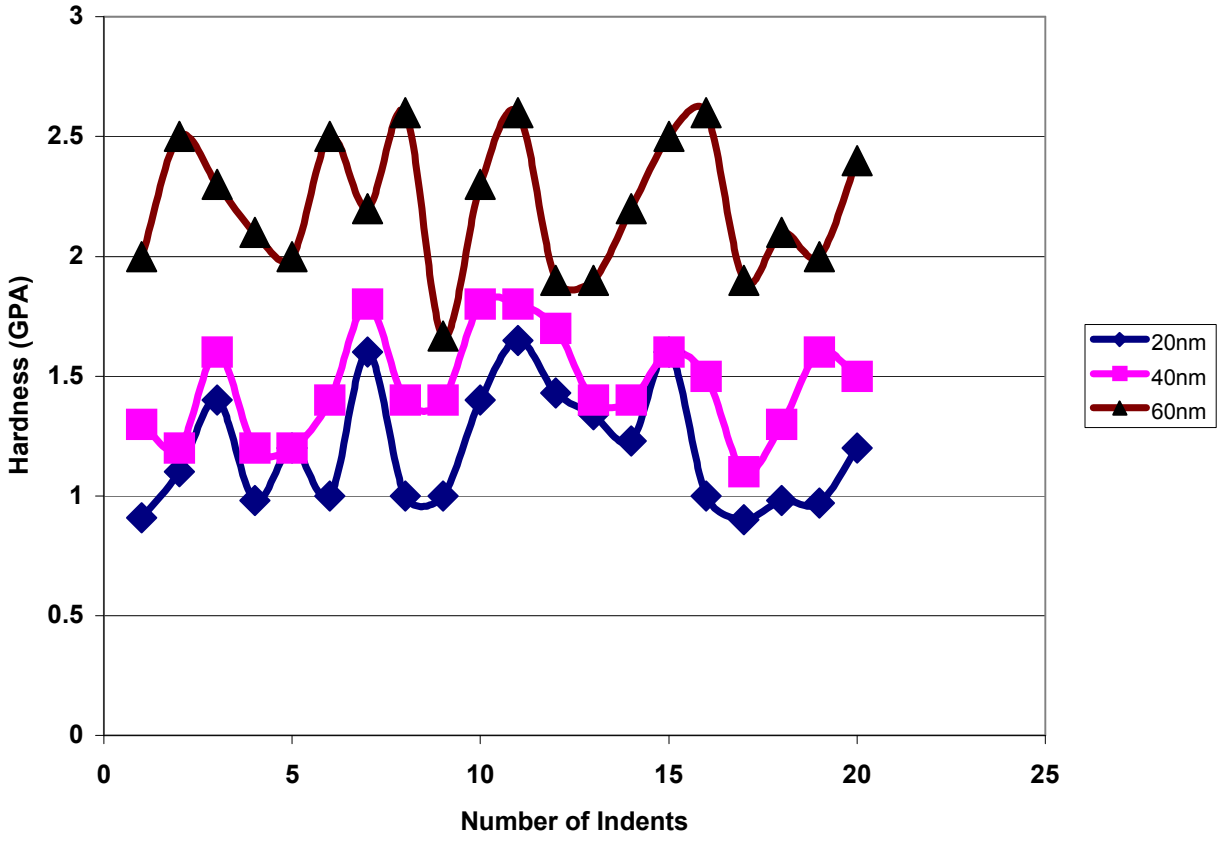

Figure 4. 23 Nano-Hardness measurement results of the as-received phase 1 steel after additional heat treatment to remove the effect of temper rolling: CR_NTR condition. The hardness is measured as a function of the constant depth of indentation and is shown for all the indents. The sample was not etched.

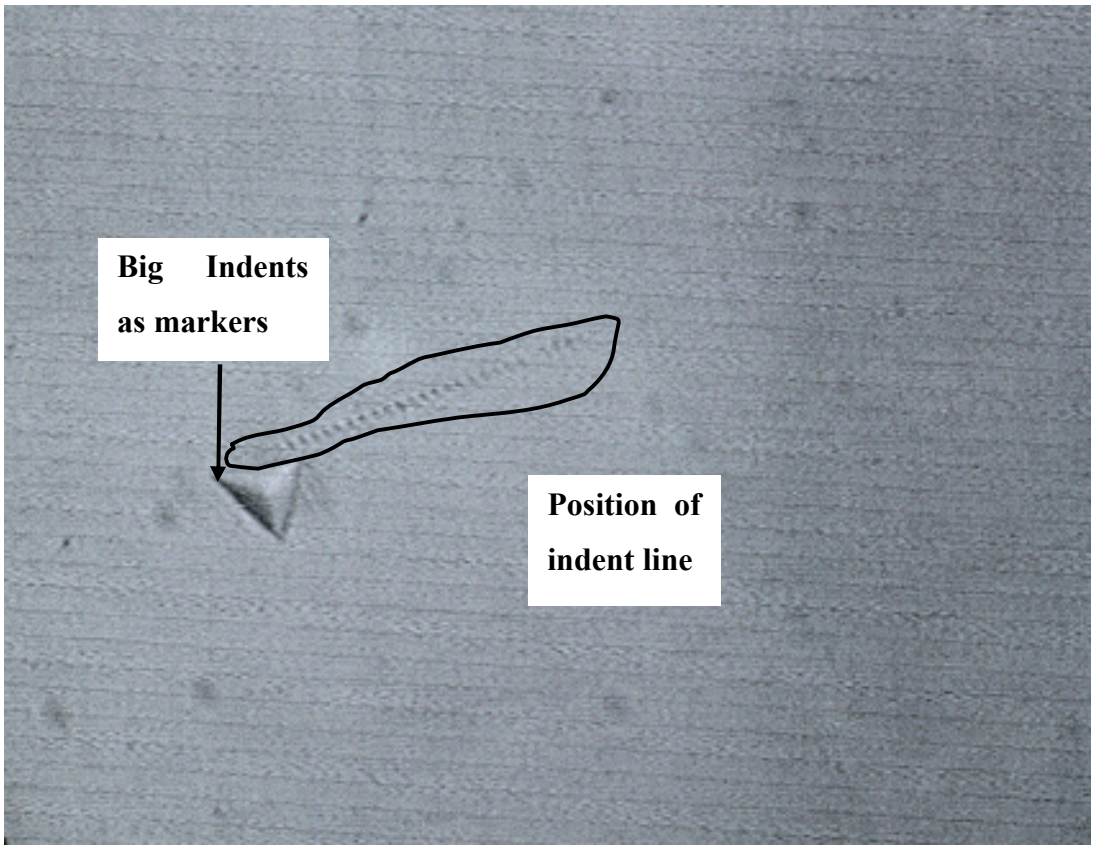

Figure 4. 24 Optical micrograph showing the position at which the indentations were taken for the as-received phase 1 steel after additional heat treatment to remove the effect of temper rolling: CR_NTR condition.

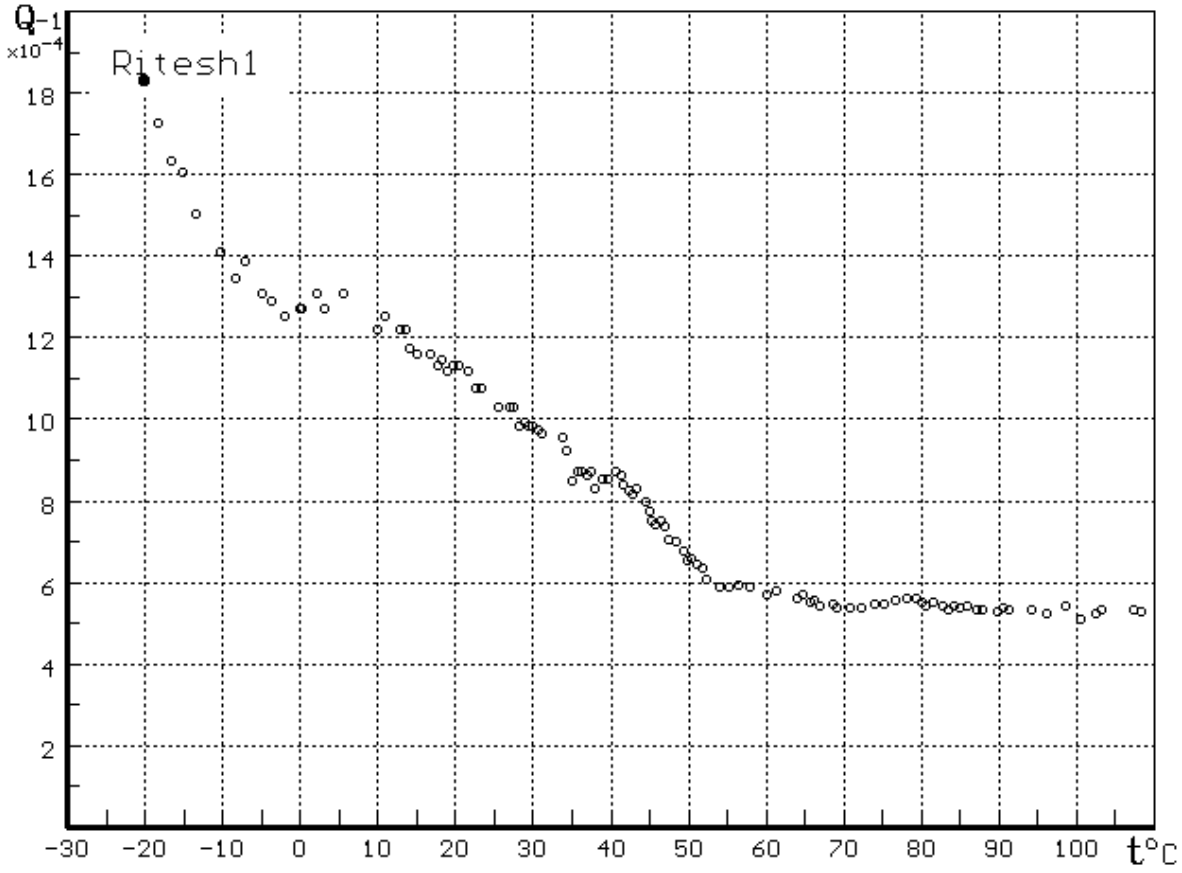

Figure 4. 25 Internal Friction results of the as-received phase 1 steel: CR_AR condition. No sharp Snoek-Koster (S-K) peaks observed for C and N at any temperature for the above as-received (1% temper-rolled) steel.

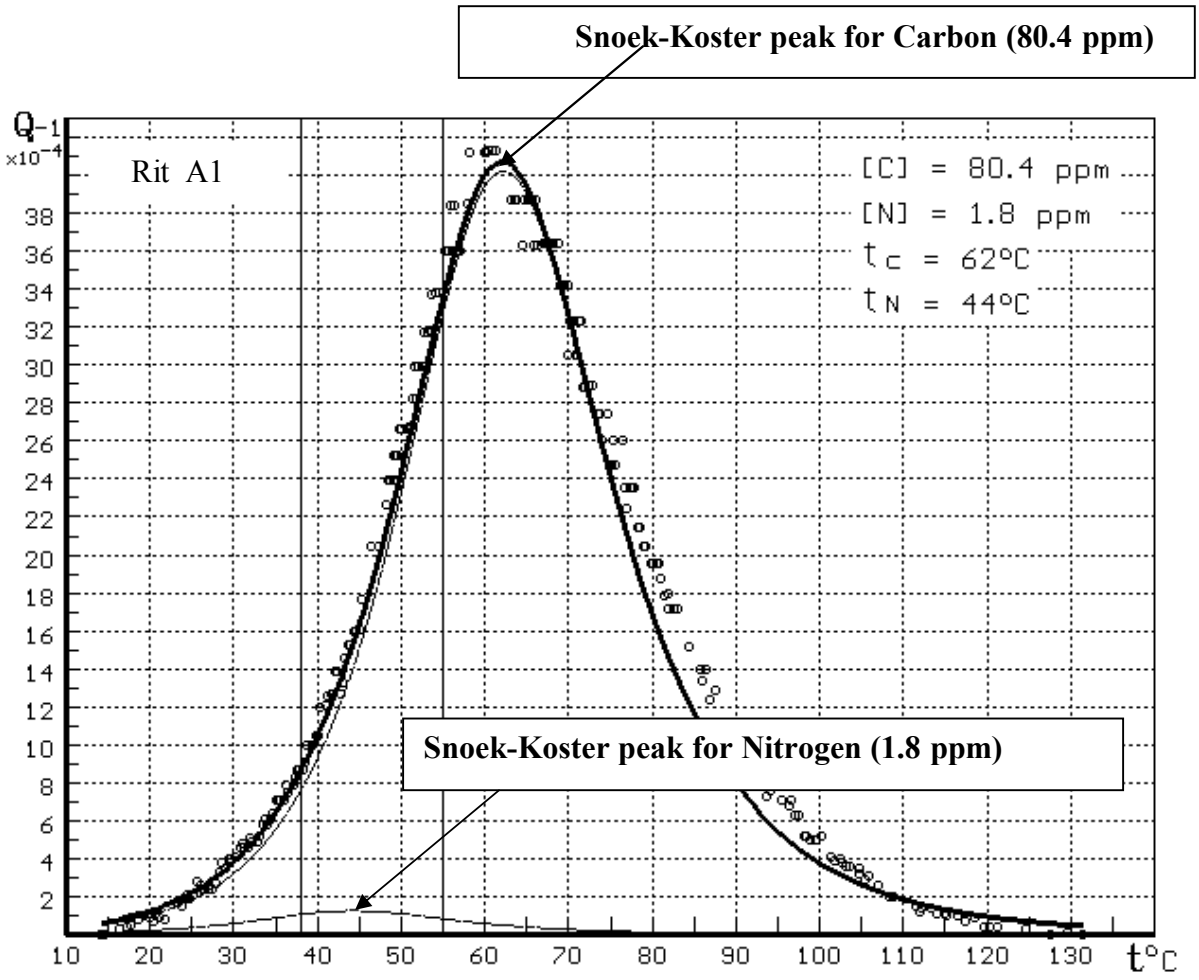

Figure 4. 26 Internal Friction results of the as-received phase 1 steel after additional heat treatment to maximize carbon in solution: CR_AR_MAX condition.

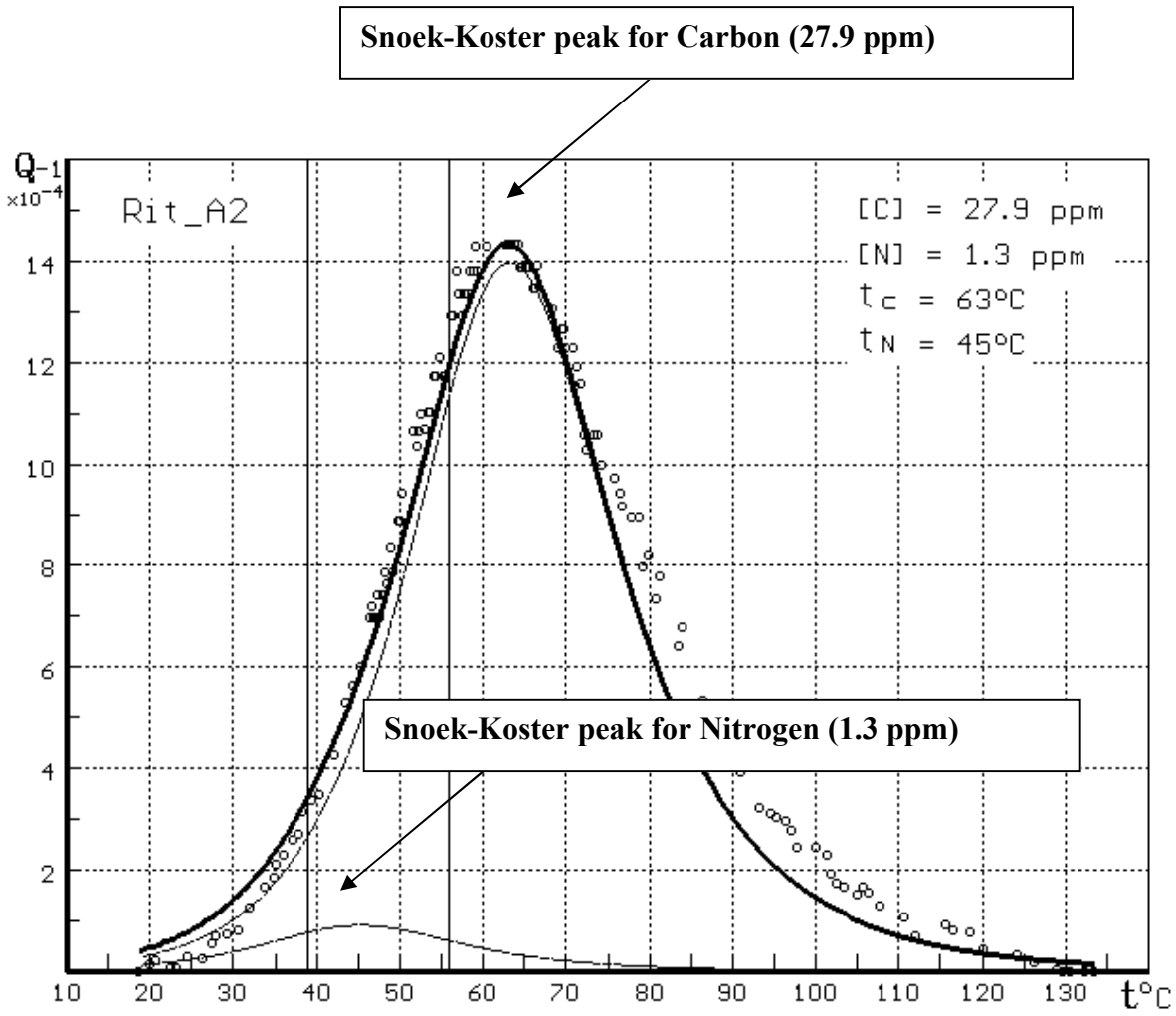

Figure 4. 27 Internal Friction results of the as-received phase 1 steel after additional heat treatment to remove the effect of temper rolling: CR_NTR condition.

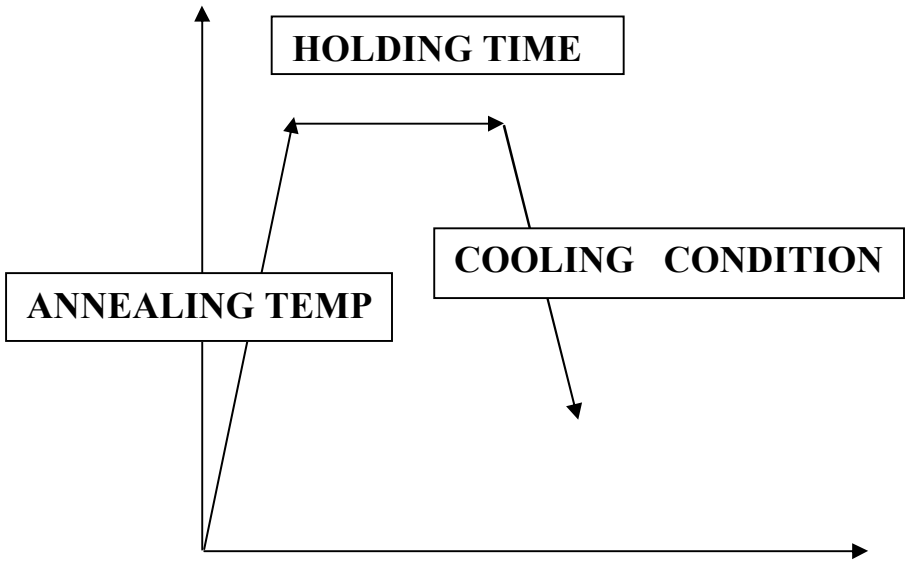

Figure 4. 28 Schematic drawing of the various annealing treatments given to both the laboratory phase 2 steels: plain carbon steel (24CA) and Mo-B steel (25CA).

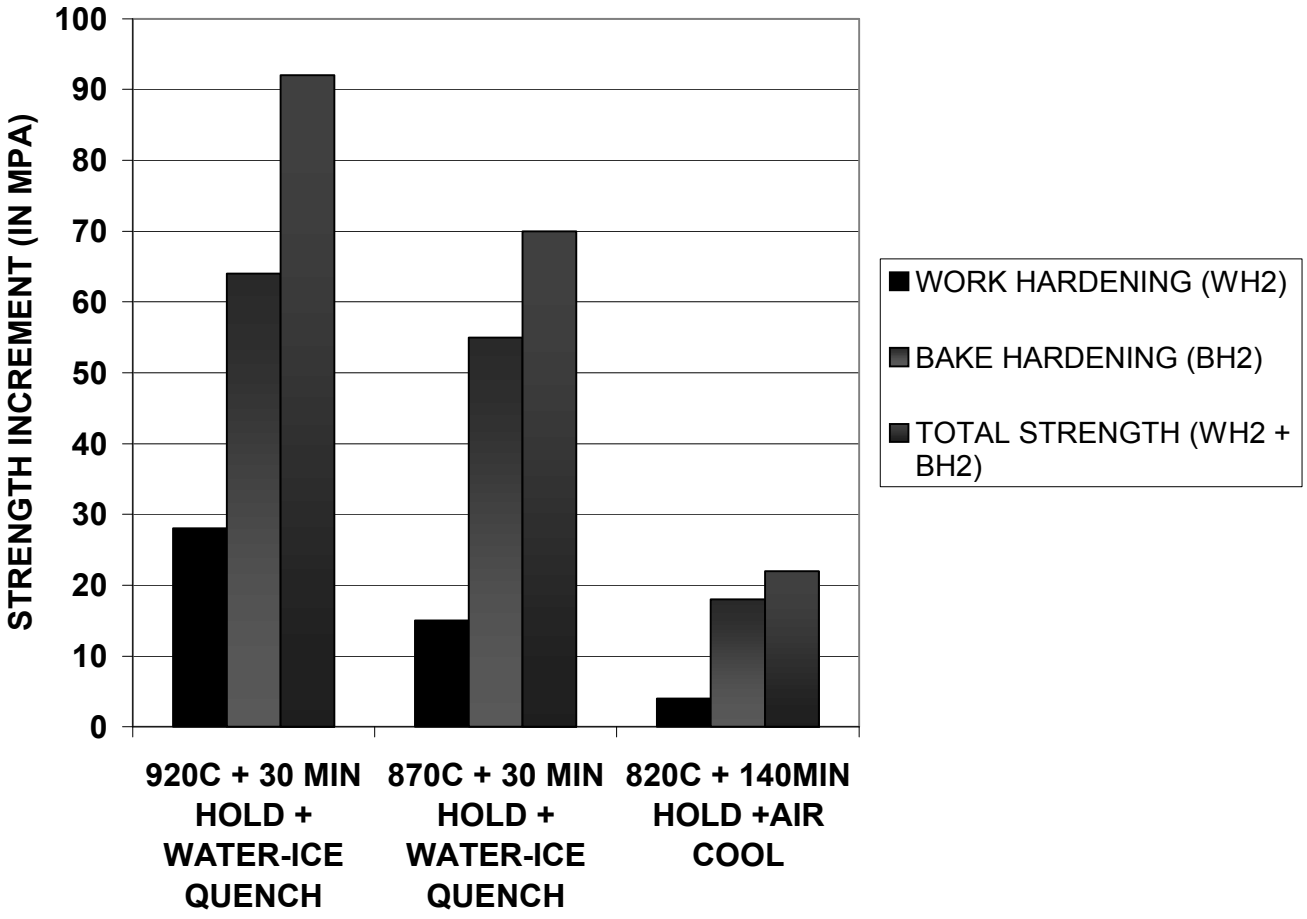

Figure 4. 29 Schematic representation of the WH, BH and total strength (WH+BH) increments at 2% pre-strain for the phase 2 plain carbon (24CA) steel as a function of the various annealing treatments.

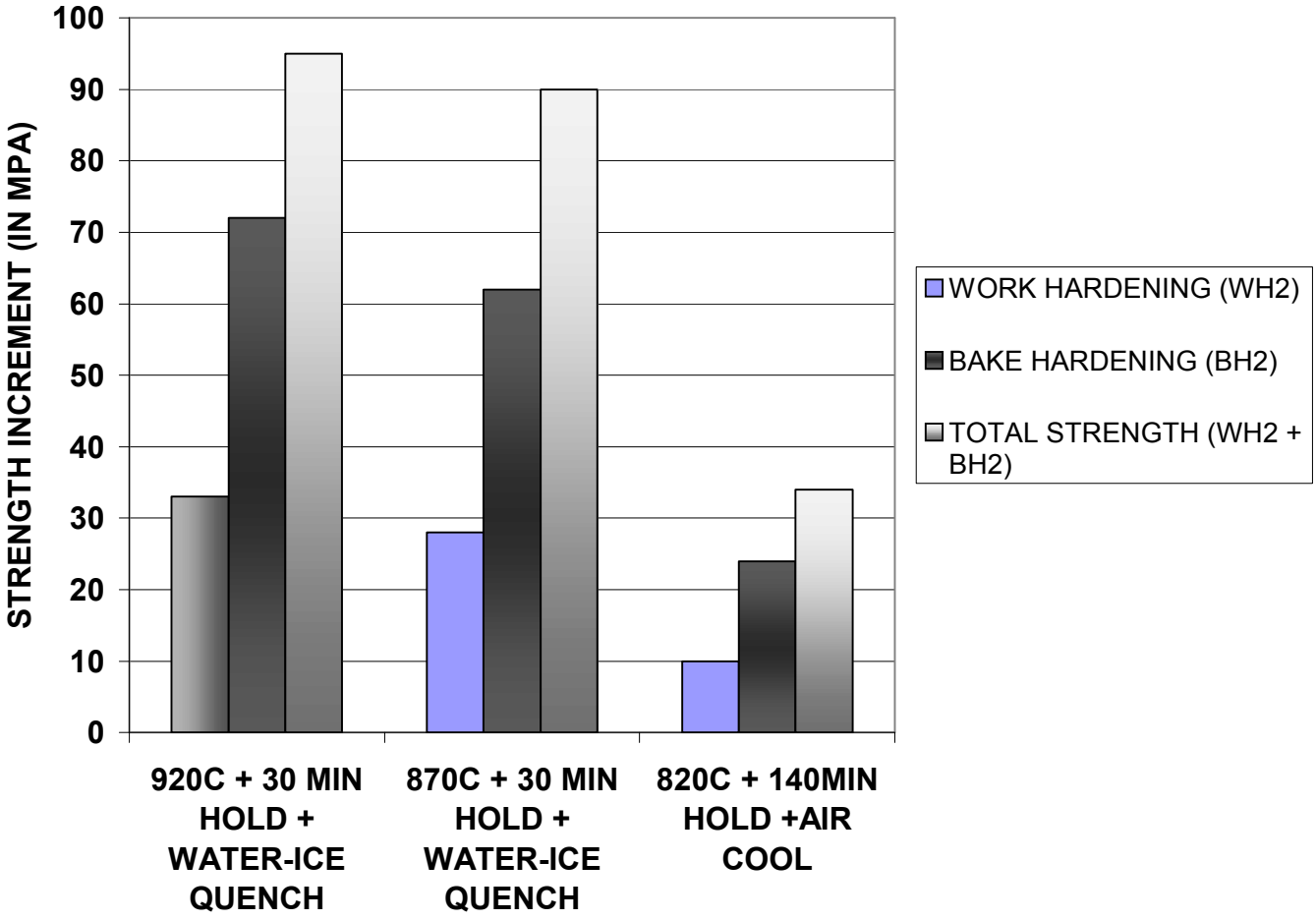

Figure 4. 30 Schematic representation of the WH, BH and total strength (WH+BH) increments at 2% pre-strain for the phase 2 Mo-B (25CA) steel as a function of the various annealing treatments.

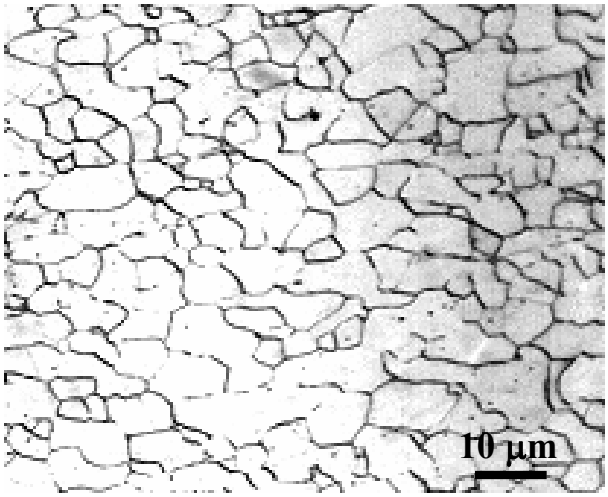

(A)

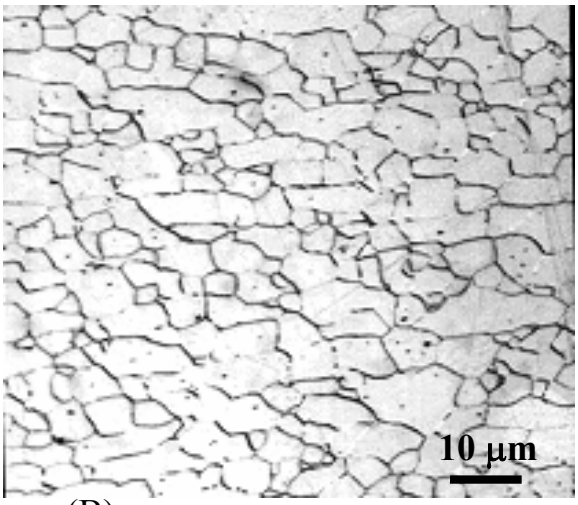

(B)

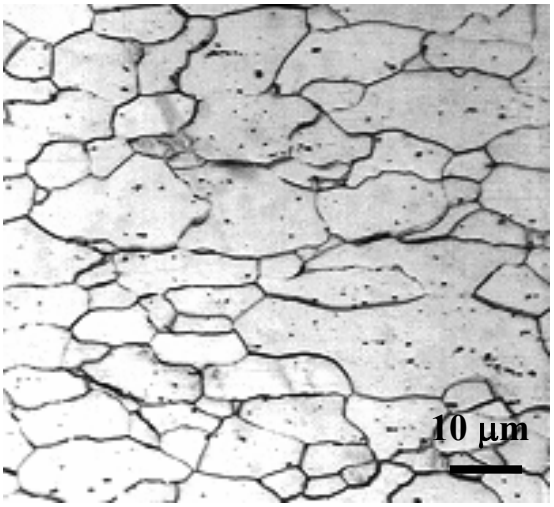

(C)

Figure 4. 31 Optical micrographs of the phase 2 plain carbon (24CA) steel as a function of the various annealing treatments. (A) 820°C heat for 140 min hold and air cool, (B) 870°C for 30 min hold and water-ice quench, and (C) 920°C for 30 min hold and water-ice quench.

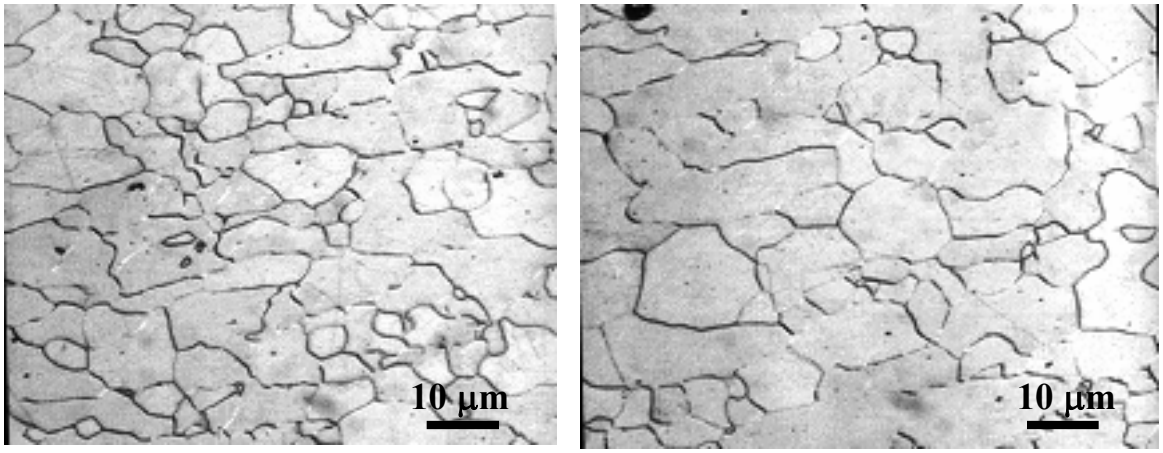

(A) (B)

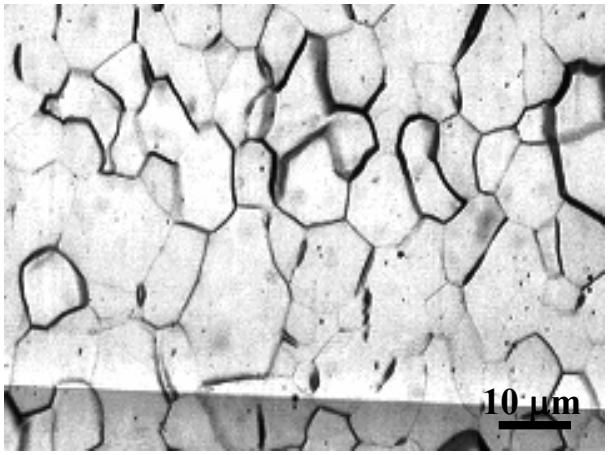

(C)

Figure 4. 32 Optical micrographs of the phase 2 Mo-B (25CA) steel as a function of the various annealing treatments. (A) 820°C heat for 140 min hold and air cool, (B) 870°C for 30 min hold and water-ice quench, and (C) 920°C for 30 min hold and water-ice quench.

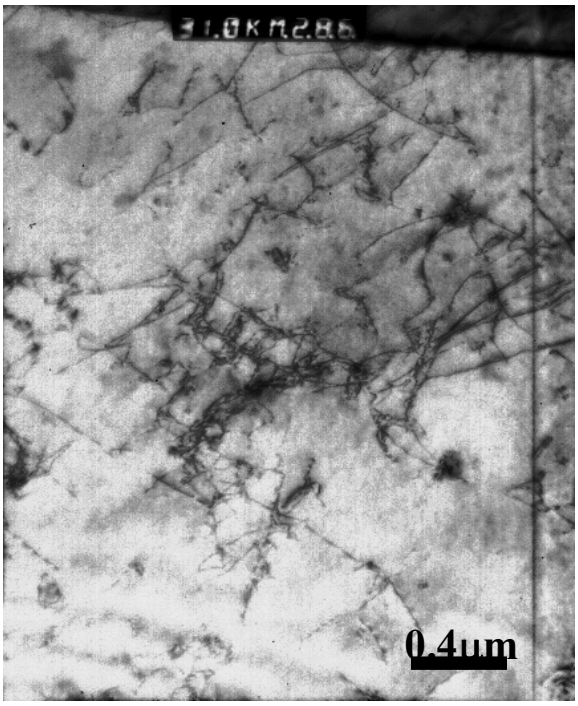

Figure 4. 33 TEM bright field micrographs of the phase 2 plain carbon (24CA) steel annealed at 870°C hold for 30 minutes and then ice-water quenched to room temperature and then 2% pre-strained before the BH test.

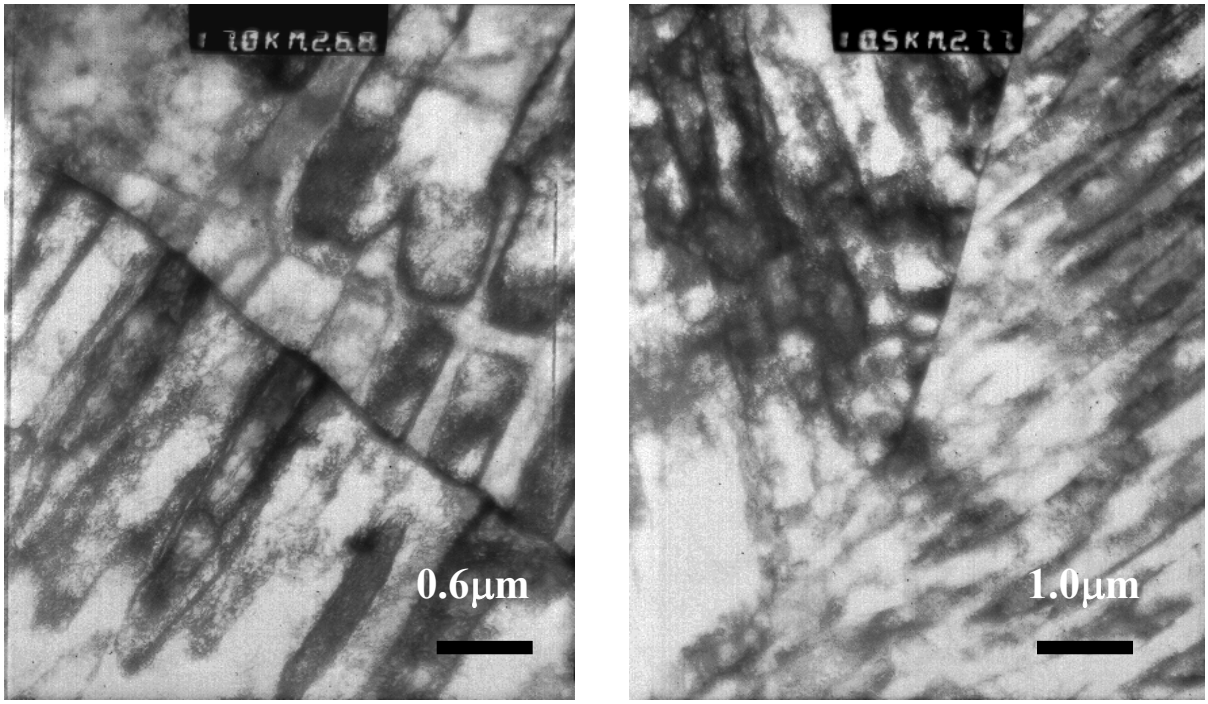

(A) (B)

Figure 4. 34 TEM bright field micrographs of the phase 2 plain carbon (24CA) steel annealed at 870°C hold for 30 minutes and then ice-water quenched to room temperature. It was then 2% pre-strained and then paint baked at 180°C and 20 minutes. (A) and (B) are the different (random) regions of the foil.

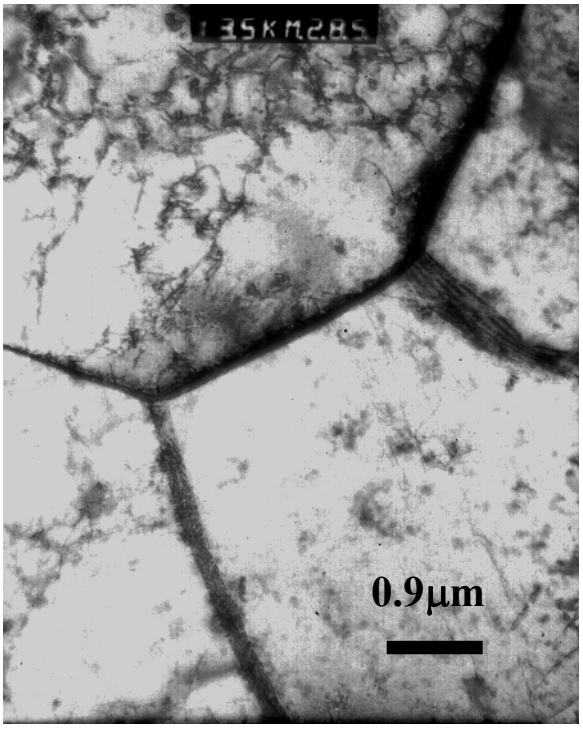

Figure 4. 35 TEM bright field micrographs of the phase 2 plain carbon (24CA) steel annealed at 920°C hold for 30 minutes and then ice-water quenched to room temperature and then 2% pre-strained before the BH test

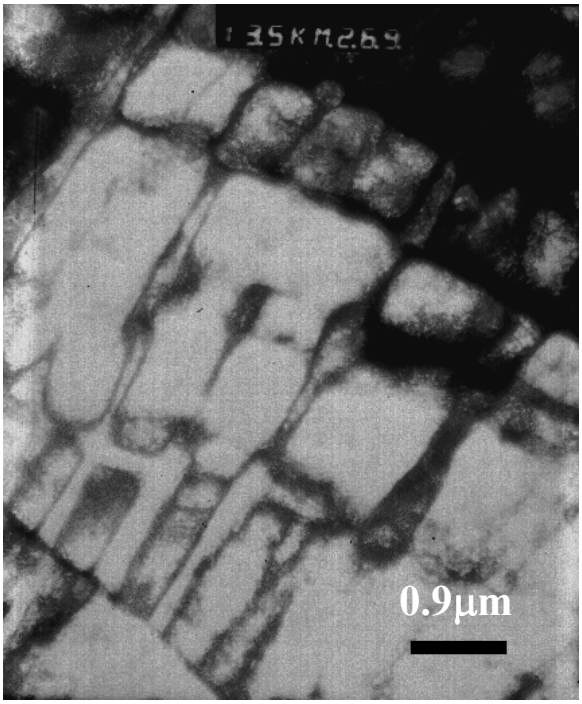

Figure 4. 36 TEM bright field micrographs of the phase 2 plain carbon (24CA) steel annealed at 920°C hold for 30 minutes and then ice-water quenched to room temperature. It was then 2% pre-strained and then paint baked at 180°C and 20 minutes.

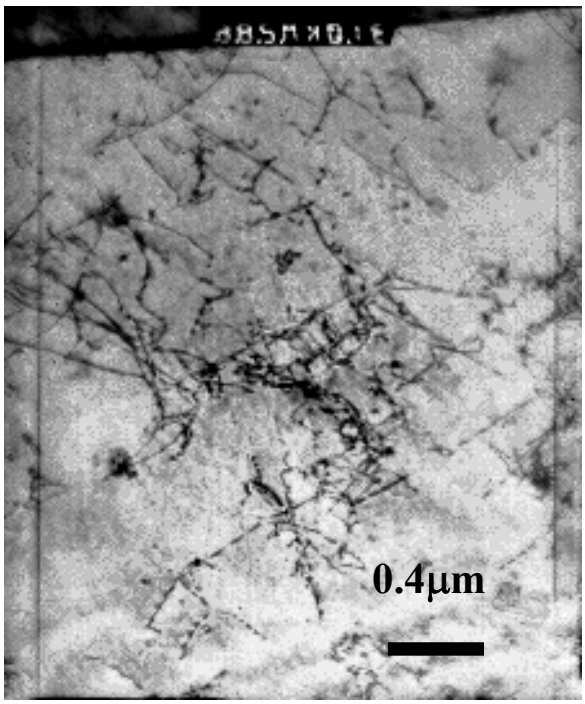

Figure 4. 37 TEM bright field micrographs of the phase 2 Mo-B (25CA) steel annealed at 870°C hold for 30 minutes and then ice-water quenched to room temperature and then 2% pre-strained before the BH test.

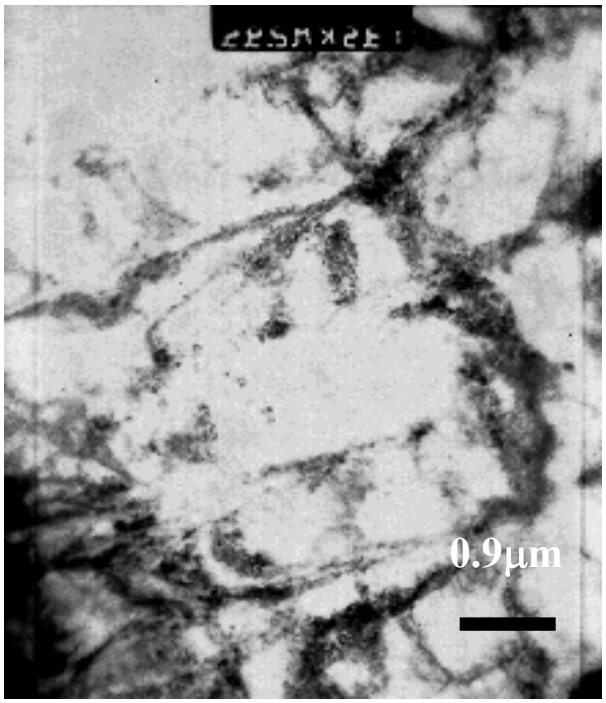

Figure 4. 38 TEM bright field micrographs of the phase 2 Mo-B (25CA) steel annealed at 870°C hold for 30 minutes and then ice-water quenched to room temperature. It was then 2% pre-strained and then paint baked at 180°C and 20 minutes.

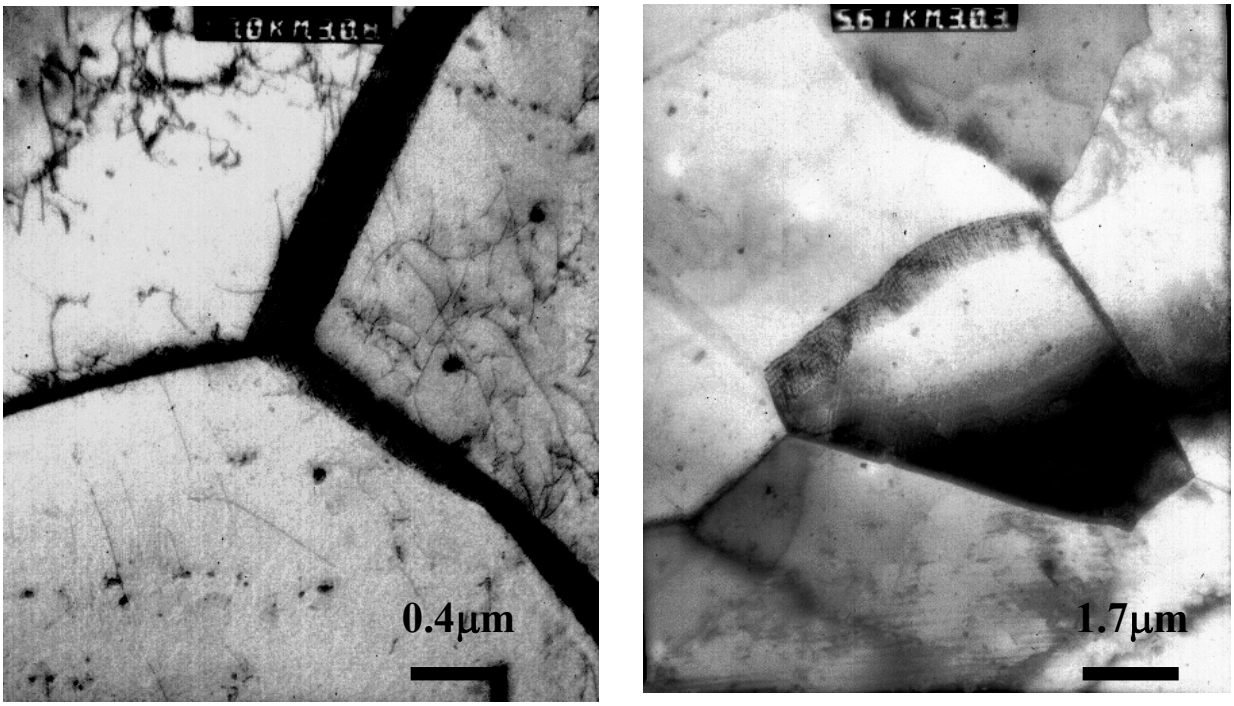

(A) (B)

Figure 4. 39 TEM bright field micrographs of the phase 2 Mo-B (25CA) steel annealed at 920°C hold for 30 minutes and then ice-water quenched to room temperature and then 2% pre-strained before the BH test. (A) and (B) are the different (random) regions of the foil.

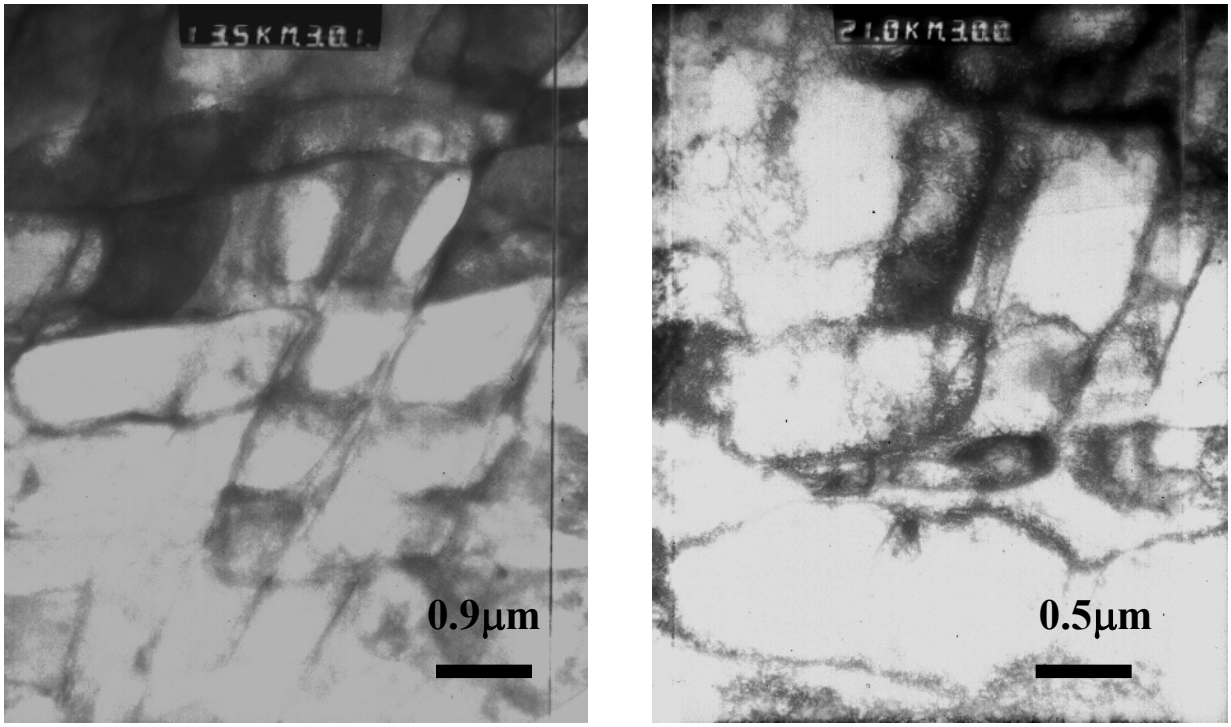

(A) (B)

Figure 4. 40 TEM bright field micrographs of the phase 2 Mo-B (25CA) steel annealed at 920°C hold for 30 minutes and then ice-water quenched to room temperature. It was then 2% pre-strained and then paint baked at 180°C and 20 minutes. (A) and (B) are the different (random) regions of the foil.

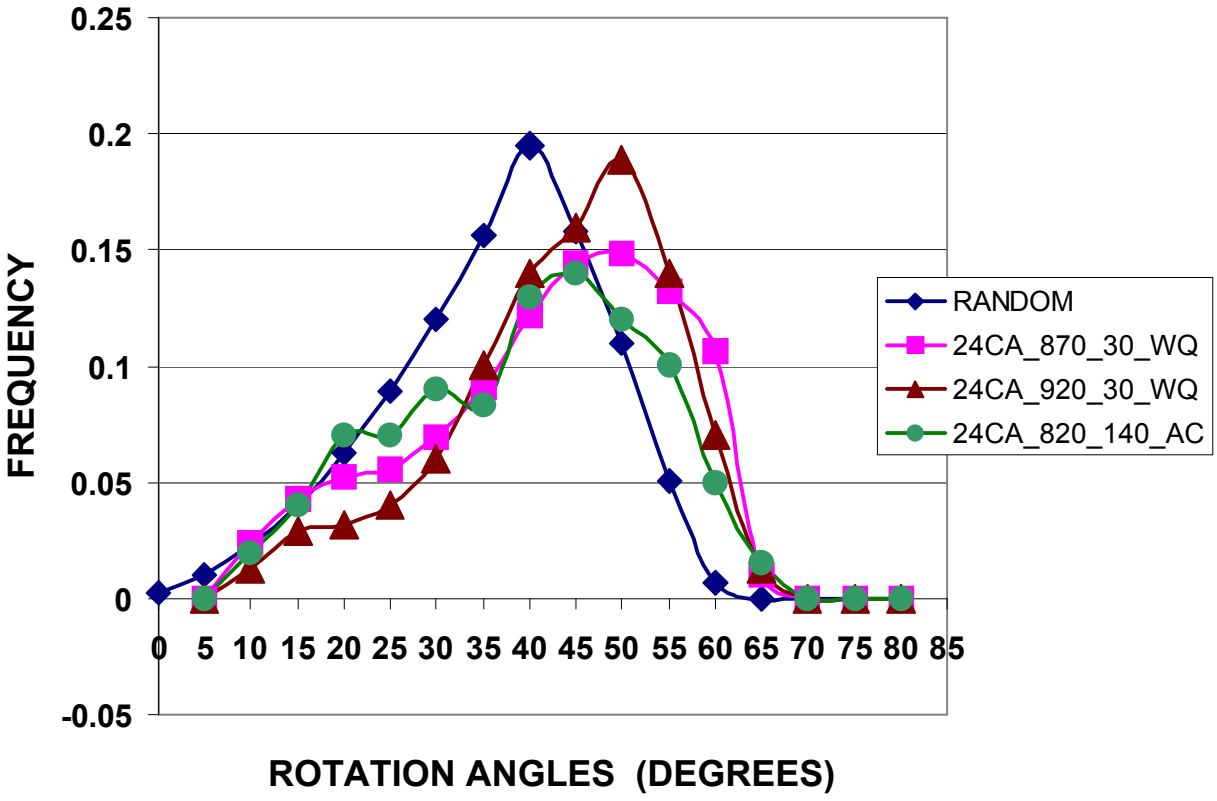

Figure 4. 41 EBSD results of the phase 2 plain carbon (24CA) steel as a function of the various annealing treatments. Comparison of the random mis-orientation with the mis-orientation in the above 3 annealing conditions is shown here.

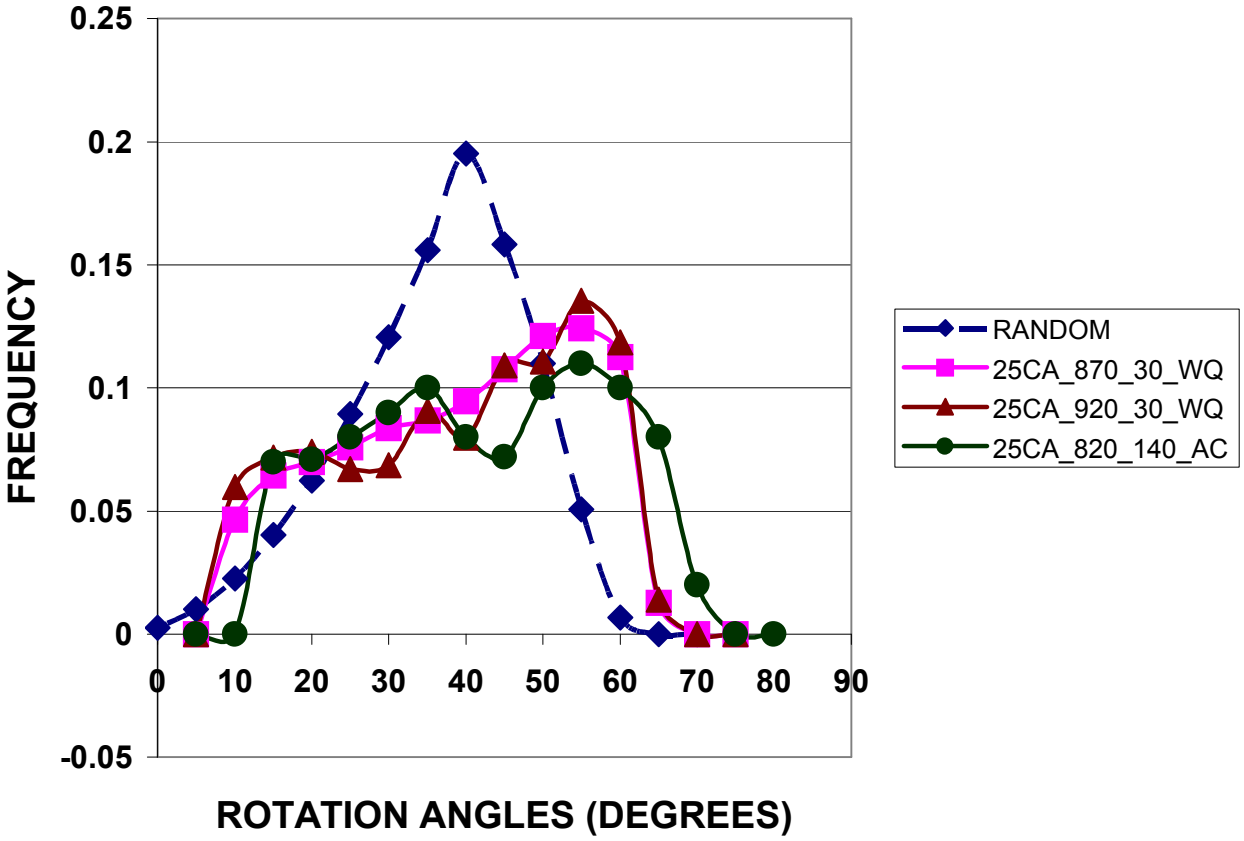

Figure 4. 42 EBSD results of the phase 2 Mo-B (25CA) steel as a function of various annealing treatments. Comparison of the random mis-orientation with the mis-orientation in the above 3 annealing conditions is shown here.

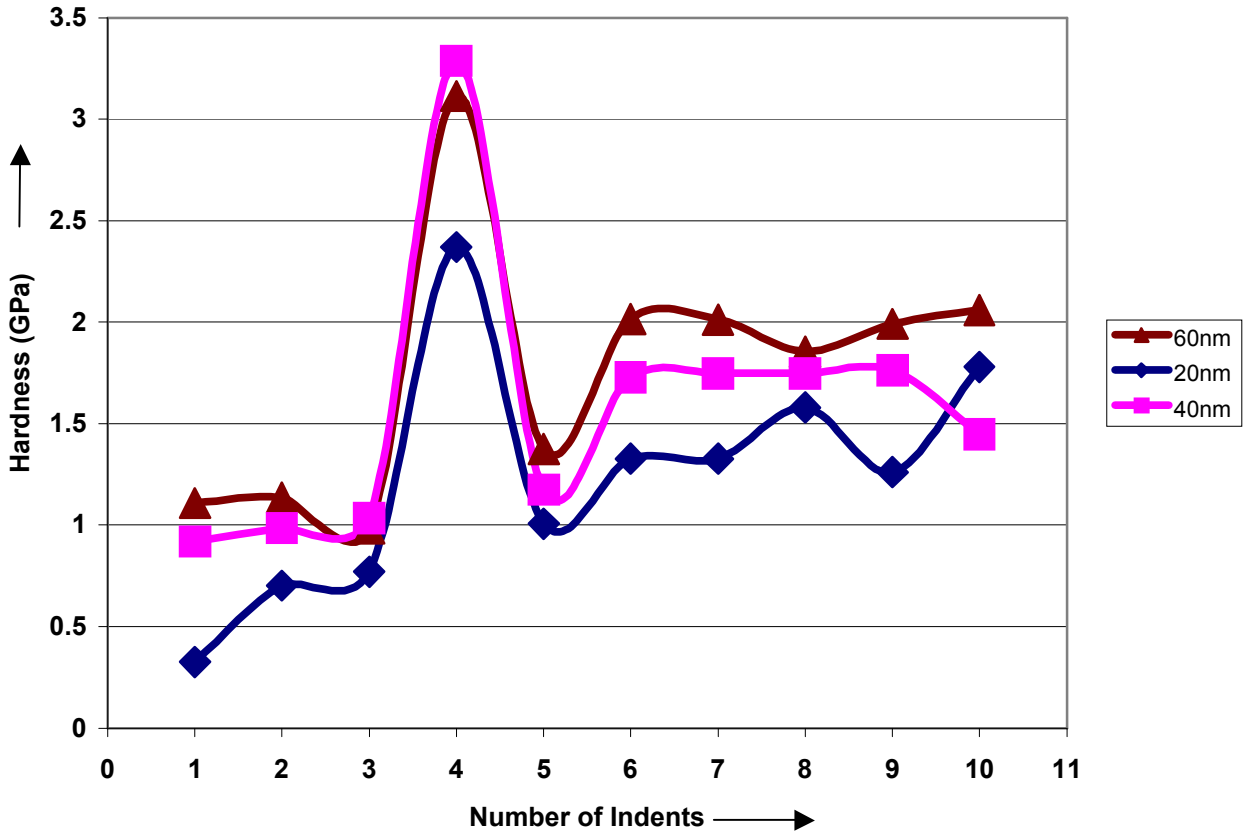

Figure 4. 43 Nano-Hardness measurement results of the phase 2 Mo-B (25CA) steel annealed at 920°C hold for 30 minutes and then ice-water quenched to room temperature. The hardness here is measured as a function of the number of indents and is shown for varying depths of indentations. Position 1 in etched condition is shown here.

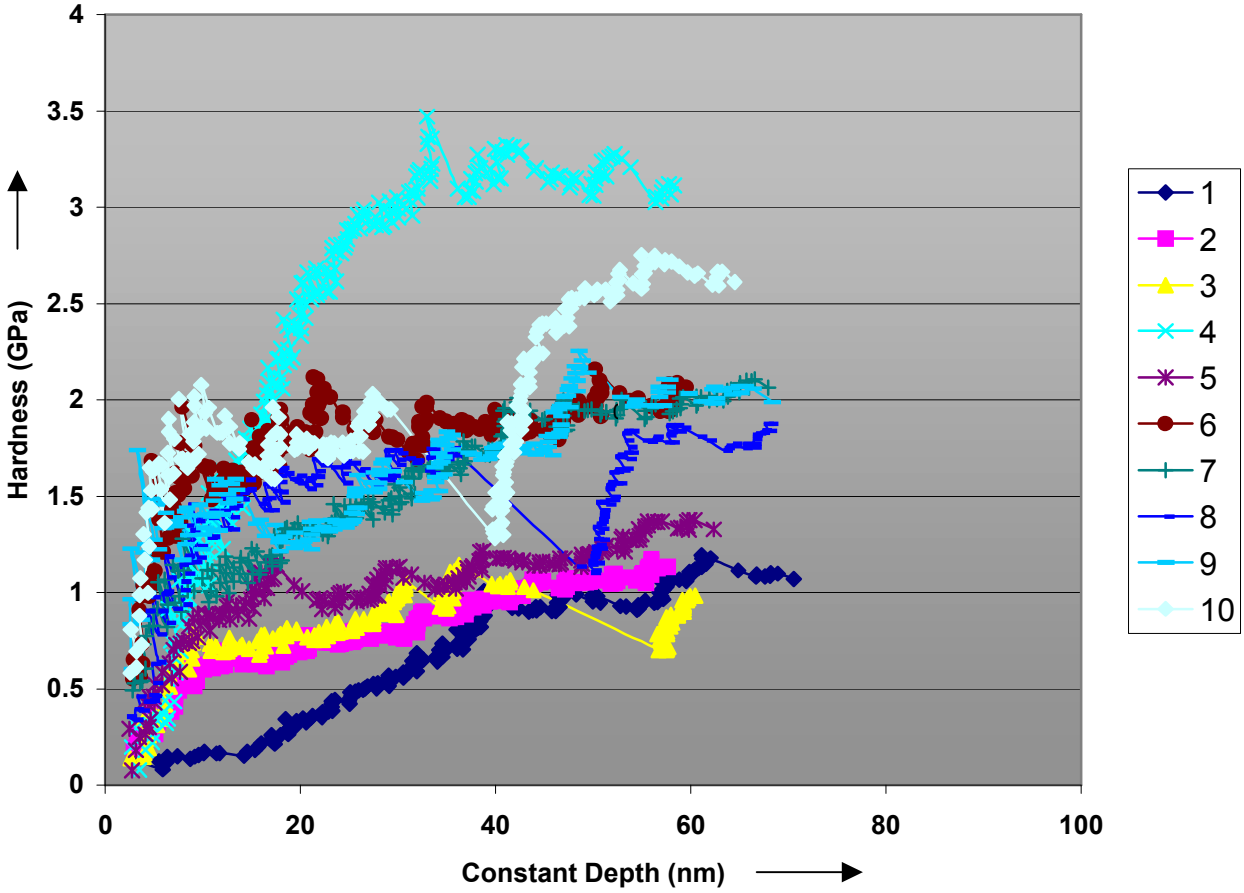

Figure 4. 44 Nano-Hardness measurement results of the phase 2 Mo-B (25CA) steel annealed at 920°C hold for 30 minutes and then ice-water quenched to room temperature. The hardness is measured as a function of the constant depth of indentation and is shown for all the indents. Position 1 in etched condition is shown here.

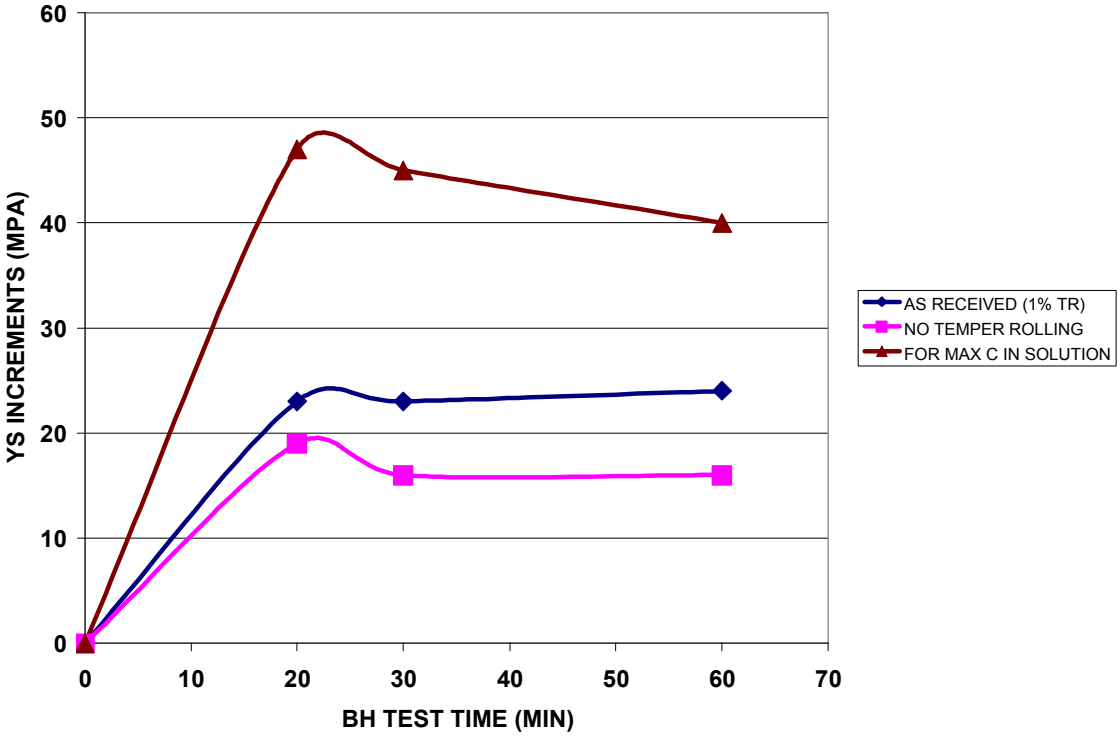

Figure 5. 1 Comparison of BH2 of the commercial phase 1 steels at various annealing conditions namely as-received steel with 1% temper rolling (CR_AR), as-received heat treated to maximize the C in solution (CR_AR_MAX) and as-received heat treated to remove the temper rolling effect (CR_NTR).

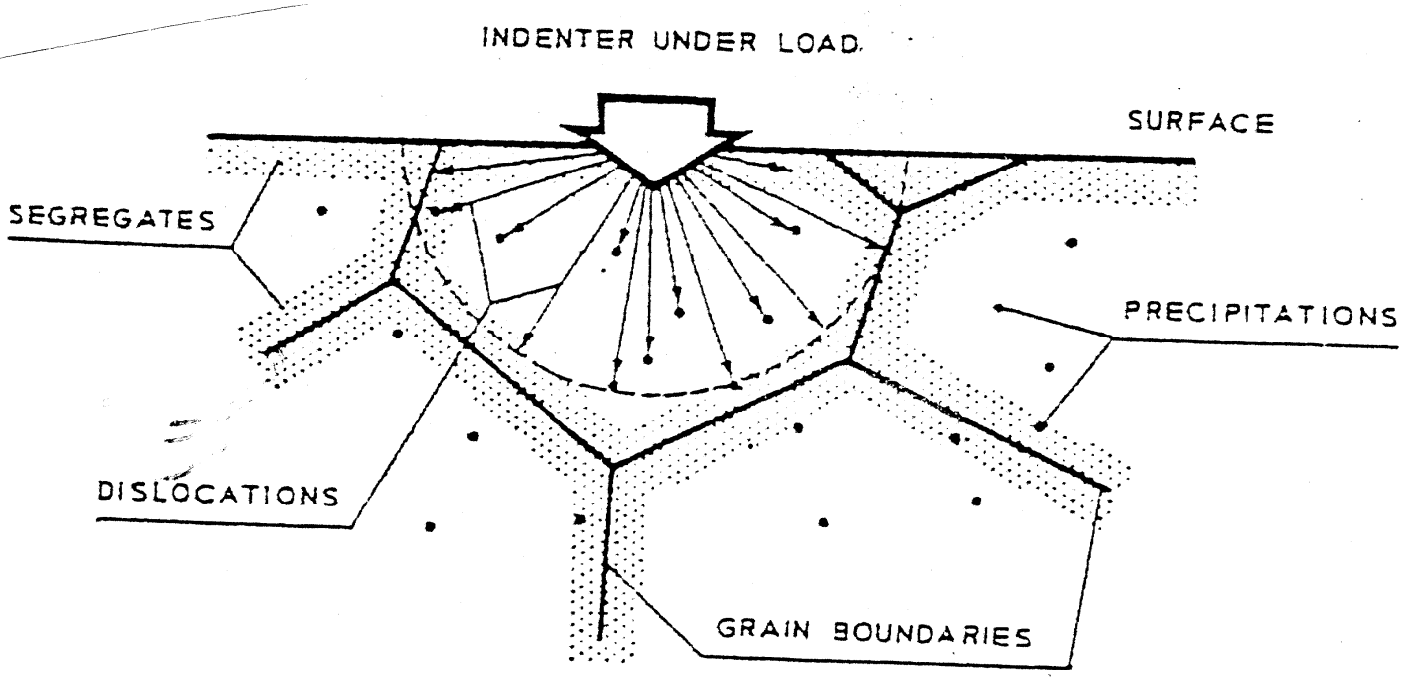

Figure 5. 2 Schematic representation of the penetration mechanism characterizing the depth of indentation [46].

Table 4. 1 Tensile properties of the as-received commercial steel: CR_AR condition. The standard deviations are also mentioned.

SAMPLE	*LYP (MPA)*	*YS @ 0.2% OFFSET (MPA)*	*UTS (MPA)*	*TE(%)*	*YPE (%)*	*N-VALUE (5-0)*	*N-VALUE (10-20)*	*%RA*
2%PRE	0	**229/1.4**	**268/1.1**	2.01	0	0	0	-
5%PRE	0	**229/0.6**	**301/0.9**	5.03	~0	0	0	-
AR	0	**229/1.1**	343/1.6	42.2/0.4	0.01	0.20/~0	0.21/~0	52.2
0% (180/20)	236/1.1	**238/1.0**	342/1.2	42.3/0.3	~0	0.19	0.19	52.1
0% (180/30)	233/0.2	**236/0.6**	342/0.9	41.2/0.8	~0	0.19/~0	0.195	51.9
0% (180/60)	238/2.7	**241/1.5**	344/2.4	40.8/0.3	0.8	0.19	0.192	51.3
2% (180/20)	**291/2.8**	296/2.7	344/1.3	38.1/2.2	1.2	0.15	0.16	50.4
2% (180/30)	**291/0.4**	293/3.2	346/0.5	42.1/1.2	1.1	0.15	0.17	56.2
2% (180/60)	**292/2.7**	293/2.7	348/1.0	41.7/0.8	1.4	0.15	0.17	55.0
5% (180/20)	**317/0.9**	320/1.6	360/0.9	40/1.3	1.6	0.12	0.14	49.3
5% (180/30)	**317/0.4**	322/1.1	355/1.0	35.9/2.4	1.6	0.12	0.145	48.6
2% (180/60)	**319/1.1**	324/2.0	361/2.3	36.6/0.6	1.8	0.12	0.14	50.4

Table 4. 2 Bake hardening and work hardening increments in as-received steel: CR_AR condition. (A) Bake hardening increments, and (B) work hardening increments

(A)

Time (min) @ 180°C Pre- Strain	***0***	***20***	***30***	***60***
0 %	**0**	**9**	**7**	**12**
2 %	**0**	**23**	**23**	**24**
5 %	**0**	**16**	**16**	**18**

ALL INCREMENTS IN STRENGTHS (SHOWN ABOVE) IN MPA

(B)

Pre-strain	**Sample No.**	**Offset @ 0.2%**	**UTS**
2%	*AVG.*	***229***	***268***
5%	*AVG.*	***229***	***301***

WH2 = 268 - 229 = 39 MPA

WH5 = 301 – 229 = 72 MPA

Table 4. 3 Tensile properties of the as-received commercial steel after additional heat treatment to maximize carbon in solution: CR_AR_MAX condition. The standard deviations are also mentioned.

SAMPLE	*LYP (MPA)*	*YS @0.2% OFFSET (MPA)*	*UTS (MPA)*	*TE(%)*	*YPE (%)*	*N-VALUE (5-0)*	*N-VALUE (10-20)*	*%RA*
2%PRE	324/0.5	**333/0.8**	**363/1.0**	2.1/0.16	0	0	0	-
5%PRE	319/0.6	**330/0.8**	**375/0.8**	5.03/0.05	~0	0	0	-
AR	323/0/9	**335/0.6**	410/1.0	33.2/1.0	2.6	0.2	0.18	48.90%
0% (180/20)	**365/0.5**	324/1.0	420/1.2	32.7/1.4	3.5	0	0.2	49.00%
0% (180/30)	**363/0.8**	321/0.9	417/1.2	32.9/1.0	3.6	0	0.2	51.50%
0% (180/60)	**361/0.7**	316/1.0	414/1.1	34.6/0.4	3.8	0.2	0.2	52.30%
2% (180/20)	**410/0.5**	370/0.5	435/4.0	21.7/0.2	2.6	0	0	46.20%
2% (180/30)	**408/1.6**	368/0.8	430/1.4	22.3	1.9	0	0	42.80%
2% (180/60)	**403/0.7**	360/0.9	425	19.47/0.4	1.8	0.13	0	44.50%
5% (180/20)	**408/0.6**	371/1.0	435/0.4	23.7/0.7	3.7	0.12	0.04	50.20%
5% (180/30)	**405/3.0**	365/1.1	431/1.5	25/1.9	3.5	0.11	0.1	51.00%
5% (180/60)	**409/0.4**	371/0.4	440/1.0	23.8/2.41	3.6	0.12	0.145	49.00%

Table 4. 4 Bake hardening and work hardening increments in as-received steel after additional heat treatment to maximize carbon in solution: CR_AR_MAX condition. (A) Bake hardening increments, and (B) Work hardening increments.

(A)

Time (min) @ 180°C Pre- Strain	***0***	***20***	***30***	***60***
0%	**0**	**30**	**28**	**26**
2%	**0**	**47**	**45**	**40**
5%	**0**	**33**	**30**	**34**

ALL INCREMENTS IN STRENGTHS (SHOWN ABOVE) IN MPA

(B)

Pre-strain	**Sample No.**	**Offset @ 0.2%**	**UTS**
2%	*AVG.*	***333***	***363***
5%	*AVG.*	***330***	***375***

WH2 = 363 - 333 = 30 MPa

WH5 = 375 - 330 = 45 MPa

Table 4. 5 Tensile properties of the as-received commercial steel after additional heat treatment to remove the effect of temper rolling: CR_NTR condition. The standard deviations are also mentioned.

SAMPLE	*LYP (MPA)*	*YS @0.2% OFFSET (MPA)*	*UTS (MPA)*	*TE(%)*	*YPE (%)*	*N-VALUE (5-0)*	*N-VALUE (10-20)*	*%RA*
2%PRE	271/0.6	**275/1.2**	**277/1.7**	2.1	0	0	0	-
5%PRE	272/1.1	**275/0.6**	**284/1.9**	5.06	~0	0	0	-
AR	270/0.9	**276/1.1**	365/1.3	40.2/0.4	2.2	0.15	0.15	50.7
0% (180/20)	**286/0.5**	277/1.0	372/1.9	40.7/0.3	2.1	0.2	2	50.1
0% (180/30)	**285/0.4**	270/.6	370/0.8	38.9	2.4	0.19/~0	0.21	50
0% (180/60)	**285/2.1**	268	372/2.4	42.2/0.8	2.3	0.13	0.18	52
2% (180/20)	**296/1.1**	284/0.2	384/1.0	39.7/1.1	1.8	0.15	0.18	48
2% (180/30)	**293/1.2**	280/1.0	380/0.9	38.3	2.1	0.21	0.17	49.1
2% (180/60)	**293/0.8**	279/1.1	381	39	2.5	0.22	0.19	46.2
5% (180/20)	**297/0.8**	275/2.2	385/0.9	37.3	1.9	0.12	0.14	50.2
5% (180/30)	**297/1.1**	277/0.9	383	36/1.1	2.1	0.15	0.17	46
2% (180/60)	**299/2.3**	281	385	37.3	2.3	0.13	0.14	48.2

Table 4. 6 Bake hardening and the work hardening increments in as-received steel after additional heat treatment to remove the effect of temper rolling: CR_NTR condition. (A) Bake hardening increments, and (B) work hardening increments.

(A)

Time (min) @ 180°C Pre- Strain	***0***	***20***	***30***	***60***
0 %	**0**	**10**	**9**	**10**
2 %	**0**	**19**	**16**	**16**
5 %	**0**	**13**	**13**	**15**

ALL INCREMENTS IN STRENGTHS (SHOWN ABOVE) IN MPA

(B)

Pre-strain	**Sample No.**	**Offset @ 0.2%**	**UTS**
2%	*AVG.*	***275***	***277***
5%	*AVG.*	***284***	***275***

WH2 = 277 - 275 = 35 MPa

WH5 = 284 - 275 = 32 MPa

Table 4. 7 Grain size measurements of the commercial steel in the as-received (CR_AR) condition, maximum carbon in solution (CA_AR_MAX) condition and removal of temper rolling effect (CR_NTR) condition. The standard deviations are also mentioned.

PHASE 1 STEEL CONDITION	PROCESSING TREATMENTS	GRAIN SIZE (IN μM)
CR_AR	AS-RECEIVED (1.0% TEMPER ROLLED	15μM (1.2)
CR_AR_MAX	ANNEALED TO 715°C + 30 MIN HOLD + WATER-ICE QUENCH (C MAX IN SOLUTION)	9.8μM (0.9)
CR_NTR	750°C + 10 MIN HOLD + AIR COOLED.(AS-RECEIVED STEEL WITH NO TEMPER ROLLING)	14.5 (1.5)

Table 4. 8 Description of the various annealing treatments given to both the laboratory phase 2 steels: plain carbon steel (24CA) and Mo-B steel (25CA).

PHASE 2 STEEL	ANNEALING TEMPERATURE (°C)	HOLDING TIME (MIN)	COOLING CONDITION
PLAIN C STEEL (24CA)	820	140	AIR COOL
PLAIN C STEEL (24CA)	870	30	WATER-ICE QUENCH
PLAIN C STEEL (24CA)	920	30	WATER-ICE QUENCH
ALLOY STEEL (25CA)	820	140	AIR COOL
ALLOY STEEL (25CA)	870	30	WATER-ICE QUENCH
ALLOY STEEL (25CA)	920	30	WATER-ICE QUENCH

Table 4. 9 Description of the bake hardening and the work hardening increments at 2% pre-strain for the phase 2 plain carbon (24CA) steel as a function of the various annealing treatments.

Heat Treatment (temp.(°C)/time (min)/cooling condition)	BH2 (MPA)	WH2 (MPA)
920/30/water-ice quench	60	28
870/30/water-ice quench	55	15
820/140/air-cool	18	4

Table 4. 10 Description of the bake hardening and the work hardening increments at 2% pre-strain for the phase 2 Mo-B (25CA) steel as a function of the various annealing treatments.

Heat Treatment (temp.(°C)/time (min)/cooling condition)	BH2 (MPA)	WH2 (MPA)
920/30/water-ice quench	72	33
870/30/water-ice quench	62	28
820/140/air-cool	24	10

Table 4. 11 Grain size measurements of the various annealing treatments given to both the laboratory phase 2 steels (A) plain carbon steel (24CA) and, (B) Mo-B steel (25CA). The standard deviations are also mentioned.

(A)

Heat Treatment (temp.(°C)/time (min)/cooling condition)		**Grain Size (μm)**
920/30/water-ice quench		17.2 (0.8)
870/30/water-ice quench		11.1 (0.7)
820/140/air-cool		12.2 (0.8)

(B)

Heat Treatment (temp.(°C)/time (min)/cooling condition)		**Grain Size (μm)**
920/30/water-ice quench		26.1 (1.3)
870/30/water-ice quench		17.9 (0.9)
820/140/air-cool		14.0 (0.6)

Table 5. 1 The relation between the increments in nano-hardness level at the grain boundary region with the mis-orientation of the grains for different steel conditions is shown.

Type of Steel	**Heat Treatment (temp.(°C)/time (min)/cooling condition)**	**Nano-hardness increment (in ΔGPA)**	**Grain mis-orientation (θ)**
Phase 1 commercial steel (CR_AR_MAX): position 1	750/30/water-ice quench	3.3	53
Phase 1 commercial steel (CR_AR_MAX): position 2	750/30/water-ice quench	2.9	48
Phase 2 Alloy steel	920/30/water-ice quench	2.1	43

APPENDIX A

NANO-HARDNESS TECHNIQUE

A.1 NANO-HARDNESS MECHANICAL PROPERTY MEASUREMENT

Measuring mechanical properties of materials is an extremely important part of the engineering design process. Mechanical testing techniques such as tensile test, creep test, and impact test have been well developed for examining specimens in bulk form. Smaller scale testing can be achieved using techniques such as the micro-hardness and micro-tensile test. However, for the last decade, there has been an increasing demand to measure mechanical properties at a much smaller scale [68-70].

A new technique capable of measuring the mechanical properties of a small volume of material is the nano-indentation technique. As the name applies, nano-indentation is an indentation technique which measures mechanical properties by making indentations at a nanometer scale. Nano-indentation is performed by an instrument such as the Nanoindentor II^{TM}, which continuously records the applied load, P, and the penetration depth of the indenter, h, into the specimen [68].

With proper calibration and instrumentation, indentations with depth as small as 20nm can be made. Relating the experimentally recorded load and displacement information to more useful parameters, such as the indentation area, hardness, and

elastic modulus, has been the major concern of load and displacement sensing indentation development.

A.2 EFFECT OF THE INDENTER GEOMETRY ON HARDNESS AND ELASTIC MODULUS MEASUREMENT

The measurement of mechanical properties such as hardness, H, and elastic modulus, E, by nano-indentation methods, has been conducted largely with indenters having the Berkovich or spherical geometries. The Berkovich indenter, a three sided pyramid with the same area-to-depth ratio as the Vickers indenter commonly used in micro-indentation testing, is useful in experiments where full plasticity is needed at very small penetration depths, such as the measurement of hardness of very thin films and surface layers. The spherical indenter, on the other hand, is useful when purely elastic contact or the transition from elastic to plastic contact is of interest.

Of the many sharp indenters, the Berkovich has proven the most useful in nano-indentation work. This is because the three-sided pyramidal geometry of the Berkovich naturally terminates at a point, thus facilitating the grinding of diamonds, which maintain their sharpness to very small scales.

Berkovich tip defects, as characterized by the effective tip radius, are frequently less than 50 nm in many of the better diamonds. For the Vickers indenter, on the other hand, it is more difficult to maintain geometric similarity at such small scales because the square based pyramidal geometry does not terminate at a point but rather at a "chisel" edge. The conical indenter is the most difficult to grind, and as a result, conical diamonds often have severe tip rounding [68].

A.3 INDENTATION SIZE EFFECT (ISE)

Over the last few decades, it has been demonstrated that the hardness of some bulk materials measured by conventional techniques or by instrumental indentation depends on the load or indentation depth. The usual observation is that the hardness increases as the load or indentation depth decreases. The change in hardness can be as much as a factor of 4. This indentation size effect (ISE) has been documented in several reviews.

There are many explanations for the ISE. Tabor has suggested that some of the ISE observations may be due to poor resolution of the indenter or statistical error. Upit and Varchenya et al., [78] suggested that the increase in the apparent hardness is due to the extra energy to egress dislocations to the surface at small indentation depths. An ISE caused by friction between the indenter and the specimen has been suggested by Atkinson and Li et al. Braunovic and Haworth suggested that polishing can affect an ISE, since mechanically polished samples have a more pronounced ISE than those electrolytically polished. An ISE caused by tip rounding effect has also been proposed.

Fleck et al., [79] have developed a model for strain gradient plasticity, which has recently been proposed as another possible origin of the ISE. This model states that in addition to the "statistically stored dislocations," plastic shear gradients result in the storage of "geometrically necessary dislocations". The density of the "Geometrically Necessarily Dislocations (GNDs)", ρ_g, can be expressed as:

$$\rho_g \sim 4\Upsilon / b\lambda$$

Where ϒ is the macroscopic plastic shear strain, b is the magnitude of the Burger's vector, and λ is a local length scale, which is related to the indentation size. As λ decreases, i.e., for smaller indentations, the density of the "GNDs" increases, which in turn increases the shear yield stress in materials subjected to strain hardening.

Ma and Clark applied this model to hardness data obtained from an epitaxially grown silver film and obtained very good agreement. They also performed TEM imaging of the indentations and found an extremely high concentration of dislocations at the edges and the apex of the indentation but very few dislocations in the face region. De Guzman et al. investigated the ISE in copper, nickel and metallic glass. They suggested that the ISE is real for materials, which can strain harden, and that it is caused by the GNDS. They suggested that at shallow depths, the dislocations from over a relatively small volume, resulting in a higher dislocation density and apparent hardness. As the indentation size increases, the volume over which they are distributed becomes greater, and this reduces the apparent hardness.

In spite of careful measurements to calculate hardness using the calibrated area function, the most confusing result of the hardness tests is the ISE. Hardness in nano-indentation tends to be overestimated compared with the conventional hardness, even after the area function is calibrated. It was also reported that the overestimation is not only limited to nano-indentation, but occurs in low- load Vickers tests.

If the ISE exists as long as hardness is defined as the result of load divided by contact area, the "unaffected" hardness must be evaluated for engineering purposes, because it is the unaffected hardness that has good correlation with other mechanical properties [68-70].

The purpose of electrolytic polishing is to diminish the surface- deformed layer introduced during mechanical polishing. It has been reported that soft, strain-hardenable metals can depend strongly on the depth of the indentation, and that hard,

finely structured materials depend less on, or do not vary significantly with, the depth of the indentation. Although this may be an intrinsic nature of the size effect, the limited dependency of hard, finely structured materials can be explained as the contribution of non-uniformity reduces or negates the amount of the size effect [68-70].

One of the major obstacles to understanding the indentation size effect has been the dearth of good experimental data describing it.

APPENDIX B

CLASSIFICATION OF ULC BAKE HARDENABLE STEELS

Bake hardenable steels can be classified on the basis of the ratio of carbon to the carbide forming elements such as titanium, niobium and vanadium. A number of approaches, which control thermal history and alloy content, have been developed to control dissolved C and N levels to obtain optimum bake hardening in ultra-low carbon steels.

B.1 FULLY STABILIZED BH STEELS

Typical fully stabilized BH steel is Nb-added ULC steel. The Nb/C ~1.0 steel was first processed by hot rolling and coiling at a temperature higher than 600°C, resulting in the stabilization of almost all C and N as NbC and AlN, respectively. After cold rolling and heating above the recrystallization temperature (~750°C), an intense {111} recrystallization texture develops. NbC and AlN are still stable at this temperature. Further heating above 850°C results in the dissolution of NbC. At this stage, the influence of solute C on the texture development is negligible since this stage

corresponds to the growth of the recrystallized grains. On the other hand, AlN dissolves little at this temperature.

Hence, according to the foregoing principle, sheet steel having both bake hardening and extra deep drawability can be produced. But high temperature annealing and subsequent rapid cooling leads to problems such as heat buckling. In addition, processing conditions must be strictly controlled to minimize the deviation of solute C. Other examples of the fully stabilized steels are Ti-Nb ULC steels and V-added IF steels [1, 6-7, 20-21, 73, 77].

B.2 PARTIALLY STABILIZED BH STEELS

Typical partially stabilized BH steel is a Ti added ULC steel. The variation of precipitates along with the steel chemistry and production conditions is the controlling factor of the degree of stabilization. In this process, it is difficult to control the solute C by adjusting the C, Ti and S contents at the same time because Ti forms complex precipitates, such as TiN, TiS, $Ti_4C_2S_2$, TiC, and FeTiP.

Ideally, if all the above processing parameters are properly controlled, Ti is completely tied up with N and S, Mn combines the remaining S as MnS, and the total C content is available for bake hardening. In other cases, the C is partially stabilized via formation of either TiC or $Ti_4C_2S_2$ and therefore is less available for bake hardening. Therefore, chemical composition must be strictly controlled to minimize the deviation of solute contents [1, 6-7, 20-21, 73, 77, 80-81].

APPENDIX C

FORMABILITY OF ULTRA LOW CARBON STEELS

The steel properties leading to good formability are relatively low yield stress, suitable texture to give an r-value greater than one, zero yield point extension or Lüders strain and high n-value in the Holloman equation $(\sigma = k(\varepsilon)^n)$. The latter two properties are strongly influenced by temper rolling of the steel prior to delivery to the stamping plant.

Many important intrinsic factors influence formability such as yield strength, n-value, m-value and r-value. These factors can be somewhat interrelated and, with the effect of geometry, influence obtainable formability as indicated by changes in the forming limit diagram. The most important factor is the n-value. Together with thickness, the n-value determines the FLC_o position of the forming limit diagram. The following equation is found valid for conventional BH, IF, AKDQ as well as for other medium steels.

$$FLC_o = (n/0.21).[23.3 + 359t]$$

Where n is the n-value from a tension test and t is the as-received sheet thickness. The relationship for the n-value and the m-value is particularly relevant for BH steels [7, 91-93]. Steels with higher m-value resist the onset of diffuse necking leading to higher uniform elongation values. The higher rate sensitivity generally leads to higher n-values.

However, dissolved C tends to decrease m-value through the dynamic strain aging process. It has been established that lowering the tensile test temperature or decreasing the dissolved carbon content both increase uniform elongation in ultra-low C steels [7, 35].

For sheet steel, the strain hardening capacity can be defined by the strain-hardening component, *n*. A sheet metal with higher n-value exhibits better stretchability. Lankford et al., found that the deep drawability of the sheet was related to a parameter called a strain ratio, *R*, which is defined as

$$R = \varepsilon_w / \varepsilon_t$$

Where ε_w and ε_t are the width and the thickness strains respectively.

Later, Whiteley defined the parameter, *R*, the average strain ratio, which is determined by this equation:

$$R = (R_0 + 2R_{45} + R_{90}) / 4.$$

Where R_0, R_{45} and R_{90} are the *R*-values measured at *0°, 45°* and *90°* respectively to the rolling direction.

The R-value reflects the degree of normal anisotropy present in the sheet material. If the strength normal to the sheet is greater than the average strength in the plane of the sheet, the R-value is greater than unity.

Based on the data obtained from various sources of literature, Hutchinson et al., showed that the carbon content in the steel significantly influenced the R-value of the sheet steel. This is because as the carbon content is lowered, favorable {111}<uvw> texture components are produced [36, 61-64, 86, 91].

Post baking yield stress increases with C (dissolved C content) in the steel. However, if C is much greater than 25-wt-ppm then undesirable strain aging occurs at room temperature leading to unacceptable yield point strain and poor surface quality of the stamping.

Consequently, the need for room temperature stability limits C and the amount of bake hardening that may be achieved. Slowing the diffusion of C would be one possibility and a study of the effect of alloying elements on the diffusion of C is recommended.

APPENDIX D

DENT RESISTANCE

Currently, bake hardening steels are frequently used for outer panels as well as for structural parts to reduce weight. These grades combine good formability with an additional increase of strength caused by the moderate heat treatment during baking in the paint shop. A reduction in weight can be reached by an adequate design and the reduction of sheet thickness using high strength steel sheets.

One of the design criteria for the selection of materials for outer panels is the dent resistance. Dent resistance of an outer body panel is a complex function of design, strain path employed during forming, assembly characteristics and of course, the material. Previous investigations determined a correlation between sheet thickness, yield strength and the load F at which the first plastic deformation is detected.

This correlation for the dent force was established as:

$$F = t^n \cdot (R_p^{0.2})^m$$

Where t is the sheet thickness, $(R_p^{0.2})^m$ the yield strength and the parameters n and m depend on the geometry of the considered part.

Many conflicting properties are desired for the sheet steel used for the outer body of the automobiles. Denting resistance requires higher strength steel than desired for

formability. For acceptable surface after forming, there must be zero yield point elongation. In addition, a high work hardening rate is desired. On the other hand, dent resistance requires a high proportional limit. These conflicting properties can be achieved by temper rolling the steel to an approximate reduction in thickness of 0.9%, which induces mobile dislocations and residual stress from grain to grain. The resulting stress –strain curve is rounded with a low proportional limit. Such strain aging is to be encouraged in the paint bake-curing step but must be subsequently prevented before the stamping operation. This puts a limit on the useful paint bake hardening that can be achieved.

Proper dent resistance in a body panel is necessary to minimize permanent damage that might occur during in-plant and in-service handling situations. In service flying rocks and road debris, hailstorm, impacts in parking lots, etc., may create dents. In-plant handling damage may occur due to one panel hitting another during transit, or during repair and assembly operations. Because metals are often strain rate sensitive, it is no surprise that the response of a panel to a projectile impact (flying objects) is different than under near static load conditions. One must therefore distinguish between static and dynamic dent resistance.

Prior work in this area indicates that the static dent resistance decreases with increase in stiffness, but increases with increase in thickness and yield strength of the panel. Thus, for the same panel design, increasing the thickness of the steel is effective in increasing both stiffness and dent resistance. Since increasing the thickness has a weight penalty associated with it, the use of high strength steel for improving dent resistance of the panel may be both weight and cost effective [2, 11, 15, 34, 92-93].

The dynamic dent problem is more complicated. Clearly, the denting energy will increase with impact velocity for the same mass. However, steels in particular have positive strain coefficients. Thus, yield strength of a steel panel increases with increasing impact velocity.

To a first approximation, it appears that a design satisfying the dent resistance criteria will meet the dynamic denting criteria as well for steels.

APPENDIX E

A MODEL FOR THE COTTRELL ATMOSPHERE FORMATION

Cottrell and Bilby analyzed the kinetics of the segregation of carbon atoms to dislocations. They developed equation (1) to describe the formation of the so-called Cottrell atmosphere surrounding dislocations.

$$N(t)/N_0 = (3/2).n_o.\lambda.V_{dis}.t^{(2/3)} \quad \ldots\ldots\ldots\ldots\ldots\ldots\ldots\ldots\ldots\ldots (1)$$

Where $N(t)$ is the number of carbon atoms diffusing to dislocations in a unit volume within time t, N_0 is the dislocation density, n_0 is the initial concentration of carbon in solution, and λ is the slip distance of the dislocation. $V_{dis} = 2.(\pi/2)^{(1/3)}.(A.D/k.T)^{(2/3)}$ with D being the diffusion coefficient of carbon, k the Boltzmann constant , T the absolute temperature and A, a parameter defining the magnitude of the interaction between the dislocation and the carbon atom.

It is well known that equation (1) is applicable only in the early stage of the formation of Cottrell atmosphere. As the dislocations are saturated, the back diffusion of carbon from the core region will tend to counter balance the inward flow due to the drift force, and also the relief of the dislocation stresses by the segregated atoms reduces the drift force. Therefore equation (1) gives an overestimate of the aging rate when $N(t)/N_0 > 0.3$ [13, 22].

Harper tried to modify Cottrell's theory. He developed equation (2) by assuming that the rate of segregation of interstitial atoms was proportional to the fraction remaining in solution. However, it has been found that his model is not really applicable to the investigation of the formation of Cottrell atmosphere.

$$Q = 1\text{-}\exp[-(3/2).L_0.V_{dis}.t^{(2/3)}]\ldots\ldots\ldots\ldots\ldots\ldots\ldots\ldots(2)$$

Where q is the fraction of the original amount of free carbon, which has precipitated during time t, $L_0 = \lambda/N_0$ is the dislocation length per unit volume.

Hence, a model was developed almost a year ago at Ghent University, Belgium, which aimed to properly describe the Cottrell atmosphere formation during aging of an ultra low carbon bake hardening steel. This model takes into account the variation in the concentration of carbon in solution, the saturation of the dislocations and the segregation of carbon to grain boundaries. The model was compared with the experiments carried out with ultra low carbon bake hardenable steel. It was demonstrated that the model developed could describe the formation of Cottrell atmosphere in ULC bake hardenable steels in industrial applications.

The model can be applied to predict the carbon redistribution during a thermal circle for continuously annealed ultra low carbon bake hardenable steel in which there are no pre-existing carbide particles. Calculations were carried out for a steel of 15 wt-ppm carbon content.

It was assumed that initially 99% of the distorted positions in grain boundaries were occupied by carbon atoms. The calculated dimensionless average carbon concentration in grains, $<n>/n_{steel}$, with n_{steel} being the atomic concentration of carbon of the steel, as well as the fractions of the positions in grain boundaries occupied by carbon atoms, C_b, is the saturation level of dislocations at the center of the grain,

$N(r=0)/N_0$, for the continuously annealed process and the followed bake hardening process [13, 22, 42, 54].

Without going into the details of their work, the final result can be put mathematically as:

$$N(t)/N_0 = [1-\exp\{(3/2).(L_0-n_0.\lambda).V_{dis}.t^{(2/3)}\}] / [1-(N_0/n_0).\exp\{(3/2).(L_0-n_0.\lambda).V_{dis}.t^{(2/3)}\}]$$

The above equation has been obtained by integrating the final equation as shown below:

$$\Delta N(t) = L(t).n(t).V_{dis}.\{\Delta t/ t^{(1/3)}\}$$

Where $L(t) = L_0-n_0.\lambda N(t)$ is the length of the effective dislocations. The instantaneous segregation of carbon atoms to dislocations is proportional to the length of the effective dislocations, $N(t)$, and the concentration of the free carbon atoms, $n(t)$. The time $t=0$ describes the formation of Cottrell atmosphere without the onset of carbon segregation to grain boundaries.

The only assumption on which the model is based is that it assumes the dislocations to be homogeneously distributed in the steel. This assumption is reasonable when the pre-strain is smaller than 5% and, therefore, no cell formation has yet occurred in the grain. This is very likely the case in most applications for bake hardening steels.

The various conclusions that can be drawn from the modeling are:

- The effect of the segregation of carbon to grain boundaries increases with the decrease of grain size. It has only a negligible small effect when the average grain diameter is larger than 16μm.

- Changing the dislocation density within a considerable range does not affect the formation of Cottrell atmosphere due to the fact that generally the dislocation density is much smaller than the concentration of free carbon in bake hardening steels in typical applications.
- The model developed can be applied to predict the carbon redistribution in a continuously annealed ULC bake hardening steel in which there are no pre-existing carbide particles.

BIBLIOGRAPHY

1. L.J.Baker, S.R.Daniel, J.D. Parker; *Metallurgy and processing of ultra low carbon bake hardening steels*; Materials Science and Technology; Vol.18; April 2002; 355-368.

2. J.Christen, J.M.Rubianes; The bake hardenable steels for automotive outer body panels: Correlation between the BH measurement and the dent resistance; 40th MWSP Proc. ISS; 1998; 77-81.

3. S.Kim; Effect on the chemical composition and processing variables on the bake hardenability of ULC high strength steel; Research work in BAMPRI and POSCO.

4. W.C.Leslie; The physical metallurgy of steels; 1981 (first published).

5. J.J.M.Exebio; Metallurgical phenomena governing the bake hardening response of bake hardenable steels; Literature Review; December 2001.

6. S.Satoh, S.Okada, T.Kato, O.Hashimoto, T.Hanazawa,H.Tsuenekawa; Development of bake hardening high strength cold rolled sheet steels for automobile exposed panels; Kawasaki Steel Technical Report No. 27; Nov. 1992; 31-38.

7. R.P.Foley, M.E.Fine, S.K.Bhat; *Bake hardenable steels: Toward improved formability and strength*; 39th MWSP Conf. Proc., ISS; VOL35; 1998; 653-666.

8. D.Vanderschueren, S.Vandeputte; *Industrial development of IF high strength steels with and without BH*; 40th MWSP Conf. Proc. ISS; 1998; 205-211.

9. R.P.Foley, D.Matlock, G.Krauss; *Metallurgical review of processes for obtaining strength and r value in galvanized sheet steels*; 42nd MWSP Conf. Proc. ISS; Vol. 38; 2000; 455-469.

10. A.J.Jones, R.P.Foley; *Effects and measurements of interstitial C and N in iron and steel*; 39th MWSP Conf. Proc., ISS; Vol.35; 1998; 955-969.

11. P.Belanger, J.Singh, P.Badgley, L.Rado; *Evolution of IF based steel for exposed applications at Daimler-Chrysler in North America*; Daimler Chrysler report; sometime after 1998.

12. W.A.Shalfan, J.G.Speer, D.K.Matlock, S.Kim, H.Ledbetter; *Internal Friction measurements of ultra- low carbon sheet steels*; 42nd MWSP Conf. Proc., ISS; Vol.38; 2000; 741-753.

13. A.K.De, B.Soenen, B.C.De Cooman, S.Vandeputte; *Carbon distribution between matrix, grain boundaries and dislocations in ultra low carbon bake hardenable steels*; 42nd MWSP Conf. Proc., ISS; Vol.38; 2000; 595-606.

14. K.Yamazaki, T.Horita,Y.Umehara, T.Morishita; *Manufacturing condition and automotive use of bake hardenable steel sheets*; Nippon Steel and Toyota Motor Corporation; 327-337.

15. M. Blainscheuin, K.M. Radlmayr, A.Pichler, E.T.Stiaszny; *Bake hardening effect in components*; Proceedings of the 19th Biennail IDDRG Congress; 10-14th June; 1996; 445-458.

16. A.H.Cottrell, B.H.Bilby; Proc. Phys. Soc.; Vol.62; 1949; 49-62.

17. K.Sakata, S.Satoh, T.Kato, O.Hashimoto; *Metallurgical principles and their applications for producing extra low carbon IF steels with deep drawability and bake hardenability*; Invited lecture; May 10-11th 1994; 279-288.

18. H.Takechi; *Metallurgical aspects of IF sheet steel from industrial viewpoints*; Invited lecture; 10th -11th May 1994; 1-8.

19. G.Krauss, D.Wilshynsky, D.Malock; *Processing and properties of IF steel*; Research at CSM.

20. D.K.Matlock, B.J.Allen, J.Speer; *Aging behavior and properties of ultra low carbon bake hardenable steels*; International Symposium-Conf. Book; Vol. 1; March 30th- April 1st; 1998; 265-276.

21. F.D.Bailey, R.P.Foley, D.K.Matlock; *Processing and prestrain path effects on the strain – aging behavior of a batch- annealed bake hardenable sheet steel*; High Strength Steels For Automotive Symposium Proceedings; 1994; 119-133.

22. J.Zhao, A.K.De, B.C. Cooman; *A model for the Cottrell atmosphere formation during aging of ultra low carbon bake hardenable steels*; ISIJ; Vol.40; No.7; March 22; 2000; 725-730.

23. O.Yakubovsky, N.Fonstein, D.Bhattacharya; *Stress- strain behavior and bake hardening of TRIP and TRIP aided multiphase steels*; Int. Conf. on TRIP- Aided high strength ferrous alloys; 263-270.

24. C.C.Cheng; *Galvannealing behavior and coating performance of Ti-IF and Nb-Ti-IF steels*; 42nd MWSP Conf. Proc., ISS; Vol.38; 2000; 255-263.

25. E.Hoggan, G.Mu Sung; *Cold rolled batch annealed bake hardening steel for the automotive industry*; 39th MWSP Conf. Proc. ISS; Vol. 35; 1998; 17-29.

26. R.W.Rathbun, D.Matlock, J.Speer; *Strain aging behavior of austenitic stainless steels containing strain induced martensite*; Scripta Materialia; Vol. 42; Issue 9; 14th April 2000; 887-891.

27. G.P.DiCostanzo, D.Matlock, R.P.Foley; *Effect of tensile properties on dent resistance of sheet steels*; SAE technical paper series; 1996; 42-53.

28. T.Wubbel; *The effects of room temperature aging on the deformation behavior and strength increase in bake hardening steels*; Diploma Thesis; Colorado School of Mines; 2001.

29. W.Shalfan; *Bake hardenability of microalloyed ULC steels*; Ph.D. Thesis; Colorado School of Mines; 2001.

30. G.M.Sung; *Bake hardening steels for the Australian automotive industry*; Prepared discussion; May 10-11th 1994; 275-278.

31. F.D.Bailey; *Effects of mill processing and pre-strain mode on the aging behavior of a commercially produced bake hardenable steels*; M.S.Thesis; 1994.

32. L.Storojeva, C.Escher, R.Bode, Hulka, D.Burko; *Effect of Nb/C ratio and processing conditions on aging behavior and BH-effect of ULC sheet steels*; 2000.

33. B.Wildemeersch, J.Penning, A.K.De, S.Vandeputte; *Influence of the grain size on the mechanical properties of Ti-ULC steel*; Belgium; 1-6.

34. R.A.Hubert, S.Vandepute, A.Snick, C.Xhoffer; *Towards a controlled bake hardening by numerical calculation of the precipitate behavior during continuous annealing of TiNb and Nb alloyed IF BH steels*; Material Science forum; Vols –284-286; 1998; 551-558.

35. X.Chen; R.P.Foley; *Effects of cold rolling reductions, solute carbon content and strain rate on the tensile properties of a 0.04wt% carbon AKDQ steel*; 40th MWSP Conf. Proc, ISS; Vol.35; 1998; 889-898.

36. B.Hance, R.P.Foley, D.Matlock; *Effects of strain path on formability and microstructural evolution in low carbon sheet steels*; SAE 970155.

37. X.Fang, Z.Fan, B.Ralph, P.Evans, R.Underhill; *Effect of temper rolling on tensile properties of C-Mn steels*; Materials Science and Technology; Vol.18; March 2002; 285-289.

38. R.D.Butler, D.V.Wilson; *The mechanical behavior of temper rolled steel sheets*; Journal of the Iron and Steel Institute; January 1963; 16-33.

39. C.Lee, B.K.Zuidema; *The effects of mill processing conditions on the mechanical behavior of bake hardenable steels*; High Strength Steels for Automotive Symposium Proceedings; 1994; 103-110.

40. M.A.Meyers, C.Chawla; *Strengthening Mechanisms- Grain size strengthening*; Part III; Chapter 14; 495-515.

41. J.P.Hirth; *The influence of grain boundaries on mechanical properties*; Metallurgical Transactions;Vol.3; December 1972; 3047-3066.

42. J.M. Papazian, D.Beshers; *Grain boundary segregation of carbon in iron*; Metallurgical Transactions; Vol.2; Feb 1971; 497-503.

43. D.V.Wilson, B.Russell; *The contribution of atmosphere locking to the strain aging of low carbon steels*; Acta Metalurgica; Vol.8; January 1960; 36-45.

44. P.J.Wray; *Recent advances in grain boundary characterization and some implications for ULC steel research*; Jan 12; 2000.

45. K.J.Kurzydlowski, B.Ralph, J.J.Bucki, A.Garbacz; *The grain boundary character distribution effect on the flow stress of polycrystals: The influence of crystal lattice texture*; Materials Science and Engineering A205; 1996; 127-132.

46. M.Braunovic, C.W.Haworth; *On the phenomena of grain- boundary hardening in iron*; Journal of Materials Science; Vol.9; 1974; 809-820.

47. B.Mintz, H.Ke, G.D.W.Smith; *Grain size strengthening in steel and its relationship to grain boundary segregation of carbon*; Materials Science and Technology; Vol.; June 1992; 537-540.

48. K.Tatsumi, N.Okumura, S.Funaki; *Dependence of grain boundary segregation of phosphorus on temperature and grain boundary misorientation in α iron*; Grain boundary Structure and related Phenomena Proceedings of JIMIS-4; 1986; 427-434.

49. V.C.Shah, G.J.Wenzolff, P.J.Belanger; *Automotive Body Materials Conference Proceedings*; IBEC 1994; 90-97.

50. K.Lucke, K.Detert; *A Quantitative theory of grain- boundary motion and recrystallization in metals in the presence of impurities*; Acta Metallurgica; Vol.5; November 1957; 628-637.

51. H.M.Otte, J.J.Hren; *The observation of crystalline imperfections and their role in plastic deformation*; Experimental Mechanics; April 1966; 177-193.

52. H.Gleiter; *On the structure of grain boundaries in metals*; Materials Science and Engineering; Vol.52; 1982; 91-131.

53. S.A.Kish (supervisor); *Departmental correspondence of Ford motor company*; Jan 18th 1997; 1-6.

54. ASTM; *E-8- Standard methods of tension testing of metallic materials*; Annual Book of ASTM Standards; Vol. 3.01; 1983.

55. No author; *Metallurgical effects during cold strip processing*; IEHK; RWTH Aachen.

56. K.A.Taylor, J.G.Speer; *Development of Vanadium alloyed, bake hardenable sheet steels for hot dip coated applications*; 39th MWSP, Conf. Proc. ISS; Vol.35; 1998; 49-61.

57. No author; *Recent developments of cold formable steels*; 1-3.

58. B.M.Hance; *Bake- hardenability and aging resistance of high- strength nitrided sheet steels*; 42nd MWSP Conf. Proc., ISS; Vol.38; 2000; 607-620.

59. B.Hance; *Bake hardenability calculation methods for high strength steels;* USS Research; April 16th 2002; unpublished.

60. *ULSAB-AVC Body Structure Materials*; ULSAB-AVC Consortium; 26th May 2001

61. J.S.Rege; *The role of phosphorous in cold work embitterment in Ti and Ti-Nb stabilized high strength ultra low carbon steels*; PhD Thesis; University of Pittsburgh; 1997.

62. R.Pradhan; *Cold rolled interstitial free steels: A discussion of some metallurgical topics*; Invited lecture; May 10-11th 1994; 165-178.

63. K.Ushioda, N.Yoshinaga, K.Koyama, O.Akisue; *Application of ultra low carbon steels to the development of super formable sheet steels, solution hardened high strength sheet steels and bake hardenable sheet steels*; Invited lecture; May 10-11th 1994; 227-244.

64. P.Elsen, H.P.Hougardy; *On the mechanism of bake hardening*; Steel research; Vol.64; No.8/9; 1993; 431-436.

65. A.F.Gourguess; *Electron backscatter diffraction and cracking; Materials Science and Technology*; Vol.1; February 2002; 119-133.

66. N.Hansen; *Cold deformation microstructure*; Materials Science and Technology; Vol.6; November 19901039-1047.

67. A.B.Doucet, S.Natarjan; *Yielding behavior of pre-strained interstitial-free steel and 70/30 brass*; Metallurgical Transactions A; Vol. 22A; Feb 1991; 393-400.

68. T.Y.Tsui; *Factors limiting the accuracy of mechanical property measurement by nanoindentation*; Ph.D.Thesis; Rice University; 1996.

69. K.Miyahara, S.Matsuoka, T.Hayashi; *Nanoindentation as a strength probe- a study on the hardness dependence of indent size for fine-grained and coarse-grained ferritic steel*; Met. And Mat. Trans A; Vol. 32A; March 2001; 761-768.

70. P.M.Rice, R.E.Stoller; *Correlation of nanoindentation and conventional mechanical property measurements*; To be published at fall MRS meeting; 160-161.

71. A.J.Jones, R.P.Foley; *Effects and measurements of interstitial C and N in iron and steels*; 39th MWSP Conf. Proc., ISS; Vol. 35; 1998; 955-969.

72. E.B.Kula, N.H.Fahey; *Effect of specimen geometry on determination of elongation in sheet tension specimens*; Materials Research and Standards; August 1961; 631-636.

73. S.Kinoshita, P.J.Wray, G.T.Horne; *Some observations on the Portevin-Le Chatelier effect in Iron*; Transactions of the Metallurgical Society of AIME; Vol. 233; October 1965; 1902-1904.

74. R.G.Faulkner; *Segregation to boundaries and interfaces in solids*; International materials review; Vol.41; No.5; 1996; 198-209.

75. J.Kwak, J.Chung, K.Cho; *A study on the edge cracking of low carbon steel sheets manufactured by mini- mill process*; 42nd MWSP Conf. Proc., ISS; Vol.38; 2000; 311-320.

76. O.Richmond, W.C.Leslie, R.Sober; *Elimination of yield point in steel sheets by rapid temperature change*, Metallurgical transactions; Vol.3; Oct. 1972; 2593-2599.

77. C.E.R.Torres, F.H.Sanchez, A.Gonzales, F.Actis, R.Herrera; *Study of the kinetics of the recrystallization of cold- rolled low- carbon steels*; Metallurgical and Materials Transactions A; Vol.33; January 2002; 25-31.

78. G.P.Upit, S.A.Varchenya; *The science of hardness testing and its research applications*; American Society for Metals; 1971.

79. N.A.Fleck, G.M.Muller, M.F.Ashby, J.W.Hutchinson; *Strain gradient plasticity: theory and experiment*; Acta Metall. Mater.; Vol 42; 1994; 475-487.

80. G.Tither, C.I.Garcia, M.Hua, A.J.DeArdo; *Precipitation behavior and solute effects in IF steels*; Invited lecture; May 10-11th 1994; 293-322.

81. M.V.Phadke; *Kinetics of the reversible in-situ transformation reaction between titanium sulfide and titanium carbosulfide in ultra low carbon steel*; M.S. Thesis; University of Pittsburgh; 1998.

82. N.P.Allen; *The mechanical properties of ferrite crystal*; Journal of the Iron and Steel Institute; January 1959; 1-19.

83. C.Cheng; *Galvannealing behavior and coating performance of Ti- IF and Nb-Ti-IF steels;* 42nd MWSP Conf. Proc., ISS; Vol.38; 2000; 255-263.

84. D.M.M.Fausto; *New approaches to higher strength in interstitial free steels*; M.S.Thesis; University of Pittsburgh; 2001.

85. T.Foecke, S.W.Banovc, R.J.Fields; *Sheet metal formability studies at the national institute of standards and technology*; JOM; February 2001; 27-30.

86. J.J.Jonas; *The hot strip mill as an experimental tool*; ISIJ International; Vol.40; 2000; No.8; 731-738.

87. W.C.Leslie; *The physical metallurgy of steels*; 1982; 73-74.

88. P.T.Wakefield, M.Hatherly; *Microstructure and texture of cold rolled Cu- 10Zn brass*; Metal Science; March 1981; 109-115.

89. K.Tiito, G.Fitzsimons, A.J.DeArdo; *The effect of dynamic precipitation and recrystallization on the hot flow behavior of a Nb-V micro alloyed steel*; Acta Metallurgica; Vol.31; No.8; 1983; 1159-1168.

90. A.M.Kumar, R.Sengupta, A.Chatterjee; *Annealing technologies for cold rolled flat sheet products: a technical assessment*; Steel World; Vol.2; No.1; 1997; 29-38.

91. C.Klinkenberg, H.P.Schmitz, H.Tamler; *Texture measurements in steel industry practice*; Proceedings of the 12th International conference on Textures of Materials; 472-480.

92. M.Kurosawa, S.Satoh, T.Obara, K.Tsunoyama; *Age hardening behavior and dent resistance of bake hardenable and extra deep drawable high strength steel*; Kawasaki Steel Technical Report No.18; May 1988; 61-66.

93. P.Baucklin, G.Bollas, P.LeBlanc, Z.Simanvic; *Stamping and dentability evaluation of a hot dip ULC rephospherized bake hardenable steel for exposed body parts*; Copyright society of automotive engineers. Inc; 1997; 45-50.

94. Y.Nakada, A.S.Keh; *Kinetics of Snoek ordering and Cottrell atmosphere formation in Fe-N single crystals*; Acta Metallurgica; Vol. 15; May 1967; 879-883.

95. P.J.Turner, J.M.Papazian; *Some applications of field- ion atom probe analysis to iron and steels*; Metal Science Journal; Vol.7; 1973; 81-86.

96. M.Goken; *Studies of metallic surfaces and microstructures with atomic force microscopy*; AFM of Metallic Surfaces and Microstructures; 5th October 2002;

97. D.Blavette, E.Cadel, A.Fraczkiewicz, A.Menand; *Three-dimensional atomic scale imaging of impurity segregation to line defects*; Science; Vol 286; 17th December 1999; 2317-2319.

98. M.K.Miller, K.F.Russel, J.Kocik, E.Keilova; *Embrittlement of low VVER 440 surveillance samples neutron-irradiated to high fluencies*; Journal of Nuclear Materials; Vol 282; 2000; 83-88.